

EXHUMATION HISTORY OF CALEDONIAN ECLOGITES IN LIVERPOOL LAND,
EAST GREENLAND, AND COMPARISONS WITH ECLOGITES IN NORWAY

Except where reference is made to the work of others, the work described in this thesis is my own or was done in collaboration with my advisory committee. This thesis does not include proprietary or classified information.

Dannena Renée Bowman

Certificate of Approval:

Willis E. Hames
Professor
Geology & Geography

Mark G. Steltenpohl, Chair
Professor
Geology & Geography

Ashraf Uddin
Associate Professor
Geology & Geography

Joe F. Pittman
Interim Dean
Graduate School

EXHUMATION HISTORY OF CALEDONIAN ECLOGITES IN LIVERPOOL LAND,
EAST GREENLAND, AND COMPARISONS WITH ECLOGITES IN NORWAY

Dannena Renée Bowman

A Thesis

Submitted to

the Graduate Faculty of

Auburn University

in Partial Fulfillment of the

Requirements for the

Degree of

Master of Science

Auburn, Alabama
May 10, 2008

EXHUMATION HISTORY OF CALEDONIAN ECLOGITES IN LIVERPOOL LAND,
EAST GREENLAND, AND COMPARISONS WITH ECLOGITES IN NORWAY

Dannena Renée Bowman

Permission is granted to Auburn University to make copies of this thesis at its discretion,
upon request of individuals or institutions and at their expense. The author reserves all
publication rights.

Signature of Author

Date of Graduation

VITA

Dannena Renée Bowman, daughter of Darrell and Dorothy Bowman, was born March 24, 1983, in Waukesha, Wisconsin. She graduated from Danville Community High School in Danville, Indiana in 2001. She attended DePauw University in Greencastle, Indiana, for four years, graduated with a Bachelor of Arts degree in Geosciences in May, 2005. After working for a year as an environmental consultant in Warrenville, Illinois, she entered Graduate School at Auburn University, in August, 2006.

THESIS ABSTRACT

EXHUMATION HISTORY OF CALEDONIAN ECLOGITES IN LIVERPOOL LAND, EAST GREENLAND, AND COMPARISONS WITH ECLOGITES IN NORWAY

Dannena Renée Bowman

Master of Science, May 10, 2008
(B.A., DePauw University, 2005)

99 Typed Pages

Directed by Mark G. Steltenpohl

Lithologic information and $^{40}\text{Ar}/^{39}\text{Ar}$ cooling dates are reported from a recently discovered high-pressure (HP) Caledonian eclogite terrane in Liverpool Land, East Greenland, its overlying hanging wall block, and an extensional detachment fault separating them (Gubbedalen Shear Zone). $^{40}\text{Ar}/^{39}\text{Ar}$ analysis had not previously been reported for rocks in Liverpool Land thereby limiting our ability to understand its metamorphic and cooling history. Muscovite grains were, therefore, separated from rocks at various structural levels and analyzed using single crystal total fusion and incremental heating in the Auburn Noble Isotope Mass Analysis Laboratory (ANIMAL).

Muscovite cooling ages (analyzed to 1σ) from paragneiss and undeformed pegmatite in the hanging wall are 381.26 ± 0.41 Ma and 391.23 ± 0.54 Ma, respectively. Footwall orthogneiss yields a muscovite age of 378.5 ± 0.63 Ma and a mylonite from the Gubbedalen Shear Zone has an age of 379.78 ± 0.37 Ma. Later cooling of the footwall block, after the hanging wall had already cooled is consistent with normal movement determined along the shear zone. This age relationship is also consistent with Devonian sediments that nonconformably overlie units in the hanging wall block.

The argon isotopic results combine with previously reported U/Pb zircon dates of ~ 395 Ma for eclogitization to constrain the Liverpool Land temperature-*time* (T-*t*) path. This T-*t* path is distinct from paths reported for the Lofoten and Bergen Arcs eclogite terranes but compares favorably with the higher temperature parts of both the North East Greenland eclogite province (NEGEP) and the Western Gneiss Region (WGR) trajectories. Divergence of the NEGEP from the Liverpool Land T-*t* path likely reflects differences in the tectonic evolution between these two areas that are not yet understood. Overlapping of the Liverpool Land and WGR T-*t* paths from eclogite-facies temperatures at ~ 395 Ma to the 350°C isotherm at ~ 380 Ma suggests similar Devonian exhumation histories. Following ~ 380 Ma the WGR continued to exhume rapidly while Liverpool Land may have experienced a slight temperature rise ($\sim 75^\circ\text{C}$) for ~ 10 m.y. before reinitiating its similar rapid exhumation to Earth's surface. These differences are consistent with Liverpool Land's inferred position in an overriding plate while the WGR occupied a position in the subducting plate.

ACKNOWLEDGMENTS

The author would like to thank Dr. Willis E. Hames, Auburn University, for assistance with statistical analyses and data plotting related to the argon isotopic data. Special thanks to Dr. Arild Andresen, Oslo University, for providing the idea for this thesis, logistical support for field investigation, background information, and contributions to technical aspects throughout this investigation. Thanks also to John Wesley Buchanan II, Auburn University, for constant support during every aspect of this thesis research and Lars Augland, Oslo University, for field support and crystallization ages.

Style manual or journal used:

GEOLOGICAL SOCIETY OF AMERICA BULLETIN

Computer software used:

Microsoft Word®

Microsoft Excel®

Microsoft Powerpoint®

TABLE OF CONTENTS

LIST OF FIGURES	x
I. INTRODUCTION	1
II. GEOLOGIC SETTING.....	6
East Greenland Caledonides	6
Liverpool Land Geology.....	8
III. LITHOLOGIES AND METAMORPHISM	10
Southern Footwall Block	10
Gubbedalen Shear Zone.....	20
Northern Hanging Wall Block	27
IV. ⁴⁰ Ar/ ³⁹ Ar THERMOCHRONOLOGY.....	36
Analytical Techniques	36
Sample Descriptions	42
Results.....	44
⁴⁰ Ar/ ³⁹ Ar Discussion and Conclusions	51
V. DISCUSSION	54
VI. SUMMARY.....	70
REFERENCES	72
APPENDIX A.....	79

LIST OF FIGURES

- Figure 1. Eclogite localities superimposed upon Early Carboniferous paleogeographic reconstruction of Norway and Greenland (modified from Steltenpohl et al., 2006). NGEP = Northeast Greenland eclogite province.....2
- Figure 2. Cartoon illustrating Caledonian tectonic evolution of Baltica subducting beneath Laurentia. Oceanic-oceanic convergence ca. 440 Ma, arc-continent collision ca. 430-425 Ma, and continent-continent collision ca. 425-390 Ma. Green circles are potential locations of eclogite formation (modified from Fossen, H., pers. comm. to Steltenpohl, 2005).....4
- Figure 3. Paleogeographic reconstruction of Norway with respect to Greenland during the Late Caledonian orogeny (Mid- Devonian blue outline, dk.blue lettering) and Late Permian (black outline, green lettering). Notice the position of Liverpool Land (LL), Lofoten (LF) and the Western Gneiss Region (WGR) (modified from Zeigler, 1988).....4
- Figure 4. East Greenland Caledonides from 70° to 82°N with lithotectonic units (modified after Andresen et al., 2007). LL = Liverpool Land, CL = Canning Land, NVF = Narhval Sund Fjord, SA = Stauning Alper, KFJF = Kejser Franz Joseph Fjord, HL = Hudson Land, HwH = Hold with Hope, AF = Alpe Fjord, DLL = Dronning Louise Land, SL = Strindberg Land, AL = Andree Land, WG = Waltershausen Gletscher, OR = Ole Rømer Land, KF = Kempes Fjord, FF = Forsblad Fjord, ACF = Ardencaple Fjord, KH = Kap Hedlund, PB = Peterman Bjerg, KD = Kneakdalen, RL = Renland, Su L = Suess Land, PL = Payer Land.....7
- Figure 5. Geologic map of Liverpool Land, East Greenland (modified from Augland, 2007). Boxed areas are detailed maps from mapping within the present thesis study areas. (KS) = Krummedal Sequence.....9
- Figure 6. A. Quartzofeldspathic gneiss with mafic layers. Field book for scale at bottom left corner. B. Photomicrograph (XPL) of quartz and feldspar competent clast with recrystallized quartz and feldspar (boxed area) surrounding clast. Qtz = quartz, Feld = feldspar, Bt = biotite.....12

Figure 7. A. Competent amphibolite near Gubbedalen Shear Zone. B. Photomicrograph (PPL) of opaque minerals surrounding chlorite and biotite grain. Chl = chlorite, Opq = opaques, Bt = biotite, AcB = acicular biotite.....	14
Figure 8. A. Phyllonite along the basal sections of the Gubbedalen Shear Zone. Notice competent mafic aggregates with felsic material deformed around them. B. Photomicrograph (XPL) displaying mafic layer (top of photo) and felsic layer (middle of photo) of phyllonite. Red line is approximate separation of layers. Qtz = quartz, Plag = plagioclase, Bt = biotite, Amp = amphibole.....	17
Figure 9. A. Granitic dikes near Gubbedalen Shear Zone. Red line is approximate outline of one dike. Yellow dashed line is projection of shear zone. Cliff face is ~150 m high. B. Photomicrograph (XPL) displaying sericitic alteration of potassium feldspar. Qtz = quartz, Plag = plagioclase, Bt = biotite, Ser = sericite.....	19
Figure 10. Chart illustrating transition from breccia (gouge) to cataclasite, mylonite, and mylonite gneiss with temperature, pressure, and metamorphic facies ranges (from Winter, 2001). Yellow zone indicates extent of rocks within the Gubbedalen Shear Zone. Thick black line is approximate location of brittle-ductile transition within the shear zone.....	21
Figure 11. A. Field photograph of migmatitic orthogneiss (right in photo) becoming progressively mylonitized (toward left in photo) near Gubbedalen Shear Zone. B. Photomicrograph (XPL) of mylonite with muscovite S-C fabrics and mica fish. Blue line is C-plane. Green line is S-plane. Qtz = quartz, Mus = muscovite, Plag = plagioclase.....	22
Figure 12. A. Hand sample photograph of carbonate cataclasite with sheared and rotated lithic grains. Lip balm is approximately 7 cm in length. B. Photomicrograph (XPL) of polymineralic and monomineralic lithic grains in fine-grained, ultra cataclasite matrix. Large lithic grains have tails and halos of undistinguishable dark material. Qtz = quartz, Cal = calcite matrix, Opx = orthopyroxene, Cpx = clinopyroxene, Poly Lith = polymineralic lithic grains.....	24
Figure 13. A. Outcrop photograph of carbonate breccia boulder. B. Photomicrograph (XPL) showing quartz, plagioclase, and calcite grains surrounded by hematite. Qtz = quartz, Plag = plagioclase, Cal = calcite, Hem = hematite.....	26
Figure 14. A. Field photograph of garnet-biotite schist/gneiss inclusions in Hurry Inlet Granite (from Augland, 2007). B. Photomicrograph (XPL) of schist with weak biotite foliation. Plag = plagioclase, Qtz = quartz, Bt = biotite, Clz = clinozoisite, Gt = garnet.....	28

Figure 15. A. Photomicrograph (XPL) of calc-silicate. B. Photomicrograph (XPL) of diorite near contact with monzodiorite. Plag = plagioclase, Qtz = quartz, Bt = biotite, Cal = calcite, Chl = chloritoid, Px = pyroxene.....	30
Figure 16. A. Field photograph of banded Hurry Inlet Granite. B. Photomicrograph (XPL) of Hurry Inlet Granite. Plag = plagioclase, Qtz = quartz, Bt = biotite, Ks = potassium feldspar.....	32
Figure 17. A. Field photograph of monzodiorite. Top of photo is gray monzodiorite and center is purple (red outline). B. Photomicrograph (XPL) of monzodiorite. Qtz = quartz, Plag = plagioclase, Bt = biotite, Amp = amphibole, Px = pyroxene.....	34
Figure 18. DRB-06-16 quartzofeldspathic gneiss with fine-grained muscovite (0.25 mm diameter grains). A. Binocular photograph of muscovite grains used for $^{40}\text{Ar}/^{39}\text{Ar}$ analysis. B. Photomicrograph (XPL) of in-situ muscovite grain. Mus = muscovite.....	37
Figure 19. DRB-06-22 quartzofeldspathic gneiss with coarse-grained muscovite (0.5-1.0 mm diameter grains). A. Binocular photograph of muscovite grains used for $^{40}\text{Ar}/^{39}\text{Ar}$ analysis. B. Photomicrograph (XPL) of muscovite fish. Mus = muscovite.....	38
Figure 20. JWB-06-CP73 quartzofeldspathic mylonite in Gubbedalen Shear Zone fault (0.5-1.0 mm diameter grains). A. Binocular photograph of muscovite grains used for $^{40}\text{Ar}/^{39}\text{Ar}$ analysis. B. Photomicrograph (XPL) of muscovite fish. Mus = muscovite.....	39
Figure 21. JWB-06-M28A center of pegmatite, felsic intrusion in Krummedal Sequence (0.5-1.0 mm diameter grains). A. Binocular photograph of muscovite grains used for $^{40}\text{Ar}/^{39}\text{Ar}$ analysis. B. Photomicrograph (XPL) of muscovite. Mus = muscovite.....	40
Figure 22. JWB-06-M28C paragneiss in Krummedal Sequence calc-silicate (0.5-1.0 mm diameter grains). A. Binocular photograph of muscovite grains used for $^{40}\text{Ar}/^{39}\text{Ar}$ analysis. B. Photomicrograph (XPL) of clusters of muscovite. Mus = muscovite.....	41
Figure 23. Panoramic view of Gubbedalen shear zone looking east. $^{40}\text{Ar}/^{39}\text{Ar}$ ages reflect incremental heating plateau ages or error-weighted average age. Hanging wall ages (391, 386, and 381 Ma) are projected. Footwall ages are approximate location of samples.....	45
Figure 24. Sample descriptions with fault locations and age results reporting 1σ at the 95% confidence level. Single crystal total fusion (SCTF); error-weighted on average age (wt. avg.).....	46

- Figure 25. Age population distributions among single crystal total fusion analyses for 1σ at the 95% confidence level. Weighted average age is displayed. Thick blue line represents the mean. n = number of samples; % = probability of normal distribution.....47
- Figure 26. Inverse isochron plots for incrementally heated samples. Axes are $^{36}\text{Ar}/^{40}\text{Ar}$ vs. $^{39}\text{Ar}/^{40}\text{Ar}$. Regression results are calculated using the y-intercept for the trapped argon $^{40}\text{Ar}/^{36}\text{Ar}$. Error crosses are 1 σ.....49
- Figure 27. Age spectra for incrementally heated samples. Red boxes are plateau steps and black boxes are rejected steps. Error estimates are 1σ.....50
- Figure 28. Cartoon illustrations of A. Early Devonian eclogite-facies metamorphism. B. Exhumation of the eclogites through the 350°C muscovite isotherm in the Middle Devonian. Blue is hanging wall block and purple is footwall block. Red “e” in green circle represents eclogitized rocks. GSZ = Gubbedalen Shear Zone.....52
- Figure 29. Temperature-*time* diagram comparing Liverpool Land and North-East Greenland eclogite province (NEGEP), East Greenland, with Western Gneiss Region (WGR), Lofoten, and Bergen Arcs, Norway (Strachan and tribe, 1994; Gilotti and Ravna, 2002; White and Hodges, 2003; Gilotti et al., 2004; McClelland et al., 2005; Hacker, 2007; Kassos, 2008). Red lines indicate closure temperature of corresponding minerals (Dodson, 1973; Boundy et al., 1997; von Blackenburg et al., 1989; Lee et al., 1997; Schmitz and Bowering, 2003). 0°C temperature data are Devonian basin formation (Siedlecka, 1975; Boundy et al., 1997; White et al., 2002). K-spar = potassium feldspar, $40/39 = ^{40}\text{Ar}/^{39}\text{Ar}$ age dating, U/Pb = U/Pb age dating.....58
- Figure 30. Numerical model of active continental margin from 150 km to 600 km of subduction. Boxed yellow area is stranded oceanic crust in continental crust. yellow=sediments, red=upper continental crust, pink=lower continental crust, dark green=upper oceanic crust, light green=lower oceanic crust, dark blue=dry mantle, light blue=hydrated mantle, purple=serpentinized mantle (Gerya and Stöckhert, 2006).....62
- Figure 31. Series of time-progressive cross sections through Liverpool Land illustrating possible origin and exhumation of eclogites. Approximately 440 Ma, 5 million years after volcanic island arc (just east of cross-section) and Baltica collide, intrusion of Hurry Inlet Granite at 445 and 438 Ma. Approximately 150 km of subduction, formational rotation of orogenic flow channel in Laurentian plate. Approximately 425 Ma, 20 million years after collision, ~450 km of subduction; oceanic crust and mantle material ascend through lower continental crust; Baltic continental crust is subducted. Light blue arrow is contractional movement (into plane of model) along Gubbedalen Shear Zone. Distances not to scale..... 64

Figure 31 (cont'd). Approximately 425-420 Ma, ~25 million years after collision, ~600 km of subduction. The Hurry Inlet Granite continues thrusting (into plane of model) west across Liverpool Land and Krummedal Sequence and monzodiorite crystallize. Fjord Region Detachment initiated as extensional. Approximately 420-400 Ma, peak collision of Caledonian orogen with episodic extension initiating Western Fault Zone. Approximately 400-370 Ma, GSZ becomes extensional and pegmatites intrude hanging wall and footwall 388-386 Ma. Distances not to scale.....65

Figure 32. Present day close-up cross section parallel to Greenland coastline (e.g. perpendicular to Liverpool Land). Red fault lines are high angle normal faults ca. 425 Ma -<Tertiary. Blue fault line is listric detachment of Fjord Region Detachment, respectively. Yellow fault line is extensional Gubbedalen Shear Zone. Dashed black line is approximate location between upper thrust and lower extension. Pegmatite intruded during extension from 388-386 Ma. Longitudinal distance is not to scale.....68

I. INTRODUCTION

Processes leading to the formation and exhumation of high- and ultra-high (UHP) pressure eclogite facies rocks are highly debated and present a challenge to our understanding of regional tectonic events and crustal evolution in general (Griffin et al., 1978; Haller, 1985; Zielger 1988; Brueckner et al., 1998; Steltenpohl et al., 2006; Hacker 2007). Caledonian eclogites along eastern Greenland and western Norway are exposed in Precambrian continental basement and in allochthonous Caledonian thrust sheets (Fig. 1; Dobrzhinetskaya, et al., 1995; Steltenpohl et al., 2003; Gilotti and McClelland, 2005). These are some of the largest, most accessible, and continuously exposed eclogite terranes on Earth. Here, high temperature and pressure metamorphic rocks record geodynamic processes of extreme crustal conditions, in this case due to continental collision (Dobrzhinetskaya, et al., 1995; White and Hodges, 2003).

Perhaps most important to tectonic studies is how these deep crustal rocks eventually are exhumed to be exposed at Earth's surface. Field and petrological information is abundant for most of the Norwegian eclogite localities (Roberts and Gee, 1985; Andersen and Jamtveit, 1990) and for the North-East Greenland eclogite province (Gilotti and McClelland, 2005; Sartini-Rideout et al., 2006). The southernmost occurrences of eclogites in the Greenland Caledonides, in Liverpool Land, have not been investigated in any detail. Geochronological and structural data from this region is key, therefore, to understanding the exhumation history of the Caledonian orogen and for the

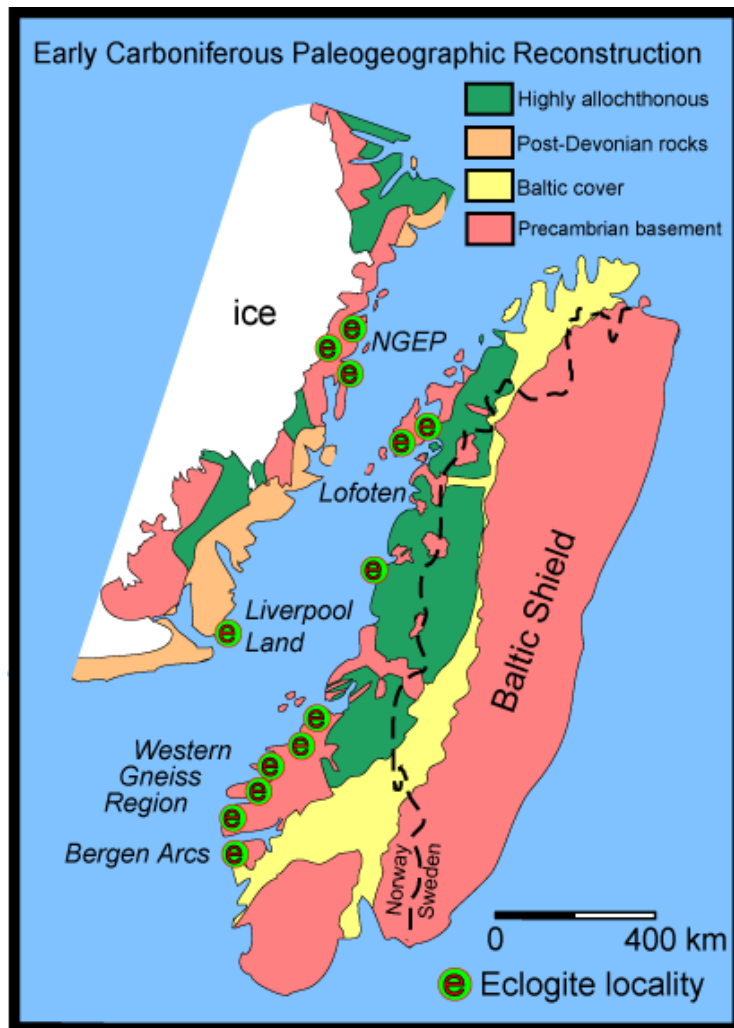


Figure 1. Eclogite localities superimposed upon Early Carboniferous paleogeographic reconstruction of Norway and Greenland (modified from Steltenpohl et al., 2006). NGEP = Northeast Greenland eclogite province.

subsequent rifting that formed the North-Atlantic Ocean. In this thesis new data collected from Liverpool Land are reported that helps to address (1) how these high-pressure (HP) rocks were exhumed and (2) how this exhumation history relates to those reported for the other eclogite provinces in Greenland and Norway.

The Caledonian orogen is thought to have formed due to collision and subduction of Baltica beneath Laurentia (Fig. 2). Paleogeographic reconstructions for the Early Devonian collision (Fig. 3) generally place Liverpool Land within the Laurentian overriding plate directly adjacent the Western Gneiss Region in the Baltic subducting plate (e.g. Ziegler, 1988; Mosar et al., 2002). Hartz et al. (2005) recently reported a date of eclogitization of ~395 Ma for eclogites in Liverpool Land basement orthogneiss, which overlaps the age of eclogitization in the Western Gneiss Region (400-390 Ma; Hacker, 2007). Furthermore, Hartz et al. (2005) report ultra-high pressure (UHP) estimates for eclogitization in Liverpool Land (>25 kbar) that are compatible with those for the Western Gneiss Region. To explain the challenge of UHP eclogite formation in both the upper (Laurentian) and lower (Baltic) plates at the same time, Hartz et al. (2005) evoke an unconventional mechanism of tectonic “overpressures”, which ignores the long-standing petrological concept that relates depths to pressures achieved during regional metamorphism. The main goal of this thesis report is to find a more parsimonious mechanism to explain the unusual setting of the Liverpool Land eclogites.

Renewed interest in the geological evolution of Liverpool Land led to the formation of a field research party that investigated the area during the summer 2006. Geological field studies were conducted in Liverpool Land by Lars Augland (University of Oslo, Norway), John Wesley Buchanan II (Auburn University), and the present author

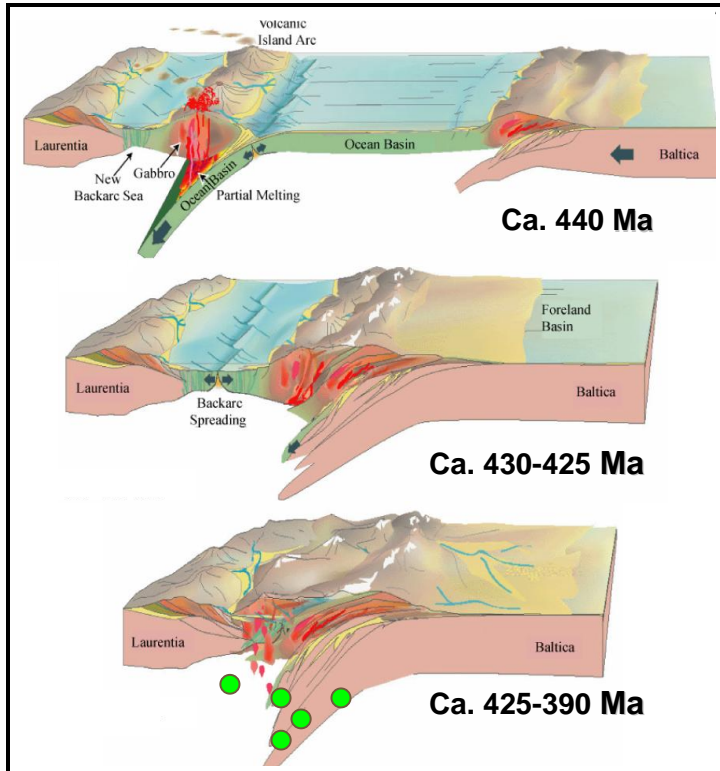


Figure 2. Cartoon illustrating Caledonian tectonic evolution of Baltica subducting beneath Laurentia. Oceanic-oceanic convergence ca. 440 Ma, arc-continent collision ca. 430-425 Ma, and continent-continent collision ca. 425-390 Ma. Green circles are potential locations of eclogite formation (modified from Fossen, H., pers. comm. to Steltenpohl, 2005).

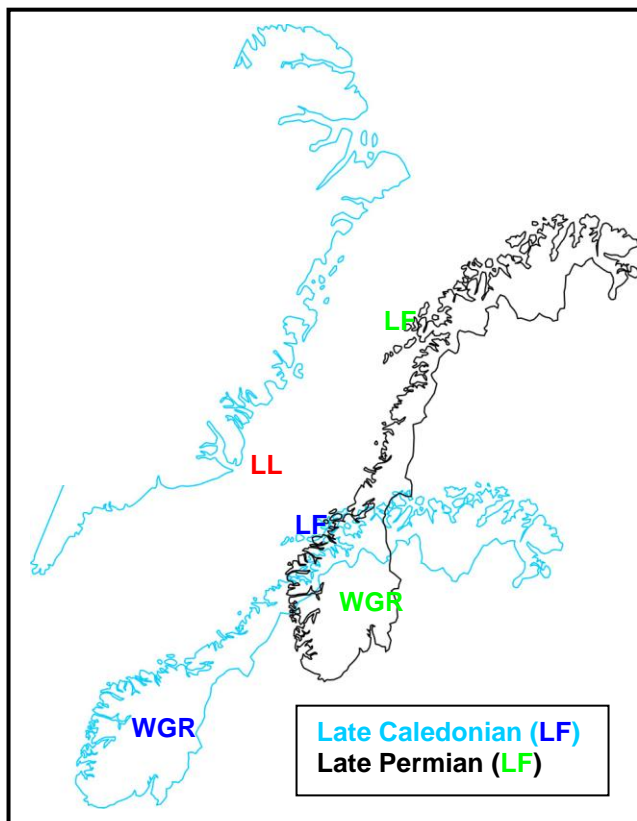


Figure 3. Paleogeographic reconstruction of Norway with respect to Greenland during the Late Caledonian orogeny (Mid-Devonian blue outline, dk. blue lettering) and Late Permian (black outline, green lettering). Notice the position of Liverpool Land (LL), Lofoten (LF) and the Western Gneiss Region (WGR) (modified from Zeigler, 1988).

to map lithologies and structures and to quantify conditions and timing of eclogite formation and exhumation. The contributions of this thesis to this geological collaboration focus on the following four objectives: (1) to characterize the field and petrographic properties of the country rocks that host the eclogites to evaluate whether they could or could not have transmitted tectonic overpressures to produce eclogitization; (2) initiate $^{40}\text{Ar}/^{39}\text{Ar}$ thermochronological work to characterize the exhumation history of Liverpool Land; (3) compare the temperature-*time* path determined for this eclogitized terrane to those reported for other eclogitized Caledonian basement terranes in Norway and East Greenland; and (4) synthesize these data to clarify eclogite exhumation along the length, and both sides of this classic Paleozoic orogen.

II. GEOLOGIC SETTING

Classically, the Caledonian orogen is thought to have formed due to collision and partial subduction of Baltica beneath Laurentia (Fig. 2). Two types of subduction occurred during the formation of the orogen. First, B-type subduction (i.e. Benioff; Andersen and Jamtveit, 1990) consumed significant amounts of oceanic crust east (present-day coordinates) of the passive continental margin of Laurentia forming a volcanic island arc (ca. 440 Ma). Second, continued B-type subduction led to the collision of the volcanic island arc (ca. 430-425 Ma) with Baltica. Finally, collision of Baltica with Laurentia led to high to ultra-high pressure A-type subduction (i.e. Ampferer; Andersen and Jamtveit, 1990) of the Baltic continental margin (ca. 425-390 Ma). The polarity of this collision (Fig. 2) is documented by a Caledonian calc-alkaline plutonic arc in the Laurentian basement of East Greenland (Gilotti and McClelland, 2005) and HP and UHP eclogites in the Western Gneiss Region of Norway (Hodges et al., 1982).

East Greenland Caledonides

The East Greenland Caledonides (70° to 82°N) consist of westward verging thrust sheets with intermittent tectonic windows exposing Archean and Paleoproterozoic metamorphic gneiss of the Laurentian continental basement complexes. Caledonian eclogites occur in reworked Archean, Proterozoic, and Lower Paleozoic rocks in more coastal regions in the NEGEP and in Liverpool Land (Fig. 4; Haller 1998; McClelland

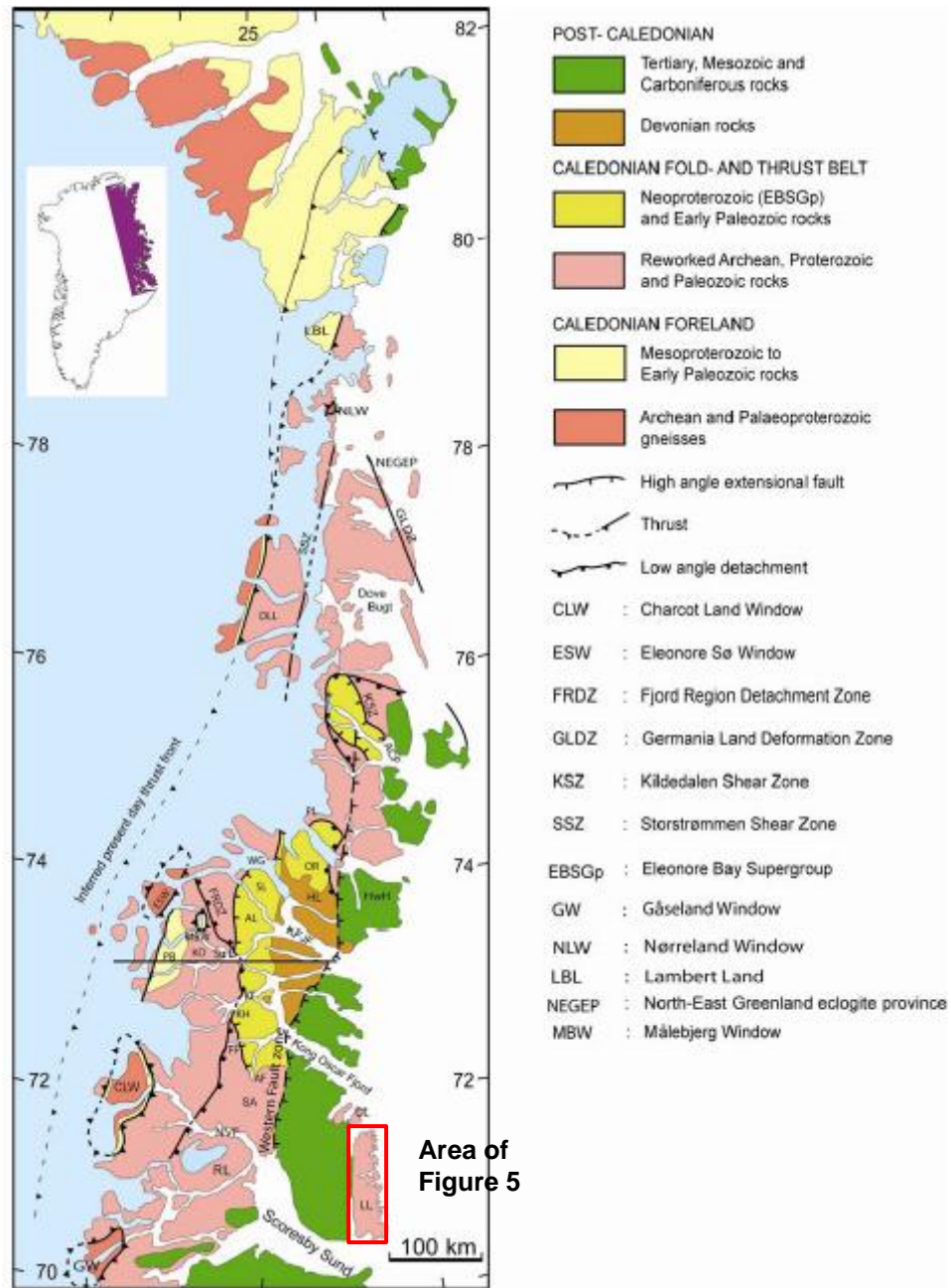


Figure 4. East Greenland Caledonides from 70° to 82°N with lithotectonic units (modified after Andresen et al., 2007). LL = Liverpool Land, CL = Canning Land, NVF = Narhval Sund Fjord, SA = Stauning Alper, KFJF = Kejser Franz Joseph Fjord, HL = Hudson Land, HwH = Hold with Hope, AF = Alpe Fjord, DLL = Dronning Louise Land, SL = Strindberg Land, AL = Andree Land, WG = Waltershausen Gletscher, OR = Ole Rømer Land, KF = Kempes Fjord, FF = Forsblad Fjord, ACF = Ardencape Fjord, KH = Kap Hedlund, PB = Peterman Bjerg, KD = Kneakdalen, RL = Renland, Su L = Suess Land, PL = Payer Land.

and Gilotti, 2003). A major, Early Devonian extensional detachment fault, the Fjord Region Detachment zone (Fig. 4), is a Late Caledonian collapse structure (Hartz and Andresen, 1995; White and Hodges, 2003; Sartini-Rideout et al., 2006). Following Devonian detachment faulting, the entire orogen has been extended about a N-S axis during pulses of rifting during Carboniferous, Permian, Triassic, Jurassic, and Cretaceous with final continental separation during Eocene (Hartz and Andresen, 1995; Leslie and Higgins, 1999; Mosar et al., 2002).

Liverpool Land Geology

Liverpool Land, northeast of Scoresby Sund (Fig. 4), contains a HP eclogite- and amphibolite-facies terrane, is cut by a major crustal shear zone, the Gubbedalen Shear Zone (Fig. 5). The southern footwall block consists mostly of 1.6 Ga quartzofeldspathic orthogneisses and migmatites with rare occurrences of variably retrograded eclogites (Hartz et al., 2005; Augland, 2007). The northern hanging wall block comprises the Hurry Inlet Granite batholith, Krummedal Sequence paragneiss, monzodiorite, and garnet-biotite gneiss. Eclogites occur as boudins and lenses encapsulated in mylonitic shears within the footwall block. Augland et al. (2007) report U/Pb dates of 400 Ma on zircon and 371 Ma on rutile extracted from the eclogites. Buchanan et al. (2008) estimated temperatures and pressures of 850 °C at >18 kbar, respectively, from several of the least retrograded eclogites. Both eclogites and country rocks have experienced weak amphibolite-facies retrogression. No $^{40}\text{Ar}/^{39}\text{Ar}$ mineral cooling dates are reported for Liverpool Land. Six samples were, therefore, collected and analyzed from the hanging wall and footwall blocks and from the Gubbedalen Shear Zone to initiate characterization of the timing of cooling of the fault blocks and for along the shear zone.

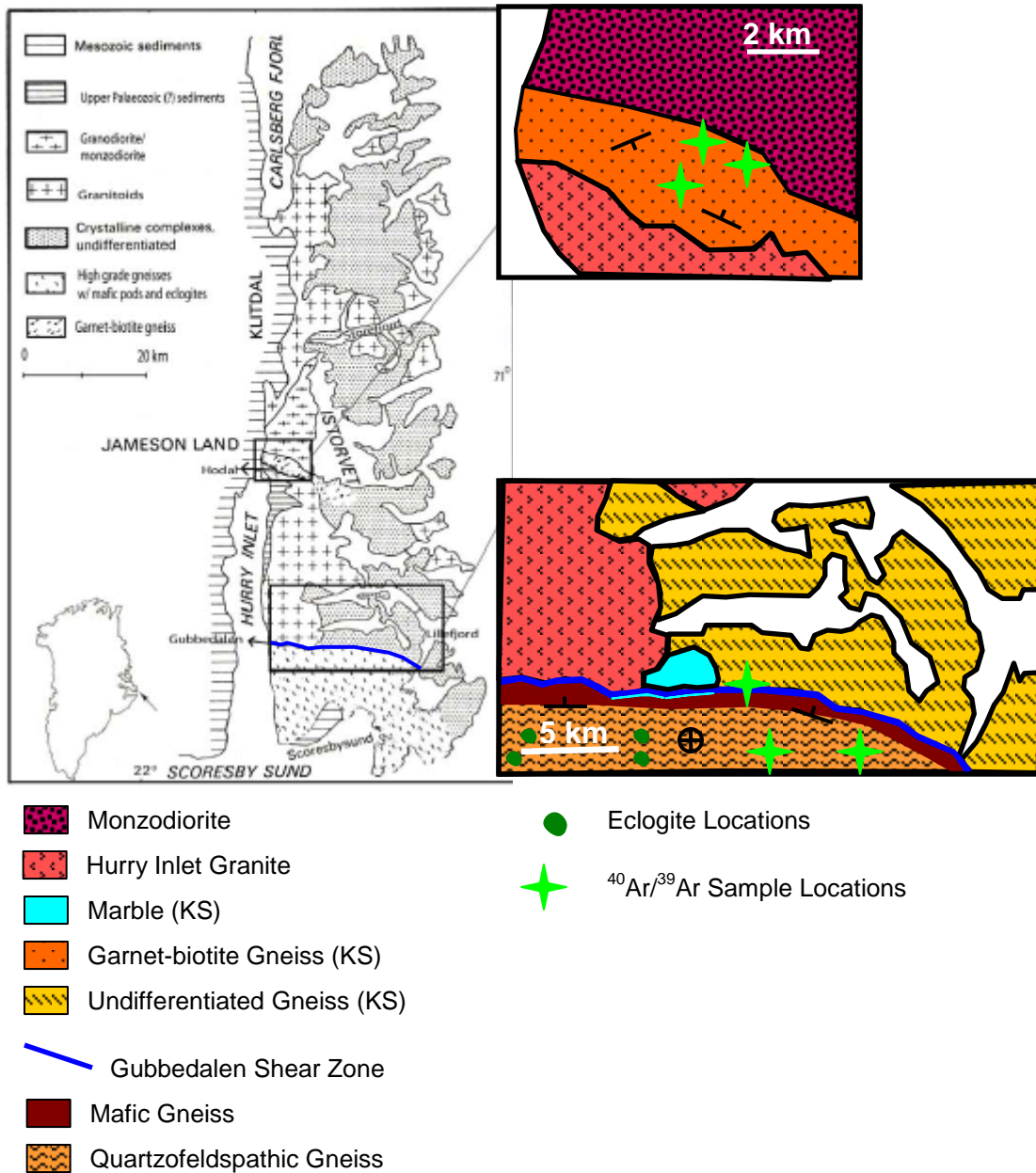


Figure 5. Geologic map of Liverpool Land, East Greenland (modified from Augland, 2007). Boxed areas are detailed maps from mapping within the present thesis study areas. (KS) = Krummedal Sequence.

III. LITHOLOGIES AND METAMORPHISM

Liverpool Land is an erosional outlier of mostly Proterozoic metamorphic rocks surrounded by nonconformably overlying Devonian, Carboniferous, Permian, Mesozoic, and Tertiary strata (Figs. 4 and 5; Andersen et al., 2007). Figure 5 illustrates the general geology and tectonostratigraphy of the two areas in Liverpool Land mapped during the summer 2006 field expedition. The tectonostratigraphy characterized within these two areas is described below in three sections: the footwall block south of the Gubbedalen Shear Zone; the Gubbedalen Shear Zone; and the hanging wall block to the north. In the following discussion of lithologies and metamorphic characteristics, units are described in order of greatest to least volumetric abundance. All volumetric mineral abundances reported are visual estimates.

Southern Footwall Block

Units of the footwall block south of the Gubbedalen Shear Zone comprise variably migmatized quartzofeldspathic orthogneiss, amphibolite, phyllonite, granitic dikes and veins, and eclogites. Rare eclogites occur within the footwall block but they are the focus of a separate thesis study by Buchanan (2008), and thus are not described herein. Likewise, Augland et al. (2007) described and isotopically dated the group of dikes and veins so these are only briefly summarized below. Refer to Figure 5 for locations of the various units.

Quartzofeldspathic Orthogneiss

Footwall quartzofeldspathic orthogneiss contains minor layers of amphibolite including a more mafic gneiss adjacent the Gubbedalen Shear Zone. The gneiss is locally migmatized and mylonitized, the latter especially near the shear zone. Orthogneiss is medium- to fine-grained (<2mm) with quartz and feldspar clasts (1-2 mm). The gneiss has tan to dark pink feldspar-rich bands alternating with dark gray layers richer in ferromagnesian silicates (biotite and amphibole; Fig 6A). The gneiss contains approximately 67% feldspar (3:1 potassium feldspar to plagioclase), 30% quartz, 1% biotite, 1% opaques, 1% amphibole, and <1% muscovite. Muscovite suitable for $^{40}\text{Ar}/^{39}\text{Ar}$ isotopic dating (DRB-06-16 and DRB-06-22) were analyzed and can be found described in the $^{40}\text{Ar}/^{39}\text{Ar}$ Thermochronology section.

Felsic layers consist of recrystallized quartz, quartz porphyroclasts (1-2 mm), feldspar porphyroclasts (1-2 mm), and fine-grained material indistinguishable using petrographic methods. Potassium feldspar grains commonly are sericitized. Clasts are surrounded by moats of recrystallized quartz and/or feldspar and altered biotite. Fine-grained, elongated grains help to define the foliation that trends 043°. Clasts of quartz and feldspar have numerous subgrains, twins, and minor amounts of myrmekite. Mafic layers consist of fine-grained biotite and minor amounts of amphibole. Minerals defining the mafic layers have been altered to chlorite/chloritoid minerals. Strongest alteration surrounds fractures in grains that may contain minor amounts of muscovite. Opaque grains are distributed throughout in minor amounts. Plastic deformation is indicated by ribbons of finely-recrystallized quartz and feldspar stretched and draped over larger, more competent grains of quartz and/or feldspar (Fig. 6B).

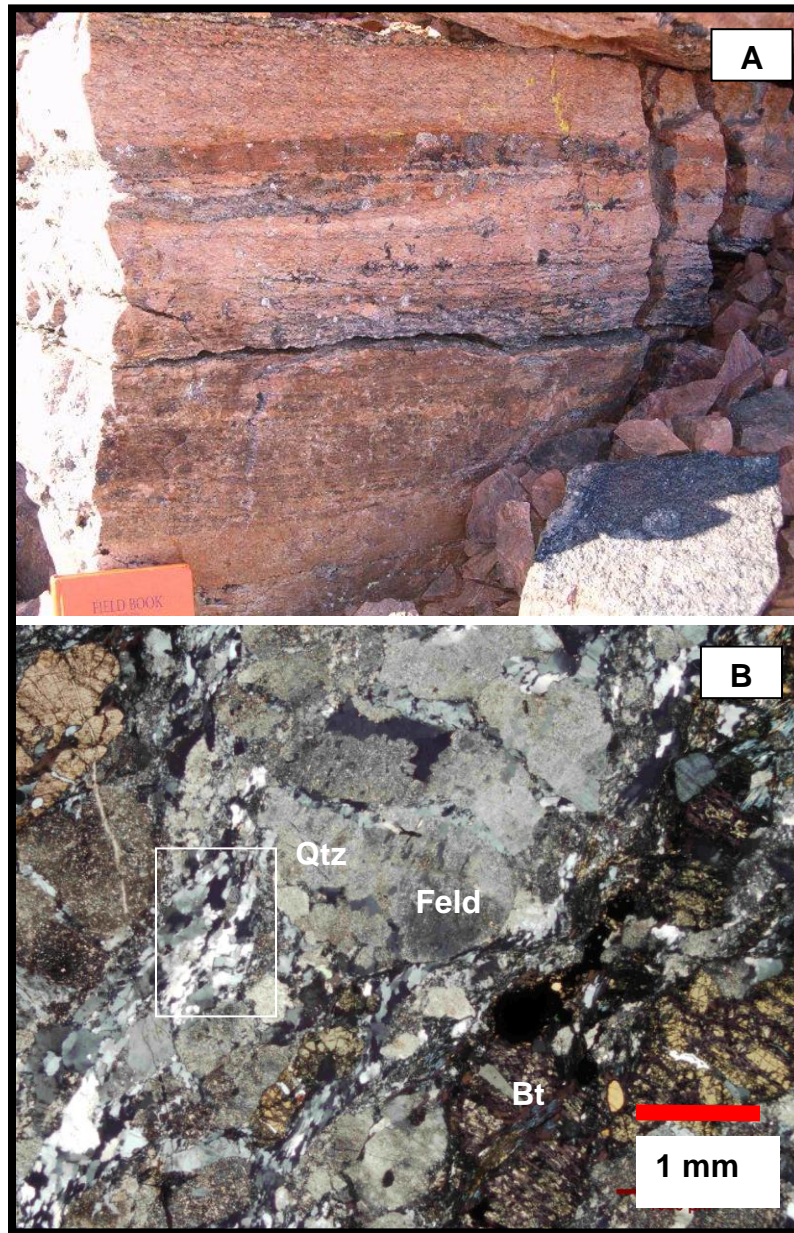


Figure 6. **A.** Quartzofeldspathic gneiss with mafic layers. Field book for scale at bottom left corner. **B.** Photomicrograph (XPL) of quartz and feldspar competent clast with recrystallized quartz and feldspar (boxed area) surrounding clast. Qtz = quartz, Feld = feldspar, Bt = biotite.

Grain shapes range from inequigranular-amoeboid to seriate-interlobate. Quartz and minor amounts of feldspar have undulose extinction and grain boundary bulges indicating grain boundary migration, and subgrain rotation. Larger feldspars have fractures in their cores and may have twins. Grains without undulose extinction are amoeboid shaped and usually contain quartz inclusions. Dynamic recrystallization of quartz and feldspar suggests lower amphibolite- to upper greenschist-facies deformational conditions. Metamorphic mineral assemblages of this granite protolith are not diagnostic of metamorphic conditions but are compatible with amphibolite-facies conditions.

Amphibolite

A larger body of competent amphibolite occurs near the Gubbedalen Shear Zone (Fig. 7A). The amphibolite, with local felsic migmatite, is approximately 40% amphibole, 20% biotite, 20% quartz, 15% feldspar, and 5% opaques. It is fine-grained (<0.5 mm) with no apparent lineations, only localized compositional banding. Overall color is black to dark green. These rocks have inequigranular-interlobate shaped grains. Most tend to be elongate but no lineation or foliation is present. Conjugate fracture patterns and no recrystallization suggest low-temperature deformation. Biotite ranges from subhedral to acicular shaped. Subhedral grains overlay one another whereas acicular grains lie parallel to one another to form clusters. Approximately half the biotite grains have altered to chlorite/chloritoid minerals. Quartz has subgrain boundaries, undulose extinction, and grain boundary bulges. Feldspars are subhedral amoeboids that have growth and deformation twinning and undulose extinction. Twin boundaries exhibit migration however, grain boundaries are not disturbed. Few grains have subgrains

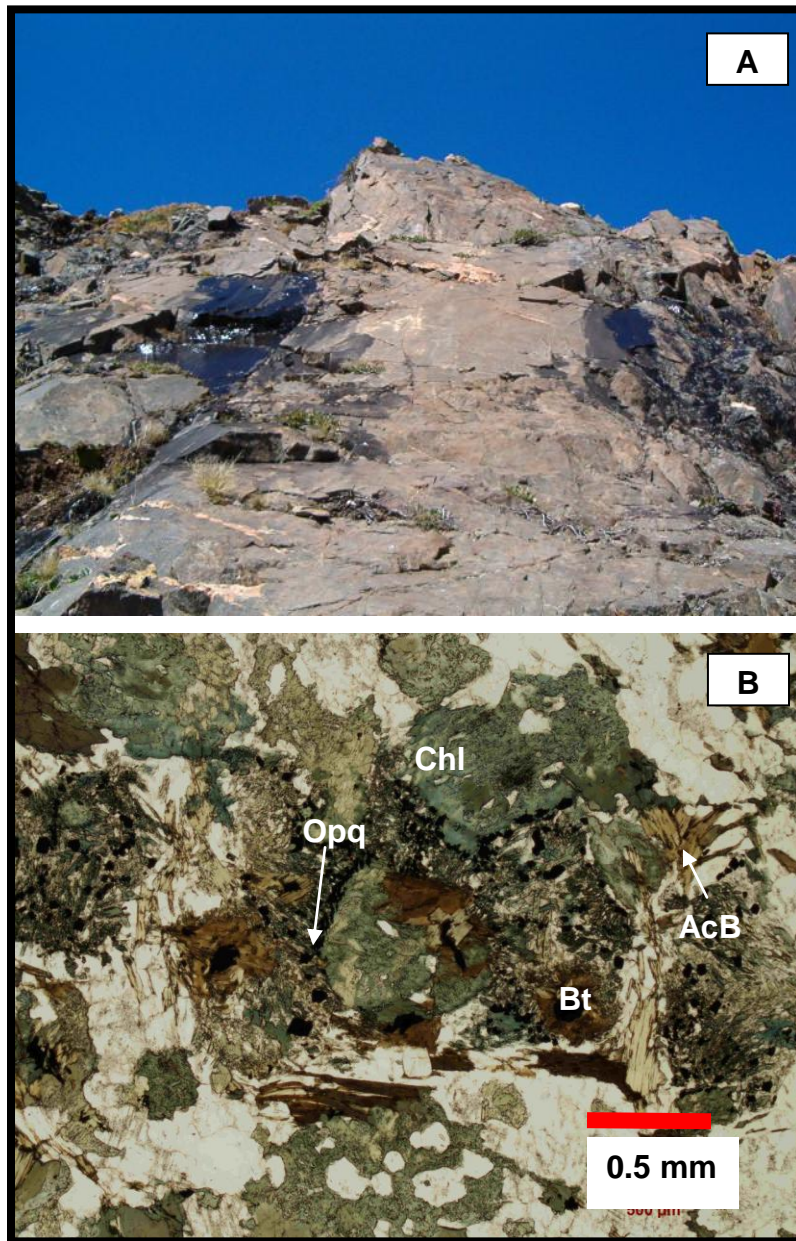


Figure 7. **A.** Competent amphibolite near Gubbedalen Shear Zone. **B.** Photomicrograph (PPL) of opaque minerals surrounding chlorite and biotite grain. Chl = chlorite, Opq = opaques, Bt = biotite, AcB = acicular biotite.

indicating high-temperature deformation. Opaque grains are abundant around biotite grains (Fig. 7B). Biotite appears to have replaced pre-existing grains as acicular crystals. Opaque grains seem to align in fractures that had cut across the pre-existing grain and partially outline the pre-existing grain shape.

Mafic Layers

Within the quartzofeldspathic gneiss are boudinaged layers of amphibolite and rarely associated eclogite boudins. Amphibolites also occur as larger bodies up to ~10m² in area near the shear zone. Around the boudins are migmatitic zones of felsic gneiss. Mafic layers range from eclogite to retrograded eclogite to amphibolite, depending on amount of fluid interactions. Veins cutting eclogites are felsic and are interpreted as decompression melts (Buchanan, 2008). Further descriptions of eclogites can be found in Buchanan (2008).

Concordant mafic layers were also found sheared in the footwall orthogneiss. In sills are veins of pure amphibole. All amphiboles have conjugate fracturing. The sills are mainly amphibole and plagioclase equigranular interlobate grains. Other veins composed of amphibole, plagioclase, and biotite cut across eclogites forming inequigranular-polygonal aggregates. Mineral assemblages are compositionally consistent throughout the amphibolites indicating gabbro to basalt protolith metamorphosed to amphibolite-facies and greenschist-facies retrogression.

Phyllonite

A distinctive phyllonite (micaceous mylonite) containing abundant biotite and porphyroclasts of mostly amphibole outcrops near the base of the Gubbedalen Shear Zone along the uppermost structural layers of the footwall block. The phyllonite is

compositionally banded with S-C fabrics in hand sample (Fig. 8A). It is a medium- to coarse-grained black rock with white layers bending around composite porphyroclasts comprise of garnet, biotite, and amphibole (Fig 8B). Mafic layers consist of 70% biotite and 30% amphiboles (<0.5 mm). Felsic layers comprise of 1-2 mm polycrystalline quartz and feldspar porphyroclasts. Around the porphyroclasts is finer grained (<0.5 mm) feldspar (2:1 potassium feldspar to plagioclase feldspar) that is dominantly altered to sericite.

Quartz grains in the phyllonite have undulose extinction, equigranular-lobate shapes, and subgrains. Feldspar grains have few growth twins, deformation lamellae, and equigranular-lobate shapes. Biotite grains (<0.3 mm) are euhedral to acicular equigranular shaped. Most grains have been altered to chlorite. Amphibole grains (<0.3 mm) are parallel to each other and non-parallel to the biotite foliation. They are subhedral to anhedral equigranular shaped grains and commonly interlaced with biotite. Garnets are 1-2 mm porphyroclasts grains in more mafic parts of the phyllonite. They are dark red in hand samples and very well rounded with intense fracturing.

The protolith to the phyllonite likely is the mafic gneiss, subsequently deformed in Gubbedalen Shear Zone. Based on crystal-plastic quartz and feldspar, dynamic crystallization likely occurred under upper greenschist- to lower amphibole-facies conditions.

Granitic Dikes and Veins

Throughout the footwall, but conspicuously absent in the hanging wall, are granitic dikes and veins from ~10 m to few cm in width that cut across all units. Dikes are meters in width and length whereas veins are centimeters in size. Near the

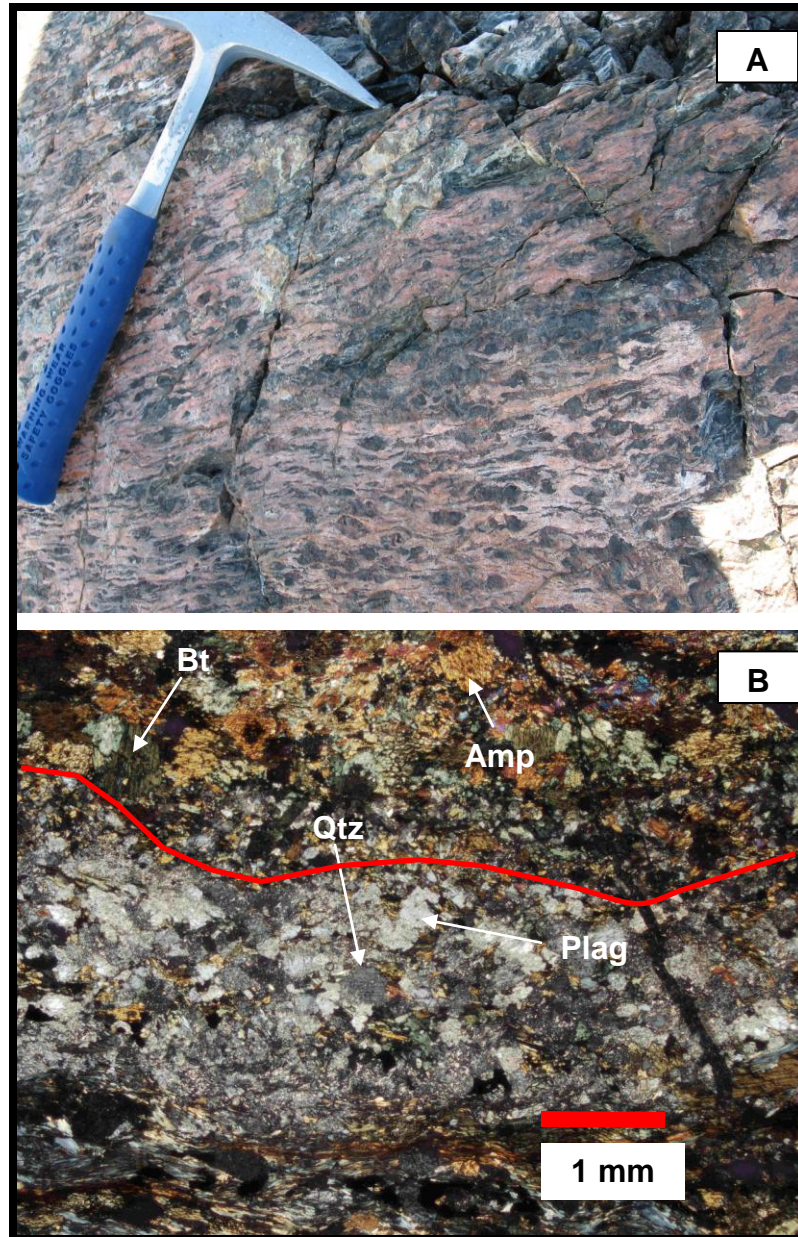


Figure 8. **A.** Phyllonite along the basal sections of the Gubbedalen Shear Zone. Notice competent mafic aggregates with felsic material deformed around them. **B.** Photomicrograph (XPL) displaying mafic layer (top of photo) and felsic layer (middle of photo) of phyllonite. Red line is approximate separation of layers. Qtz = quartz, Plag = plagioclase, Bt = biotite, Amp = amphibole.

Gubbedalen Shear Zone, these dikes are swept into the fault zone but do not cross the shear zone (Fig. 9A). Away from the fault (south), most dikes are unaffected by the shear zone. Overall, the dikes are orangish-pink to white and medium-grained (1-2 mm). Detailed petrographic, structural, and geochronology analyses on these rocks are reported in Augland (2007). Below are summarized descriptions.

Compositional proportions of dikes and veins are relatively similar. Feldspars (3:1 potassium feldspar to plagioclase) are most abundant followed by quartz, amphibole, biotite, and garnet. Potassium feldspar is dominantly sericitized and equigranular (Fig. 9B). Plagioclase growth twins are mostly preserved with few deformation twins. Quartz grains are equigranular interlobate-shaped grains. Low degrees of strain are indicated by grain boundary bulges and subgrains that document grain boundary migration and subgrain rotation crystallization in <0.25 mm patches. Most quartz and feldspar have undulose extinction. Biotite is altered to chlorite/chloritoid minerals and sometimes defines a weak foliation in the granite. Garnets are dark red (1-2 mm) subhedral grains with parallel fractures. Finer-grained feldspars and quartz do not form tails, shadows, or halos around garnets indicating low- to moderate-temperature deformation rather than moderate- to high-temperature deformation. Deformation microstructures of undulose extinction in quartz and feldspars indicate low- to moderate-temperatures as well. Late fluid infiltration producing pegmatitic quartz and potassium feldspar veins are associated with some granitic dikes. The granitic dikes are most likely decompressional melts of high grade rocks.

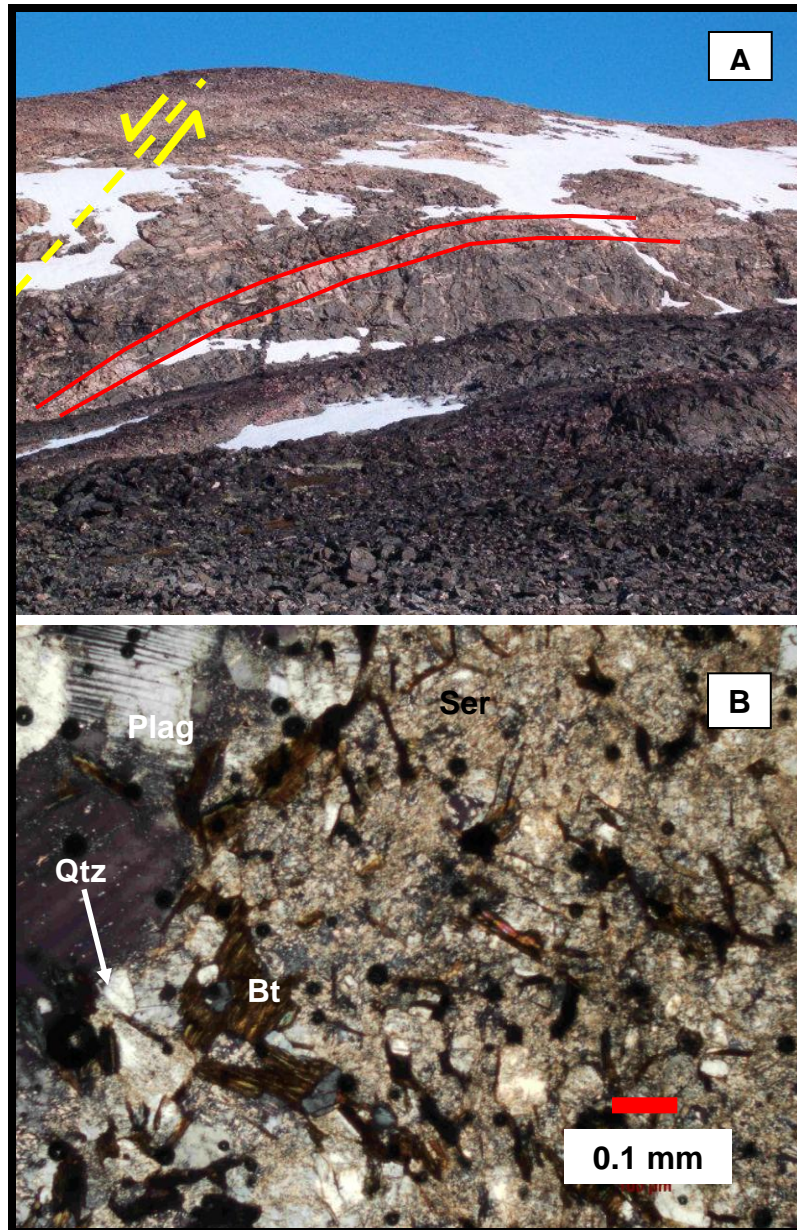


Figure 9. **A.** Granitic dikes near Gubbedalen Shear Zone. Red line is approximate outline of one dike. Yellow dashed line is projection of shear zone. Cliff face is ~150 m high. **B.** Photomicrograph (XPL) displaying sericitic alteration of potassium feldspar. Qtz = quartz, Plag = plagioclase, Bt = biotite, Ser = sericite.

Gubbedalen Shear Zone

A ~500 m thick shear zone, the Gubbedalen Shear Zone, consists of crystal-plastic to brittle rock fabrics within mylonitized gneisses and granites of the footwall block, and carbonate cataclasites and carbonate breccia of the hanging wall block (Fig. 10). Buchanan (2008) reports shear sense indicators to indicate two components of movement. Mylonite occurs within the lower contractional zone whereas cataclasites and breccias are within the upper extensional zone. Units are discussed below from ductile to brittle fabric development.

Footwall Mylonite

Approaching the Gubbedalen Shear Zone, footwall orthogneisses, mafic layers, and granitic injections are progressively mylonitized (Fig. 11A). The area of severe mylonitization is adjacent to the fault. Grain textures and sizes decrease towards the fault (northward).

Mineral abundance remains the same as previously discussed for footwall block units. The quartzofeldspathic mylonitic orthogneiss contain ~10% muscovite (Fig. 11B). Grain shapes change from seriate-interlobate and amoeboid to stretched, equigranular polycrystalline quartz and feldspar. Subgrain recrystallization is dominant. Few clasts are present; larger grained quartz and feldspar preserve some grain boundary bulges. Clasts are elongate and ribbon-like indicating ductile deformation. Grain boundaries are higher angled than non-mylonitized orthogneiss.

Grains begin to have a preferred orientation as they become mylonitized. Within the fault, all grains are stretched parallel to the N-S trending slip-line. One sample with the least amount of mylonitization is oriented 040° with parallel foliation. An

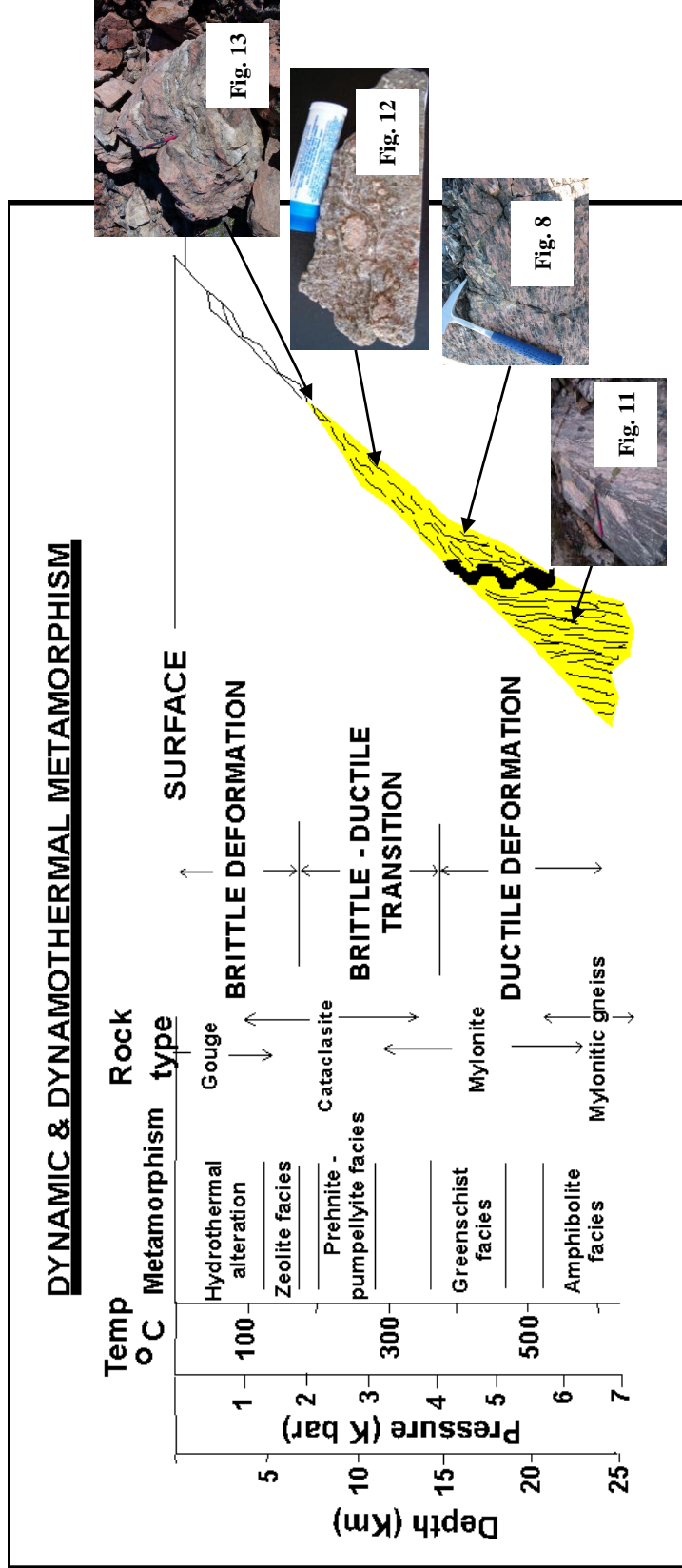


Figure 10. Chart illustrating transition from breccia (gouge) to cataclasite, mylonite, and mylonite gneiss with temperature, pressure, and metamorphic facies ranges (from Winter, 2001). Yellow zone indicates extent of rocks within the Gubbedalen Shear Zone. Thick black line is approximate location of brittle-ductile transition within the shear zone.

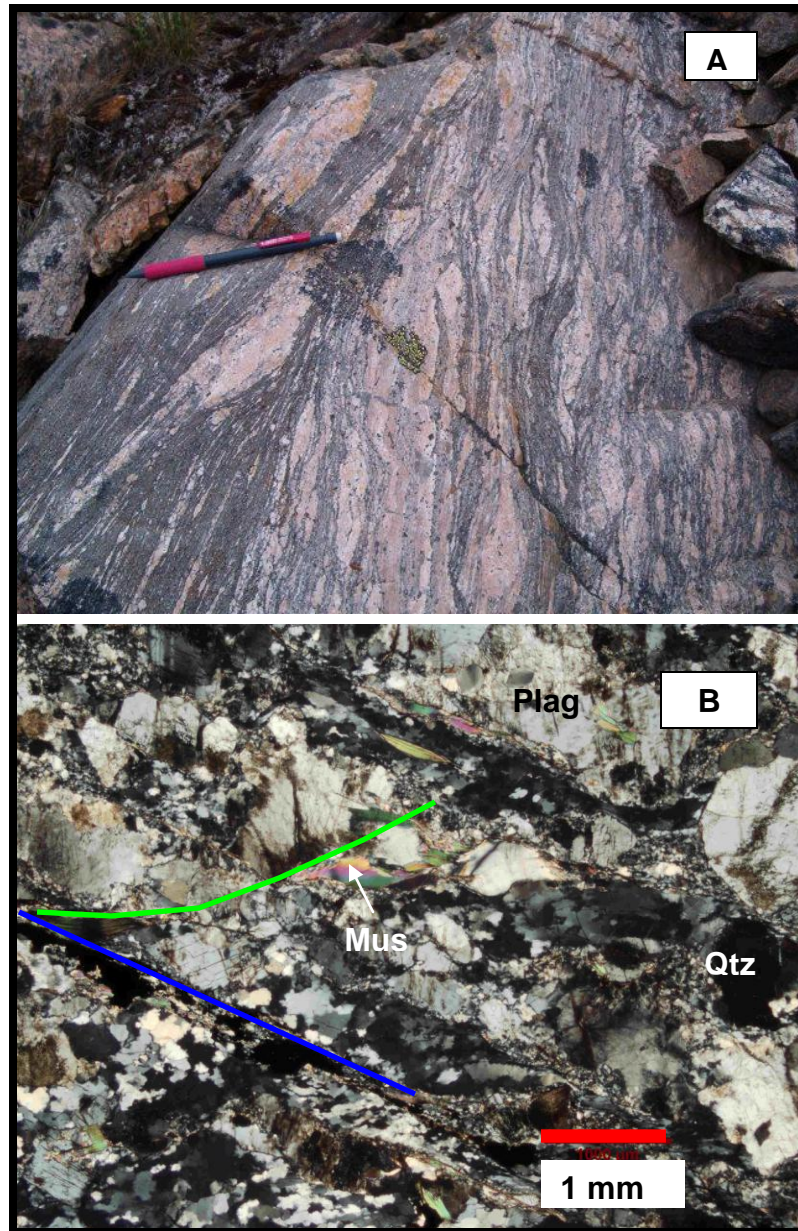


Figure 11. **A.** Field photograph of migmatitic orthogneiss (right in photo) becoming progressively mylonitized (toward left in photo) near Gubbedalen Shear Zone. **B.** Photomicrograph (XPL) of mylonite with muscovite S-C fabrics and mica fish. Blue line is C-plane. Green line is S-plane. Qtz = quartz, Mus = muscovite, Plag = plagioclase.

ultra-mylonitized sample trends east-west 20°S with parallel foliation. See Buchanan (2008) for oriented samples of Gubbedalen Shear Zone. Within the shear zone, dynamic recrystallization is most abundant with no grain boundary bulges. The contractional component mylonitized the footwall gneiss and contains coarse-grained (1-2 cm) muscovites suitable for $^{40}\text{Ar}/^{39}\text{Ar}$ isotopic dating. JWB-06-CP73 results can be found in the $^{40}\text{Ar}/^{39}\text{Ar}$ Thermochronology section.

Carbonate Cataclasite

Within the upper structural levels of the Gubbedalen Shear Zone carbonate cataclasites are a medium-gray color with sigma clast lithic fragments (Fig. 12A). Oriented samples of this material were not collected due to their occurrences in inaccessible cliff faces; samples were collected from float blocks at the base of the cliff. Grain shapes range from well-rounded to angular. Grain sizes range from 2 cm to <0.1 mm (Fig. 12). The cataclasite consists of fine-grained calcite matrix, polymineralic lithic grains with undulose extinction, and monomineralic grains in matrix (Fig. 12B). No veins are apparent in hand sample or thin section indicating low fluid pressures. Overall, cataclastic flow occurred in low-grade metamorphic conditions.

Fine-grained calcite matrix is homogenous and flows around lithic grains. Darker material within the matrix is indistinguishable using petrographic methods. The darker material forms tails and halos around rounded and rotated lithic grains. Larger grains (0.3-0.5 mm) of calcite are present in some polymineralic lithic grains.

Polymineralic lithic grains consist of quartz, indistinguishable dark materials, orthopyroxene, clinopyroxene, amphibole, and calcite. These grains are rounded to subrounded shapes. Individual mineral grain shapes are anhedral, arranged as seriate



Figure 12. A. Hand sample photograph of carbonate cataclasite with sheared and rotated lithic grains. Lip balm is approximately 7 cm in length. **B.** Photomicrograph (XPL) of polymineralic and monomineralic lithic grains in fine-grained, ultra cataclasite matrix. Large lithic grains have tails and halos of indistinguishable dark material. Qtz = quartz, Cal = calcite matrix, Opx = orthopyroxene, Cpx = clinopyroxene, Poly Lith = polymineralic lithic grains.

polygonal to interlobate inequigranular aggregates. Quartz and calcite form interlobate aggregates whereas pyroxene, amphibole, and dark material are polygonal.

Polymineralic lithic grain rock types are indeterminate due to the variation among grains.

Monomineralic lithic grains are well-rounded to angular and range from 0.2-1.0 mm. These fragments consist of quartz, orthopyroxene, clinopyroxene, and untwined feldspar. Quartz fragments have undulose extinction and subgrains. Pyroxene fragments have fractures along cleavage planes in larger grains. Orthopyroxene has pink to green color birefringence, whereas clinopyroxene has yellow to orange color birefringence. Few clinopyroxene grains have light green color birefringence indicating Na/K-rich (MacKenzie and Adams, 2001). Feldspars have twins and undulose extinction.

Carbonate Breccia

Within the second, northern-most, area of the Gubbedalen Shear Zone, shearing is opposite (i.e. thrusting). The Krummedal metasedimentary sequence lies structurally above this unit in the hanging wall. In the fault zone, a coarse-carbonate breccia formed from brittle deformation of a marble. The breccia is brownish-red with white veinlets separating individual breccia clasts (Fig. 13A). Shear-sense is not apparent in hand sample but can be seen in outcrop and thin section.

The breccia contains approximately 40% hematite, 25% quartz, 20% plagioclase, and 15% calcite. Fine grains of hematite (<0.1 mm) create the matrix of the breccia and coats rims of other grains. Quartz grains have inequigranular interlobate shapes. Most finer grained quartz and plagioclase (<0.5 mm) float in the hematite matrix. Clusters of quartz and plagioclase that are connected are equigranular with high-angle boundaries. Most quartz has undulose extinction and subgrains. Plagioclase grains are similar in

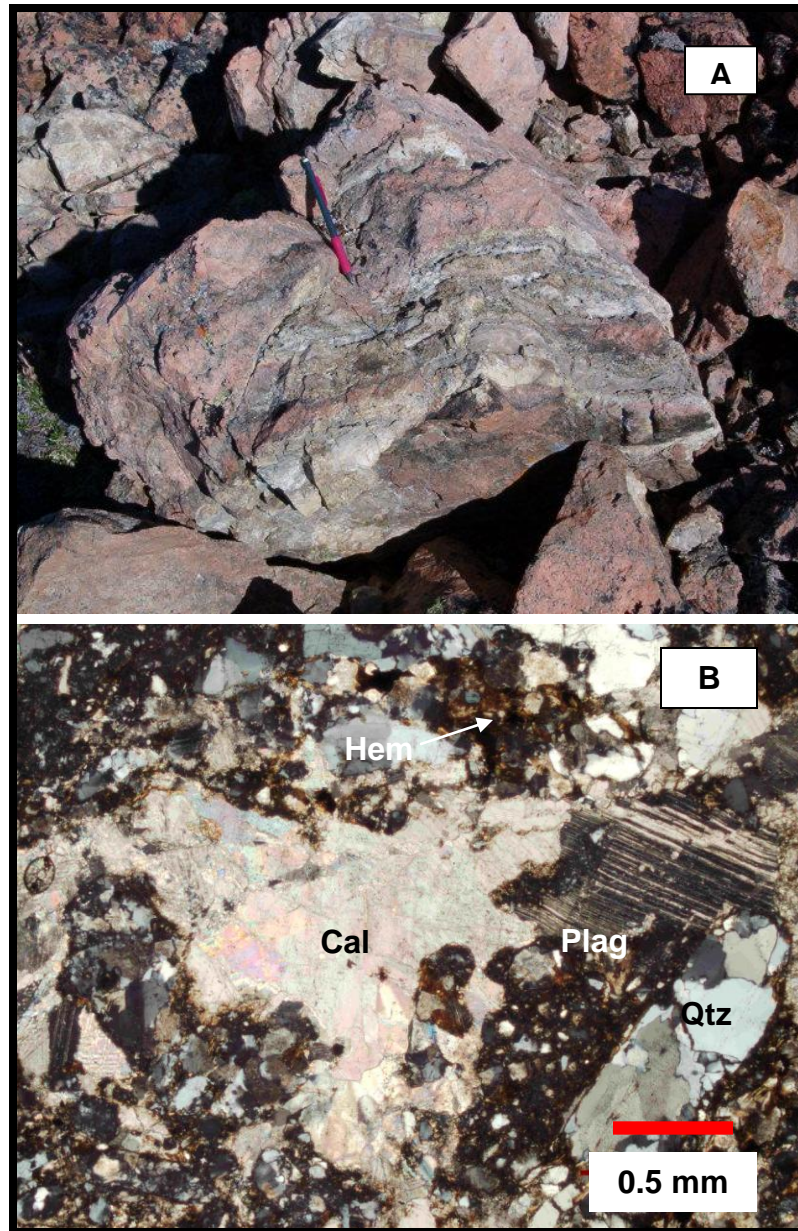


Figure 13. A. Outcrop photograph of carbonate breccia boulder. B. Photomicrograph (XPL) showing quartz, plagioclase, and calcite grains surrounded by hematite. Qtz = quartz, Plag = plagioclase, Cal = calcite, Hem = hematite.

shape and size to quartz grains and contain quartz inclusions but no myrmekite. Calcite forms euhedral equigranular polygonal shapes (1-0.2 mm). Most grains have several twins and undulose extinction. Twins are oriented in several directions. Twin orientation and population have been used to determine strain and stress magnitude and paleopressures in carbonates, but this particular fault did not deform coaxially, therefore, nullifying this approach (Passchier and Trouw, 2005).

Northern Hanging Wall Block

North of the Gubbedalen Shear Zone lies the hanging wall block. Within this block are the Krummedal Sequence, Hurry Inlet Granite, and monzodiorite. Units are discussed in order of greatest to least volume. See Figure 5 for location of units.

Krummedal Sequence

The hanging wall of the Gubbedalen Shear Zone consists mainly of a Proterozoic metasedimentary sequence (Augland, 2007). The sequence is dominated by quartzites and metapelites with lesser voluminous calc-silicates and marbles. Metapelites (garnet-biotite schist/gneiss) and calc-silicates are most abundant in the north study area (Fig. 5) with a few marbles. No marbles from the hanging wall were collected. Carbonate cataclasites described above, are similar in appearance to these marbles, however, textures differ significantly. Quartzite, least voluminous, is exposed as veins and as a thick basal unit to the sequence but no sample was collected for petrographic analysis.

Along the northern contact of the Hurry Inlet Granite is a garnet-biotite schist of the Krummedal Sequence that grades into migmatitic gneiss (Fig. 5). Within the schist/gneiss are inclusions of granite, and inclusions of schist/gneiss are found in the granite inclusions (Fig. 14A). The schist/gneiss is a medium-grained black to dark red

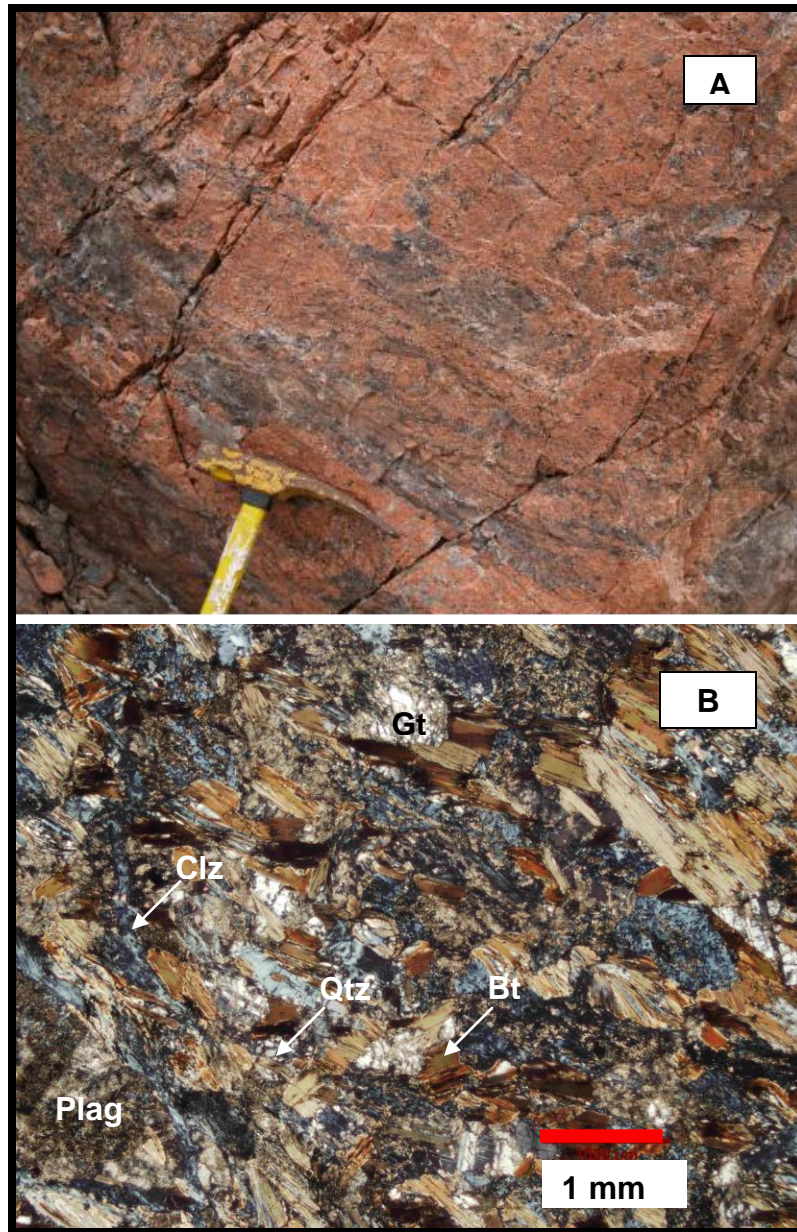


Figure 14. **A.** Field photograph of garnet-biotite schist/gneiss inclusions in Hurry Inlet Granite (from Augland, 2007). **B.** Photomicrograph (XPL) of schist with weak biotite foliation. Plag = plagioclase, Qtz = quartz, Bt = biotite, Clz = clinozoisite, Gt = garnet.

color consisting of 50% plagioclase, 20% quartz, 20% biotite, 5% garnet, 5% clinozoisite, < 1% opaques, and accessory zircon. Plagioclase (1-2 mm) is anhedral shaped and altered to sericite. Quartz (0.5-1 mm) is anhedral and forms seriate polygonal aggregates with plagioclase. Biotite (0.5-1 mm) is euhedral and forms a weak foliation (Fig. 14B). Between layers rich in biotite are layers rich in clinozoisite (<0.5mm), quartz, and plagioclase. Garnet (0.5-1 mm) is subhedral, highly fractured, and light pink in thin section. Clinozoisite (steel-blue birefringence) has deformational lamellae, unidirectional fractures, and sericite alteration. Grains are subhedral inequigranular in shape. The assemblage garnet + biotite + plagioclase + clinozoisite + quartz is compatible with metamorphic conditions ranging from lower to middle amphibolite-facies (Winter, 2001).

Concordant, tabular calc-silicate bodies ~10 m thick are interlayered within the garnet-biotite gneiss. Calc-silicates are white to light-gray colored and coarse-grained (1-3 mm) with coarser-grained varieties displaying pinkish tints. These rocks mostly consist of 70% plagioclase, 18% quartz, 12% calcite, and <1% pyroxene (Fig. 15A). Plagioclase and quartz (1-3 mm) are subhedral inequigranular-interlobate shaped grains. Calcite (<0.5-1 mm) is euhedral, inequigranular grains with deformation twins. Pyroxenes (<0.5 mm) are well-rounded fractured, equigranular polygonal grains. Recrystallization of plagioclase, quartz, and calcite by grain boundary migration as grain boundary bulges occurs only around fractures. This suggests low- to moderate temperature deformation. Based on the mineral assemblage plagioclase + quartz + calcite + pyroxene, metamorphism is upper amphibolite-facies retrograded to lower temperature amphibolite-facies (Winter, 2001).

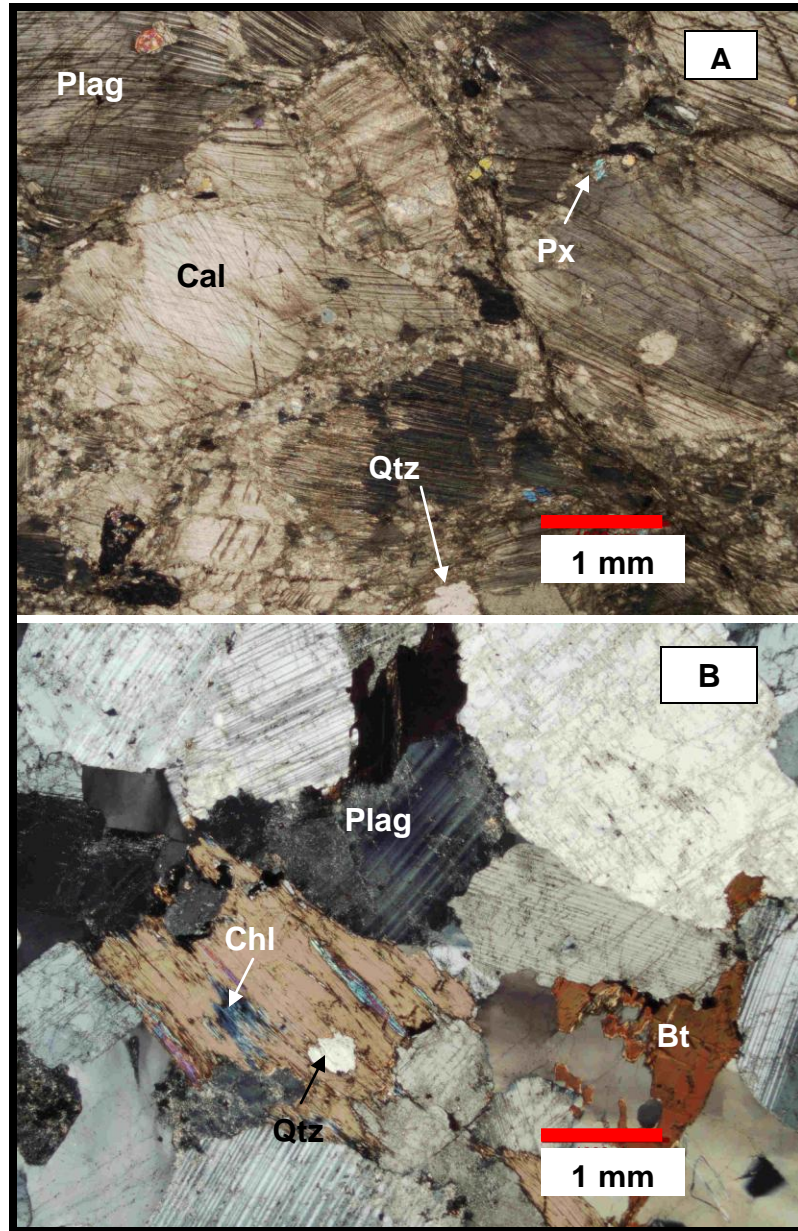


Figure 15. **A.** Photomicrograph (XPL) of calc-silicate. **B.** Photomicrograph (XPL) of diorite near contact with monzodiorite. Plag = plagioclase, Qtz = quartz, Bt = biotite, Cal = calcite, Chl = chloritoid, Px = pyroxene.

The contact between the monzodiorite is a sharp igneous intrusion representing an igneous equivalent to the garnet-biotite schist/gneiss (Augland, 2007). The igneous rocks are massive coarse-grained (1-2 mm), white and black to light purple diorite (Fig. 15B). No mineral lineations are present. Feldspar foliations are present at the contact only. The diorite consists of 80% plagioclase, equal amounts of quartz and biotite (10% each), and trace amounts of opaque minerals and zircon. Quartz and biotite rich layers occur with large (1-3 cm) plagioclase grains. Plagioclase (1-3 cm) is euhedral inequigranular-polygonal shaped. Growth twins and few deformation twins are present and few kink bands were observed. Minor grain boundary bulges suggests some recrystallization. Quartz (1-2 mm) is subhedral inequigranular-polygonal shaped with weak undulose extinction. Biotite (<0.5-1 mm) is subhedral equigranular-polygonal shaped and are altered to chlorite/chloritoid. Overall, recrystallization suggests deformation was at low-temperatures with minor affects on the diorite. Later igneous dikes, dolerites, and lamprophyres, cut across the monzodiorite, the garnet-biotite schist and gneiss, and the Hurry Inlet Granite. Lamprophyre dikes are described and discussed by Buchanan et al. (2008).

Hurry Inlet Granite

The Hurry Inlet Granite intrudes the Krummedal sequence. This granite batholith is exposed for several hundred square kilometers in north Liverpool Land (Fig. 5). Several phases are recognized throughout the intrusion and are interpreted as multiple pulses of magma. Overall, the granite is a medium-pink color with lighter and darker phases depending on feldspar and quartz amounts (Fig. 16A). Most phases are medium-grained (1-2 mm) containing 45% potassium feldspar, 25% quartz, 20% plagioclase, 5%

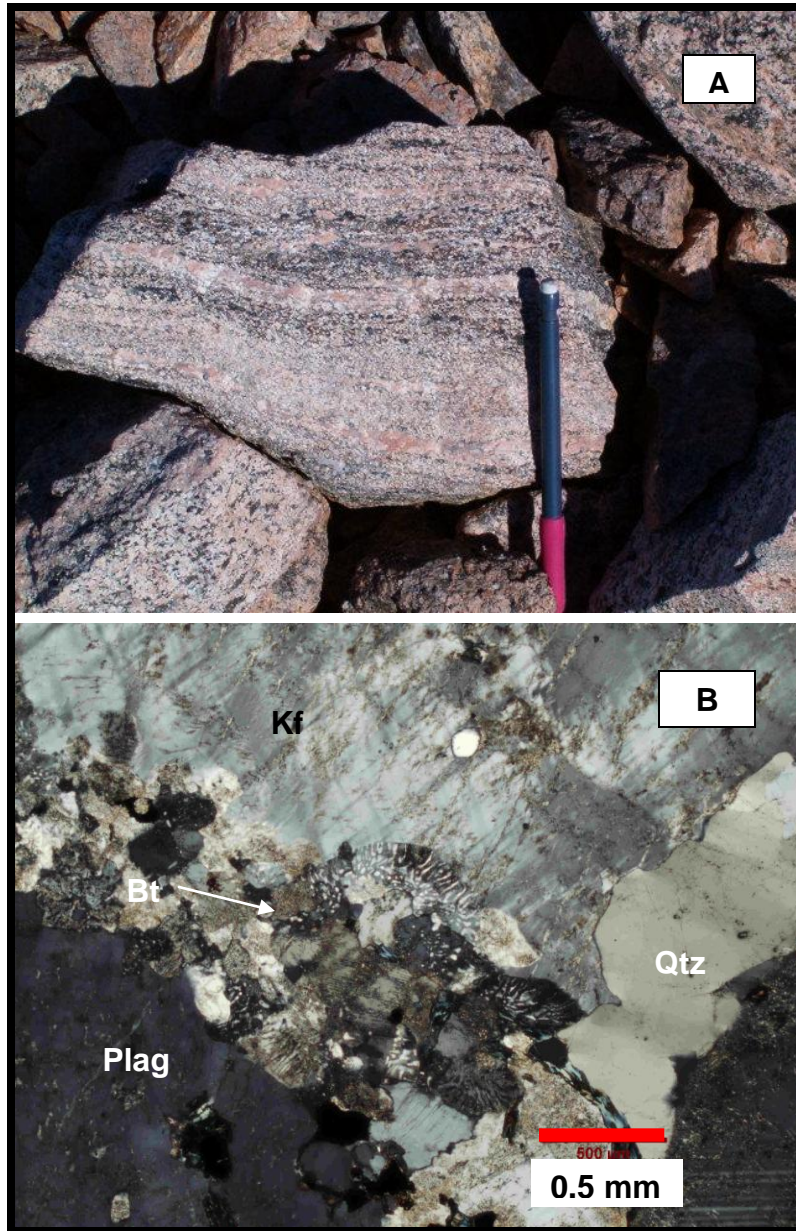


Figure 16. **A.** Field photograph of banded Hurry Inlet Granite. **B.** Photomicrograph (XPL) of Hurry Inlet Granite. Plag = plagioclase, Qtz = quartz, Bt = biotite, Ks = potassium feldspar.

biotite, and 5% amphibole, with accessory zircon. Feldspars (1-2 mm) are subhedral with sericite alteration. Plagioclase has growth twins and minor amounts of deformation twins whereas potassium feldspar may or may not have tartan cross-hatch twins (Fig. 16 B). Quartz (0.5-1 mm) is anhedral with undulose extinction. Grain boundary bulges in quartz indicates recrystallization. Feldspar and quartz occur as inequigranular-interlobate aggregates of myrmekite (Fig. 16B). Biotite and amphibole (<0.3 mm) are anhedral and variably replaced by chlorite/chloritoid. Combined microstructures imply greenschist-facies conditions for dynamic recrystallization.

Monzodiorite

Monzodiorite is a medium- to coarse-grained (1-2 mm), light-gray to purple colored unit with coarse biotite grains (Fig. 17A). The monzodiorite comprises 50% plagioclase, 15% potassium feldspar, 10% quartz, 10% pyroxene, 5% amphibole, 5% biotite, and 5% opaques. Plagioclase (<0.5-1 mm) occurs as subhedral inequigranular-interlobate to amoeboid shaped grains. Growth twins and deformation twins taper indicating low- to moderate-temperature deformation (Fig. 17B). Potassium feldspar (0.5-1 mm) is subhedral with sericite alteration and faint exsolution lamellae. Quartz occurs as (0.5-1 mm) anhedral grains containing subgrains, undulose extinction, and grain boundary bulges. Quartz and plagioclase form inequigranular-amoeboid masses of myrmekite with quartz filling areas between plagioclase grains. Pyroxene, equal amounts of clinopyroxene and orthopyroxene, (<0.5 mm) is anhedral and highly fractured. Pyroxene, biotite, and amphibole occur as inequigranular-interlobate aggregates. Amphibole (0.1-0.5 mm) is subhedral and highly fractured. Biotite (0.1-0.5 mm) occurs as euhedral to acicular grains. Acicular grains form clusters with other minerals or as

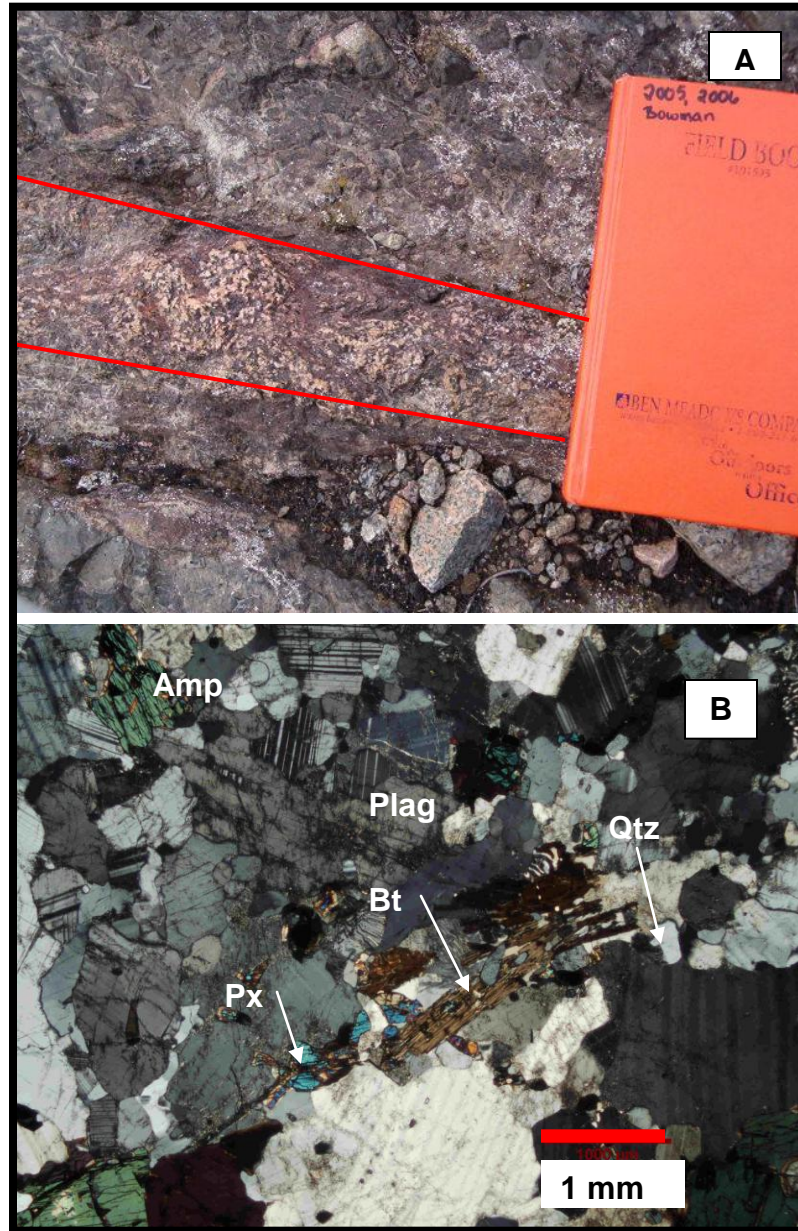


Figure 17. **A.** Field photograph of monzodiorite. Top of photo is gray monzodiorite and center is purple (red outline). **B.** Photomicrograph (XPL) of monzodiorite. Qtz = quartz, Plag = plagioclase, Bt = biotite, Amp = amphibole, Px = pyroxene.

inclusions within euhedral biotite grains. Biotite and pyroxene both are altered to chlorite/chloritoid.

IV. $^{40}\text{Ar}/^{39}\text{Ar}$ THERMOCHRONOLOGY

Analytical Techniques.

Isotopic analyses were performed at the ANIMAL laboratory, Auburn, Alabama. Six samples containing muscovite were prepared for laser analyses. Each sample was crushed, cleaned, and sieved. Standard picking techniques were used under a binocular microscope to pick uncontaminated grains. These grains were then packed into an irradiation disc and sent to McMaster University Research Reactor in Hamilton, Ontario. The standard used was FC-2, 28.03 ± 0.09 Ma, Fish Canyon hornblende (Renne et al., 1998; see Appendix A for monitor mineral data). Ten irradiated grains for each sample were placed in a copper holding disc and nine grains were analyzed using single crystal total fusion and one grain using incremental heating. Laser power percentages were adjusted accordingly to increase temperature for step-wise heating. Incremental heating was not performed on DRB-06-16 because muscovite grains are too small to yield sufficient argon for incremental heating (0.25 mm; Fig. 18A). All other sample grain sizes range 0.5 – 1.0 mm in diameter (Figs. 19A, 20A, 21A, 22A). The data was reduced using Microsoft® Excel and Isoplot 3 (Ludwig, 2003). All samples were corrected for background measurements of atmospheric argon contamination. Lengthwise gradients of fast neutron flux were monitored by determining the J-values from five crystals on each layer. Ca and K decay interferences were corrected for by using ^{37}Ar . Mass

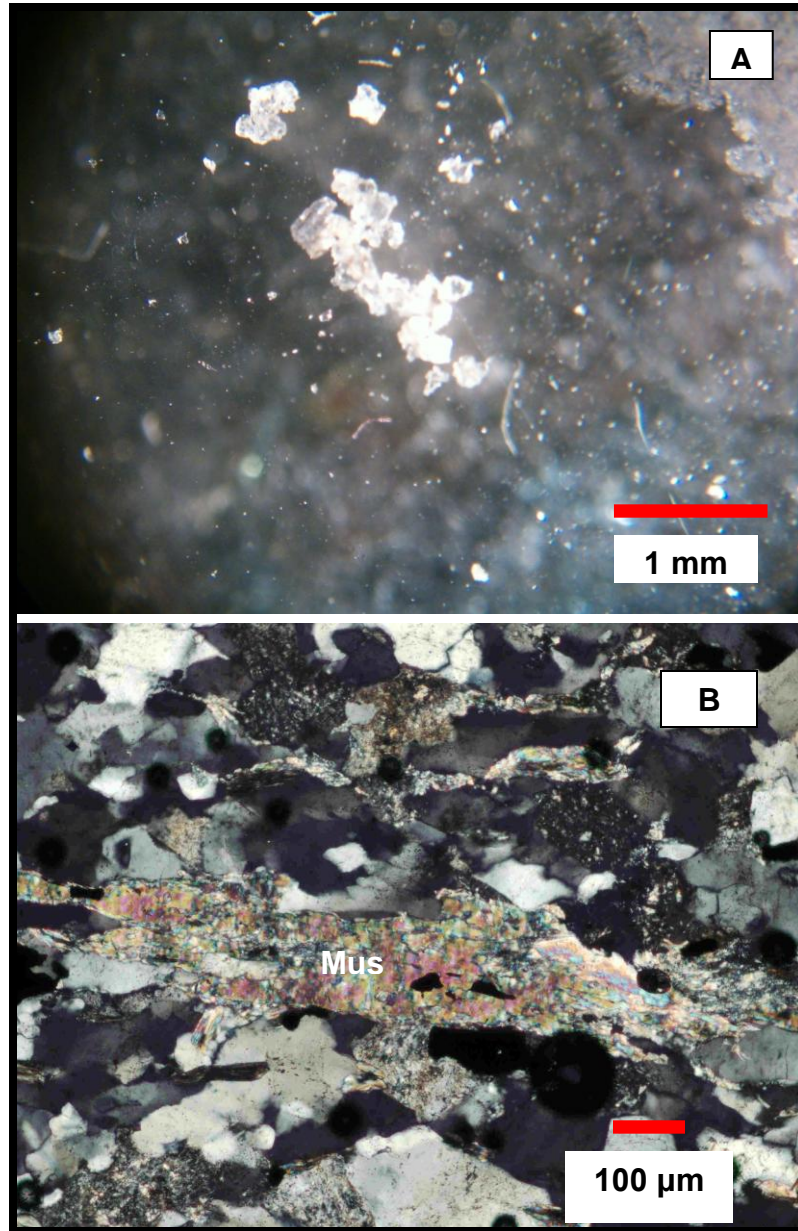


Figure 18. DRB-06-16 quartzofeldspathic gneiss with fine-grained muscovite (0.25 mm diameter grains). **A.** Binocular photograph of muscovite grains used for $^{40}\text{Ar}/^{39}\text{Ar}$ analysis. **B.** Photomicrograph (XPL) of in-situ muscovite grain. Mus = muscovite.

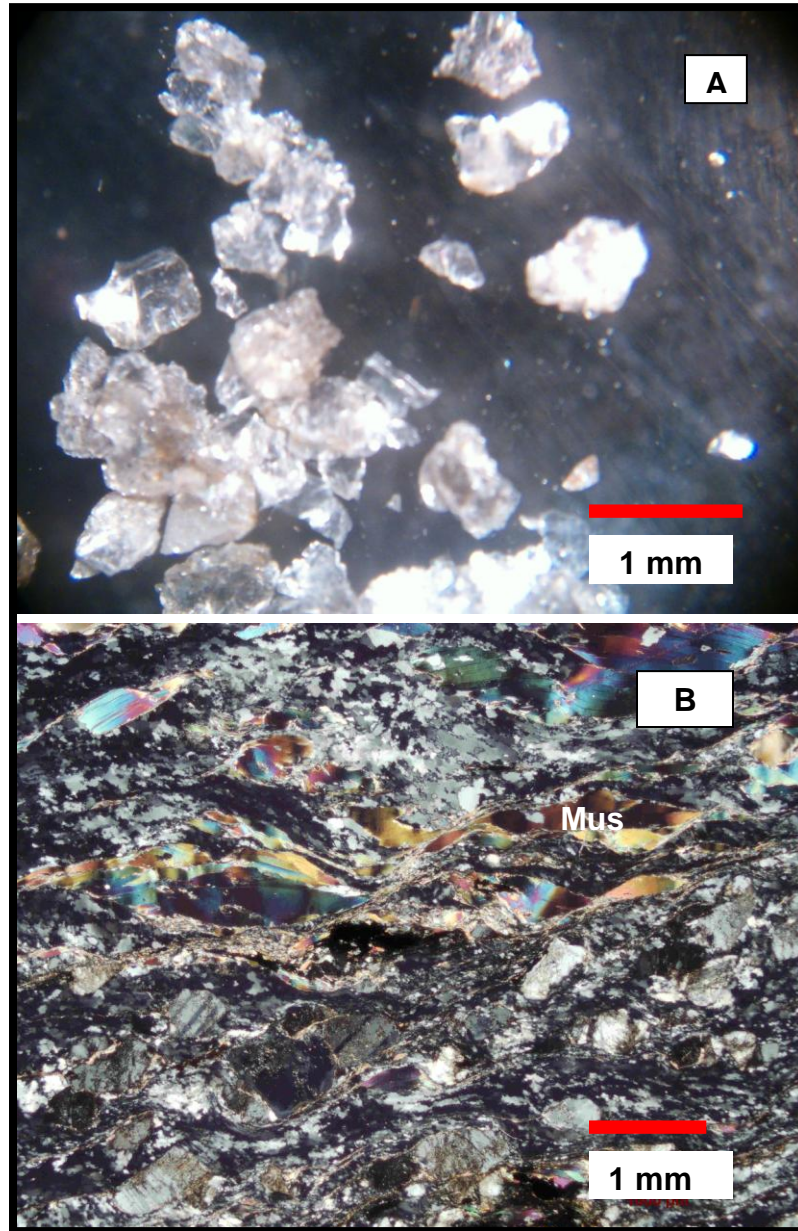


Figure 19. DRB-06-22 quartzofeldspathic gneiss with coarse-grained muscovite (0.5-1.0 mm diameter grains). **A.** Binocular photograph of muscovite grains used for $^{40}\text{Ar}/^{39}\text{Ar}$ analysis. **B.** Photomicrograph (XPL) of muscovite fish. Mus = muscovite.

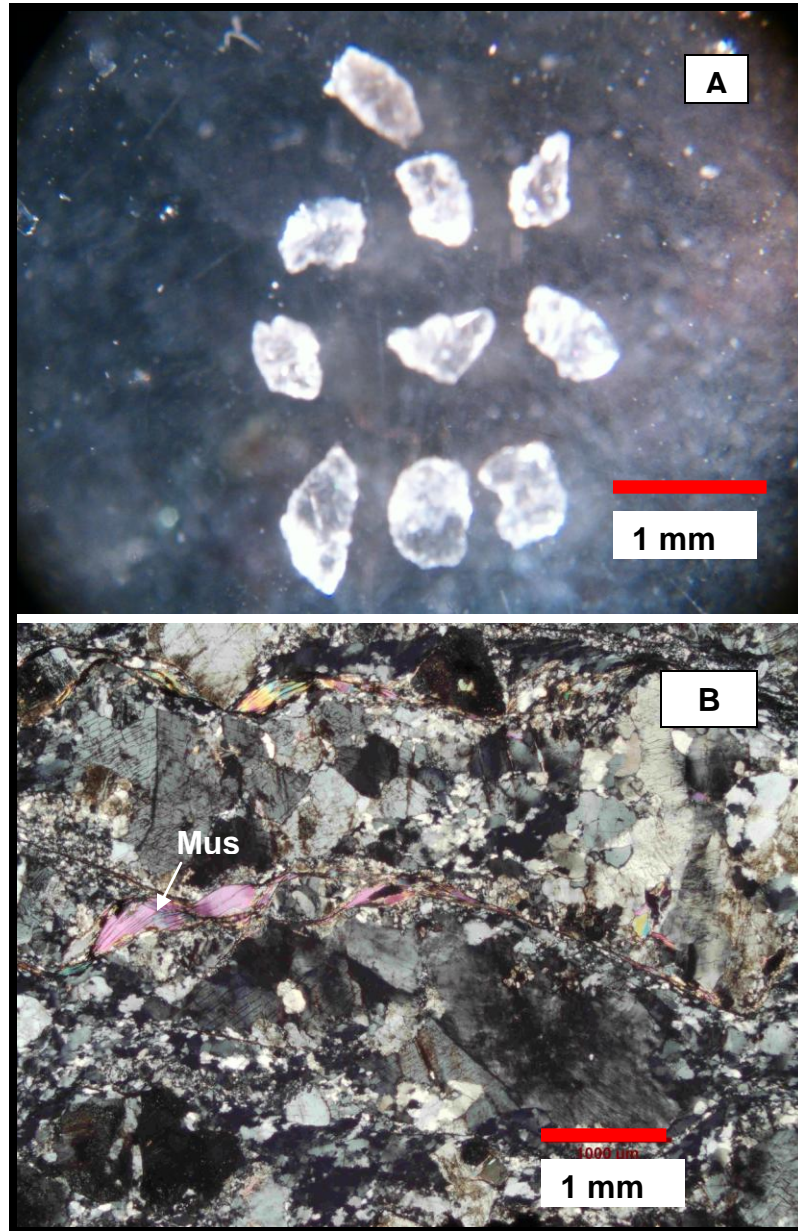


Figure 20. JWB-06-CP73 quartzofeldspathic mylonite in Gubbedalen Shear Zone fault (0.5-1.0 mm diameter grains). **A.** Binocular photograph of muscovite grains used for $^{40}\text{Ar}/^{39}\text{Ar}$ analysis. **B.** Photomicrograph (XPL) of muscovite fish. Mus = muscovite.

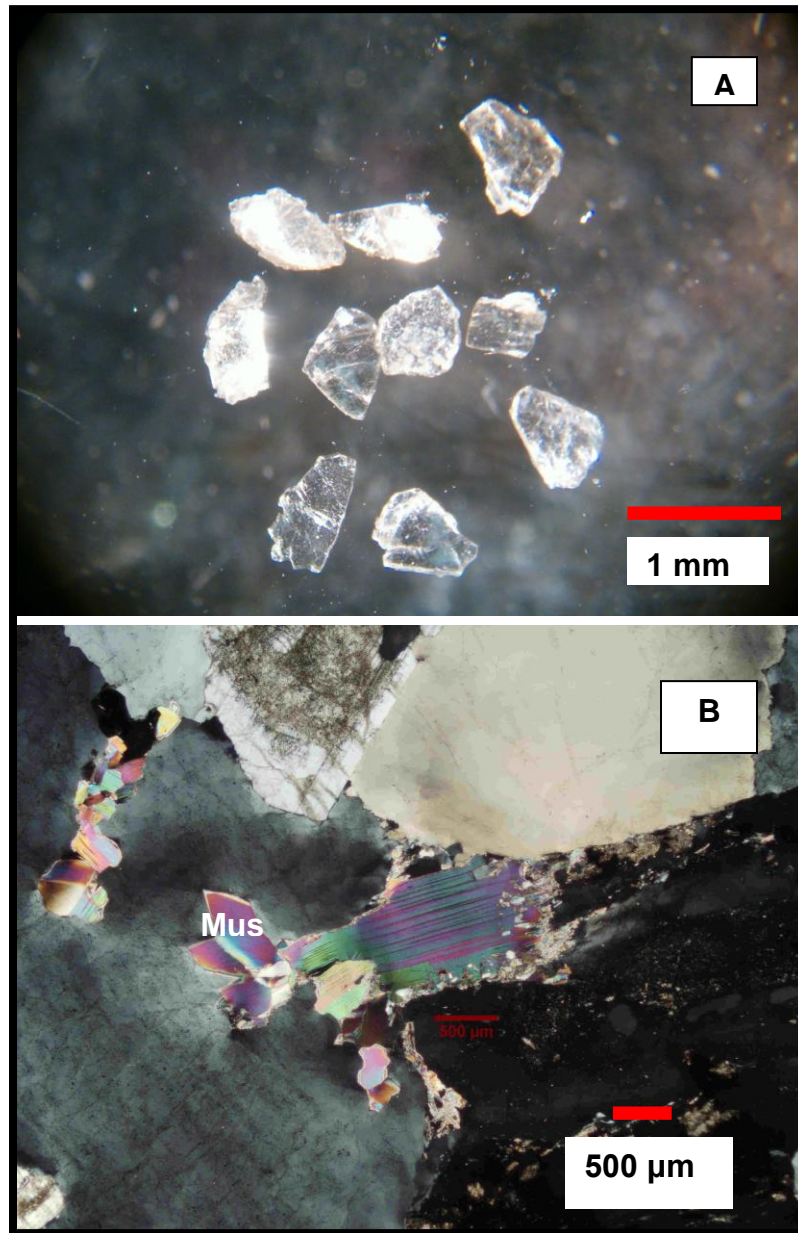


Figure 21. JWB-06-M28A center of pegmatite, felsic intrusion in Krummedal Sequence (0.5-1.0 mm diameter grains). **A.** Binocular photograph of muscovite grains used for $^{40}\text{Ar}/^{39}\text{Ar}$ analysis. **B.** Photomicrograph (XPL) of muscovite. Mus = muscovite.

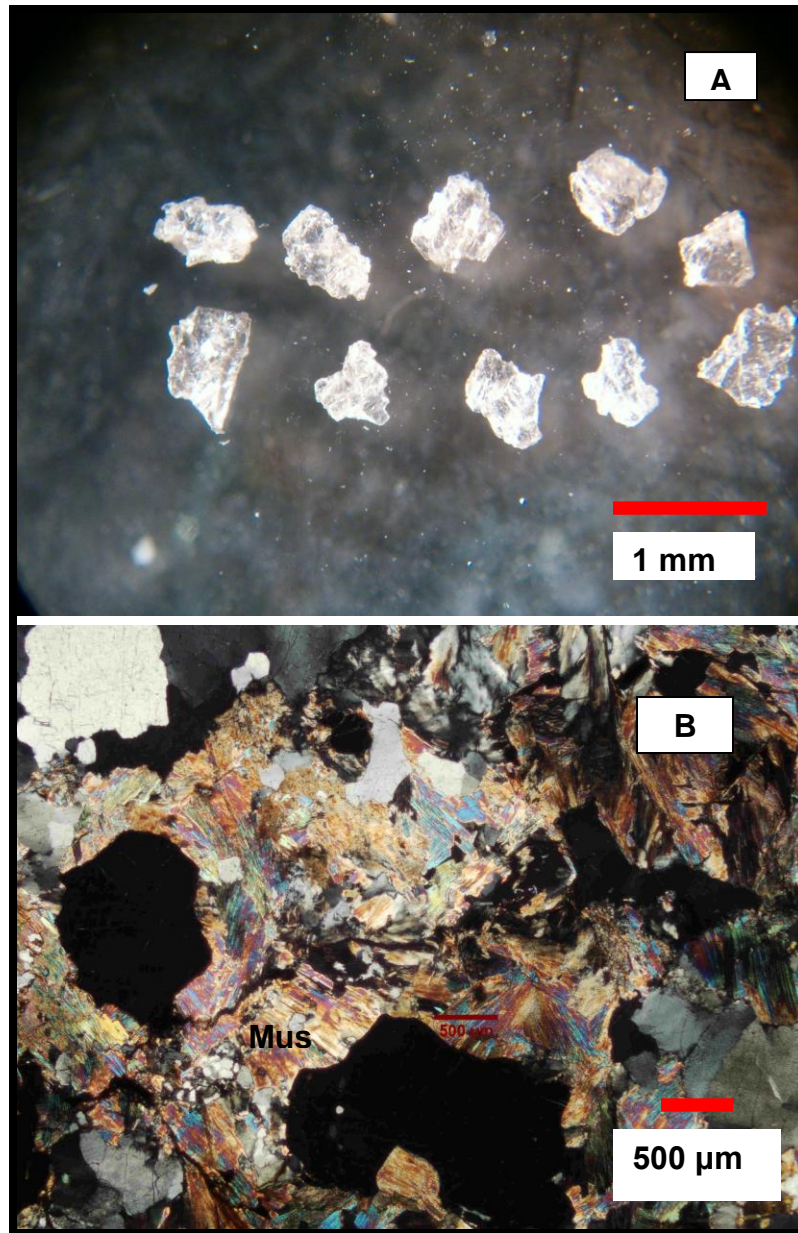


Figure 22. JWB-06-M28C paragneiss in Krummedal Sequence calc-silicate (0.5-1.0 mm diameter grains). **A.** Binocular photograph of muscovite grains used for $^{40}\text{Ar}/^{39}\text{Ar}$ analysis. **B.** Photomicrograph (XPL) of clusters of muscovite. Mus = muscovite.

discrimination and mass spectrometer sensitivity were measured by running air and blank samples every ten and five samples, respectively. Analyses comprise 10 cycles of measurement over the range of masses and half-masses from $m/e = 40$ to $m/e = 35.5$, and baseline corrected values are extrapolated to the time of inlet, or averaged, depending upon signal evolution. Hornblende and biotite were not analyzed from these samples. Petrography showed uralitization of pyroxene, replacement of pyroxene by biotite, and biotite altered to chlorite/chloritoid minerals (see Lithologies). Potassium feldspar was not analyzed due to ANIMAL capabilities.

The ANIMAL facility is equipped with an ultra-high vacuum, 90-degree sector, 10 cm radius spectrometer. The spectrometer employs second-order focusing (Cross, 1951), and is fitted with a high sensitivity electron-impact source and a single ETP electron multiplier (with signal amplification through a standard pre-amplifier). Analyses are typically made using a filament current of 2.75 A, and potentials for the source and multiplier of 2000 V and -1300 V, respectively. Measurement of atmospheric argon passed through an air pipette monitored sensitivity and mass discrimination. Sensitivity was measured at 8.09×10^{-15} moles/volt and mass discrimination at 0.21% for 298 ± 2 $^{40}\text{Ar}/^{36}\text{Ar}$ during analyses. The high sensitivity and low blank of the instrument permits measurement of 10^{-14} mole samples to within 0.2% precision.

Sample Descriptions

Six samples containing muscovite were collected from five locations around the Gubbedalen Shear Zone (Fig. 5); latitude and longitude coordinates for each sample are reported in Appendix A. Each sample contained muscovite visible in hand sample: DRB-06-16, DRB-06-22, JWB-06-CP73, JWB-06-M28A, JWB-06-M28B, and JWB-06-

M28C. Muscovite grains are described below. For further descriptions of rock unit, see the previous section on Lithologies.

Sample DRB-06-16 contains the finest grained muscovite (0.25 mm) in footwall quartzofeldspathic gneiss (Fig. 18A). Muscovite (<1% in gneiss) is subhedral with few inclusions of opaque minerals. Well defined cleavage planes are observable in thin section and third-order green to pink color birefringence (Fig. 18B). Grains are dispersed among recrystallized quartz defining a weak foliation with very little to no internal grain deformation.

The second footwall quartzofeldspathic gneiss sample, DRB-06-22, contains 5% muscovite. Kinked and sheared medium-grained muscovites (0.5-1.0 mm) occur as fish in a well defined S-C fabric with undulose extinction across the grains (Fig. 19).

Birefringence is second-order yellow to purple color.

In the extensional part of the Gubbedalen Shear Zone, mylonitized quartzofeldspathic gneiss, JWB-06-CP73, contains medium-grained muscovite (2% in mylonite; 0.5-1.0 mm) displaying third-order pink birefringence color (Fig. 20). Muscovite fish define weak S-C fabric with undulose extinction indicating deformation and shearing (Fig. 20B). Grains between C-planes are larger whereas smaller grains are between S-planes.

A pegmatite intruding the Krummedal Sequence of the hanging wall (samples JWB-06-M28A and JWB-06-M28B) contains 7% medium-grained muscovite (0.5-1.0 mm; Fig. 21A). M28A and M28 B are from the center and edge of the pegmatite, respectively. Muscovite occurs as euhedral grains with slight undulose extinction indicating a low degree of internal strain with second-order green to third-order pink

birefringence color. Well defined cleavage planes are observable in thin section (Fig. 21B).

Hanging wall sample JWB-06-M28C occurs in a felsic-rich layer of the Krummedal Sequence calc-silicate containing 7% medium-grained muscovite (0.5-1.0 mm; Fig. 22A). Muscovite occurs as clusters of subhedral to acicular grains with no strain indicators (Fig. 22B). Cleavage planes are recognized in thin section with third-order green to pink birefringence color.

Results

$^{40}\text{Ar}/^{39}\text{Ar}$ isotopes for muscovite were measured for samples from various structural levels of the Gubbedalen Shear Zone (Fig. 23). The age results, brief sample descriptions, and fault locations are summarized in Figure 24. Complete analytical results are reported in Appendix A for both single crystal total fusion and incremental heating ages. Results are discussed from youngest to oldest for each method.

Ten to nine grains from each sample were analyzed using single crystal total fusion. This method was used to determine an unbiased spread of intercrystalline ages of each sample. Incremental heating tends to yield an average age for a crystal, or population of crystals (Hodges et al., 1993). For each sample, age population distributions were constructed for 1σ at 95% confidence level and error-weighted average ages were calculated to interpret the data (Fig. 25). Samples DRB-06-16 (376.1 ± 2.0 Ma), DRB-06-22 (380.7 ± 1.4 Ma), JWB-06-M28B (387.40 ± 1.2 Ma), and JWB-06-M28C (380.2 ± 1.6 Ma) are normally distributed. Single-crystal age distributions of samples JWB-06-CP73 and JWB-06-M28A are more complex. For normally distributed data, standard errors range from ± 0.46 Ma to ± 1.24 Ma. Complex distribution standard



Figure 23. Panoramic view of Gubbedalen shear zone looking east. $^{40}\text{Ar}/^{39}\text{Ar}$ ages reflect incremental heating plateau ages or error-weighted average ages. Hanging wall ages (391, 386, and 381 Ma) are projected. Footwall ages are approximate location of samples.

Sample	Sample Description (Location near Fault)	SCTF		Incremental Heating Plateau Age (Ma)
		Wt. Avg. Age (Ma)		
DRB-06-16	Fine-grained orthogneiss (footwall)	376.1 ± 2.0		None performed
DRB-06-22	Schistose orthogneiss (footwall)	380.7 ± 1.4		378.5 ± 0.63
JWB-06-CP73	Orthogneiss mylonite in shear zone (fault)	378.5 ± 0.86		379.8 ± 0.37
JWB-06-M28A	Center of felsic pegmatite (hanging wall)	386.5 ± 1.5		391.2 ± 0.54
JWB-06-M28B	Outer edge of felsic pegmatite (hanging wall)	387 ± 1.2		Total gas age: 385.7
JWB-06-M28C	Paragneiss surrounding pegmatite (hanging wall)	380.2 ± 1.6		381.3 ± 0.41

Figure 24. Sample descriptions with fault locations and age results reporting 1σ at the 95% confidence level. Single crystal total fusion (SCTF); error-weighted on averaged ages (wt. avg.).

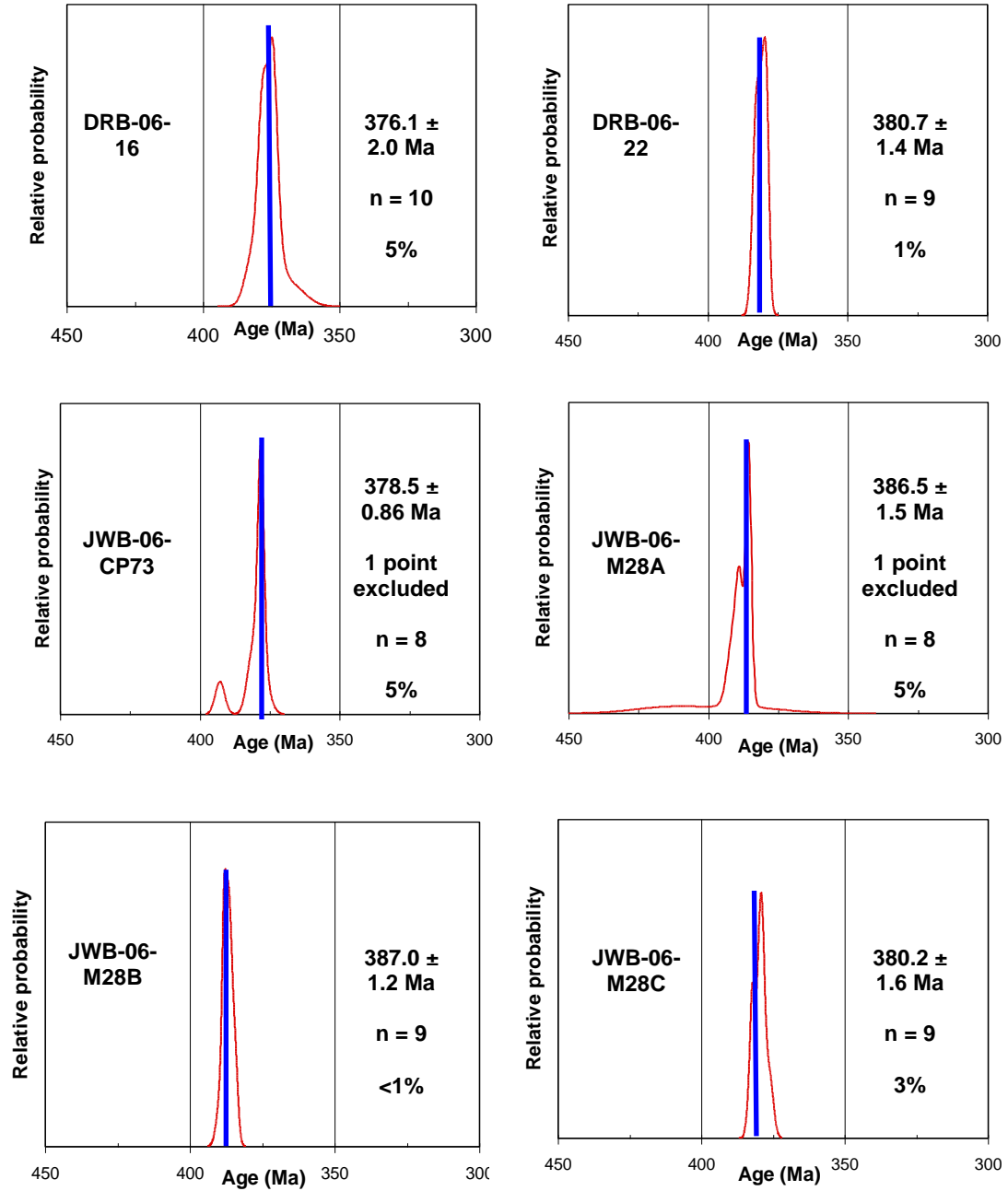


Figure 25. Age population distributions among single crystal total fusion analyses for 1σ at 95% confidence level. Weighted average age is displayed. Thick blue line represents the mean. n = number of samples. % = probability of normal distribution.

errors are greater than normally distributed data, ± 1.64 Ma to ± 3.01 Ma. Samples JWB-06-CP73 and JWB-06-M28A average ages were calculated using eight of nine grains analyzed. Both samples display one outlying data point, therefore, these points were excluded from calculations. These points may signify resetting of muscovite cooling.

One grain from each sample, except DRB-06-16, was incrementally heated. Inverse isochron plots were constructed to determine the amount of, if any, extraneous argon had affected potential plateau ages (Fig. 26). Radiogenic yields for incremental heating analyses varied between 236 ± 370 to 345 ± 81 with the resulting $^{36}\text{Ar}/^{40}\text{Ar}$ fraction less than 0.001 and $^{39}\text{Ar}/^{40}\text{Ar}$ fraction less than 0.06. These low values indicate no extraneous argon will affect plateau spectra age calculations (Fig. 27).

Plateau ages from incrementally heated grains are plotted in Figure 27 with 1σ error estimates. Sample DRB-06-22, from quartzofeldspathic gneiss in the footwall, has a plateau age of 378.50 ± 0.63 Ma and includes 90.5% of ^{39}Ar . Sample JWB-06-CP73, from mylonitized gneiss near the base of the Gubbedalen Shear Zone, has a concordant spectrum. The plateau age is 379.78 ± 0.37 Ma and includes $\sim 100\%$ of ^{39}Ar . Sample JWB-06-M28C, from hanging wall calc-silicate, has an increasing release spectrum as temperature increases. The plateau age is 381.26 ± 0.41 Ma and includes 68.2% of ^{39}Ar . Younger ages over the first $\sim 25\%$ of ^{39}Ar release may reflect diffusive loss of ^{40}Ar upon cooling. Two samples were collected from a pegmatite in the hanging wall. Sample JWB-06-M28A, from the center of the pegmatite, displays no trend in the release spectrum. The plateau age is 391.23 ± 0.54 Ma and includes 67.3% of ^{39}Ar . Sample JWB-06-M28B, from the edge of the pegmatite, yields a discordant release spectrum with a total gas age of 385.7 Ma.

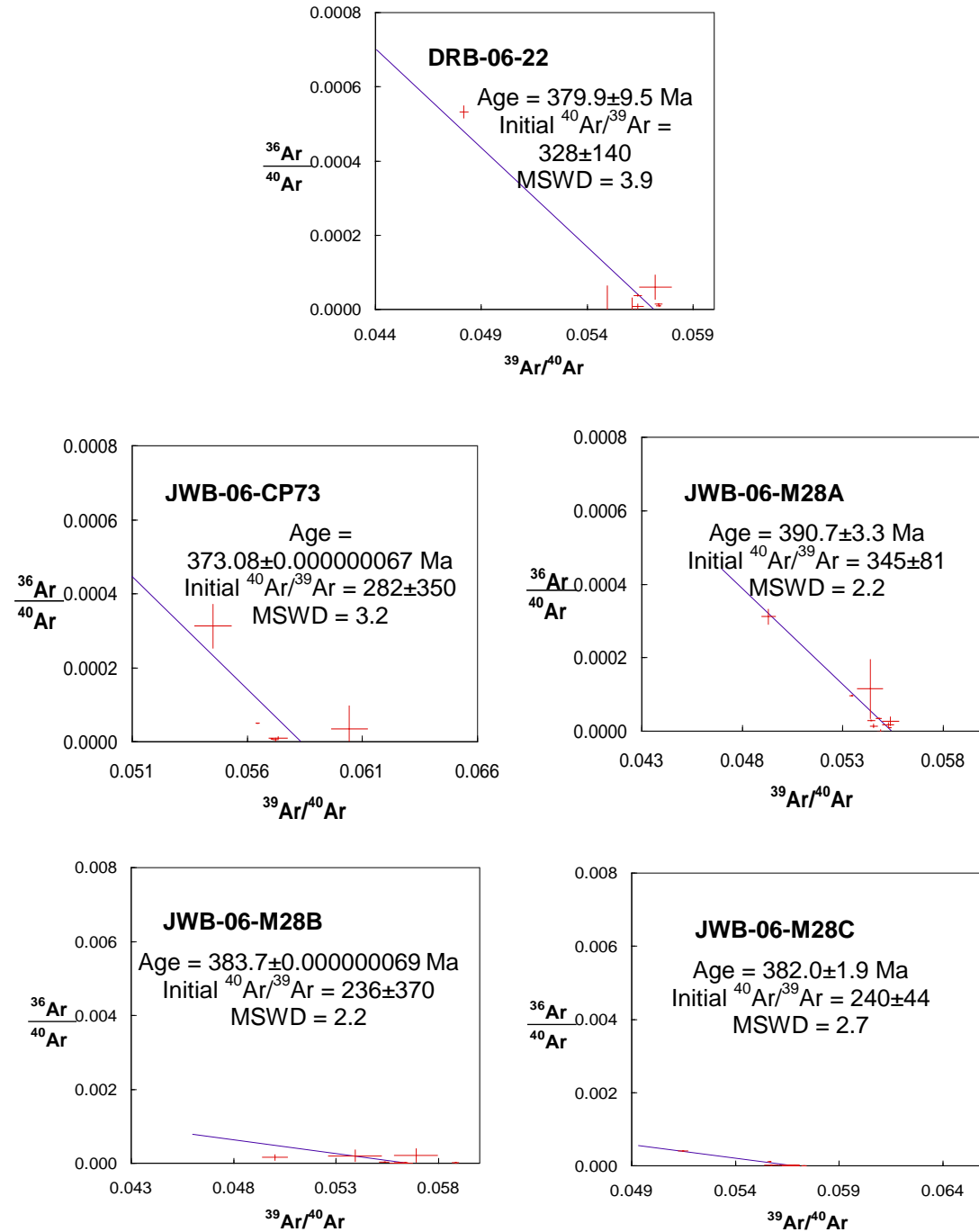


Figure 26. Inverse isochron plots for incrementally heated samples. Axes are $^{36}\text{Ar}/^{40}\text{Ar}$ vs. $^{39}\text{Ar}/^{40}\text{Ar}$. Regression results are calculated using the y-intercept for the trapped argon $^{40}\text{Ar}/^{36}\text{Ar}$. Error crosses are 1σ .

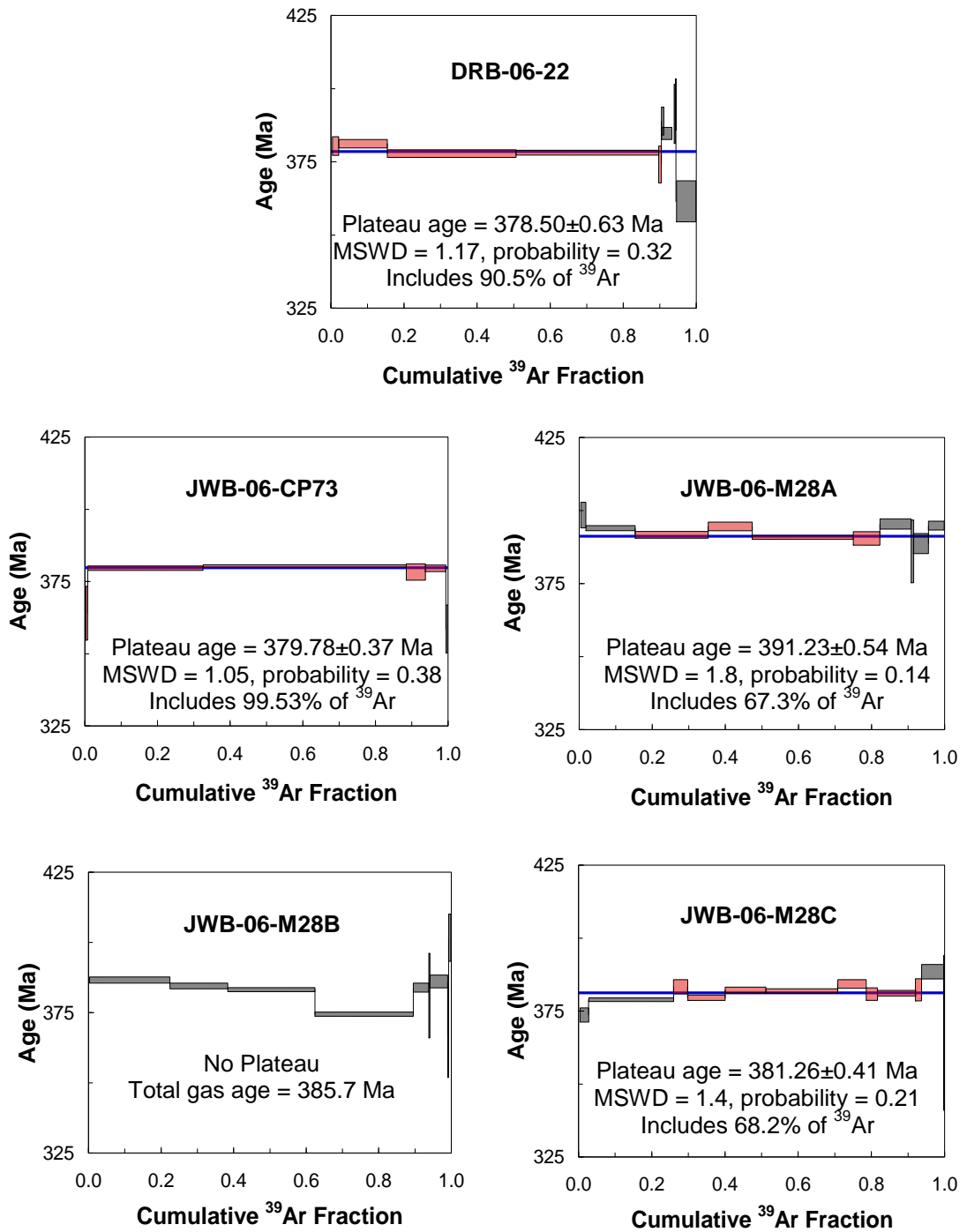


Figure 27. Age spectra for incrementally heated samples. Red boxes are plateau steps and black boxes are rejected steps. Error estimates are 1σ .

⁴⁰Ar/³⁹Ar Discussion and Conclusions

The ⁴⁰Ar/³⁹Ar single crystal total fusion and incremental heating techniques yield similar ages. The incrementally heated analyses of single crystals yield ages within the ranges of the age populations from the single crystal total fusion analyses. This indicates incrementally heated samples are biased measurements not representative of a regional cooling trend. However, incrementally heated ages represent the cooling trend across an individual grain within the single crystal total fusion age populations. Therefore, age populations more accurately represent regional trends, whereas plateau ages represent argon behavior within one grain of each age population.

Figure 28 shows an approximate time progression of the region along the Gubbedalen Shear Zone of eclogitization at 395 Ma and its exhumation to the ~350°C isotherm at Devonian sedimentation (376 Ma;). Sample JWB-06-CP73, from along the fault, has a single crystal total fusion average age at 378.5 ± 0.86 Ma constraining the latest contractional movement. Samples from the footwall, DRB-06-16 and DRB-06-22, are within the range of the respective fault single crystal total fusion age distribution, 376.1 ± 2.0 Ma and 380.7 ± 1.4 Ma, respectively. The hanging wall paragneiss, JWB-06-M28C, also has similar ages to the footwall within the range of those respective single crystal total fusion age distributions, 380.2 ± 1.6 Ma. Younger footwall and older hanging wall ages are consistent with field evidence for late-stage normal movement along the Gubbedalen Shear Zone. Muscovite cooling along the fault suggests hanging wall movement was concurrent with footwall emplacement. Pegmatite ages from the hanging wall lie within the age distribution range of JWB-06-M28A and JWB-06-M28B.

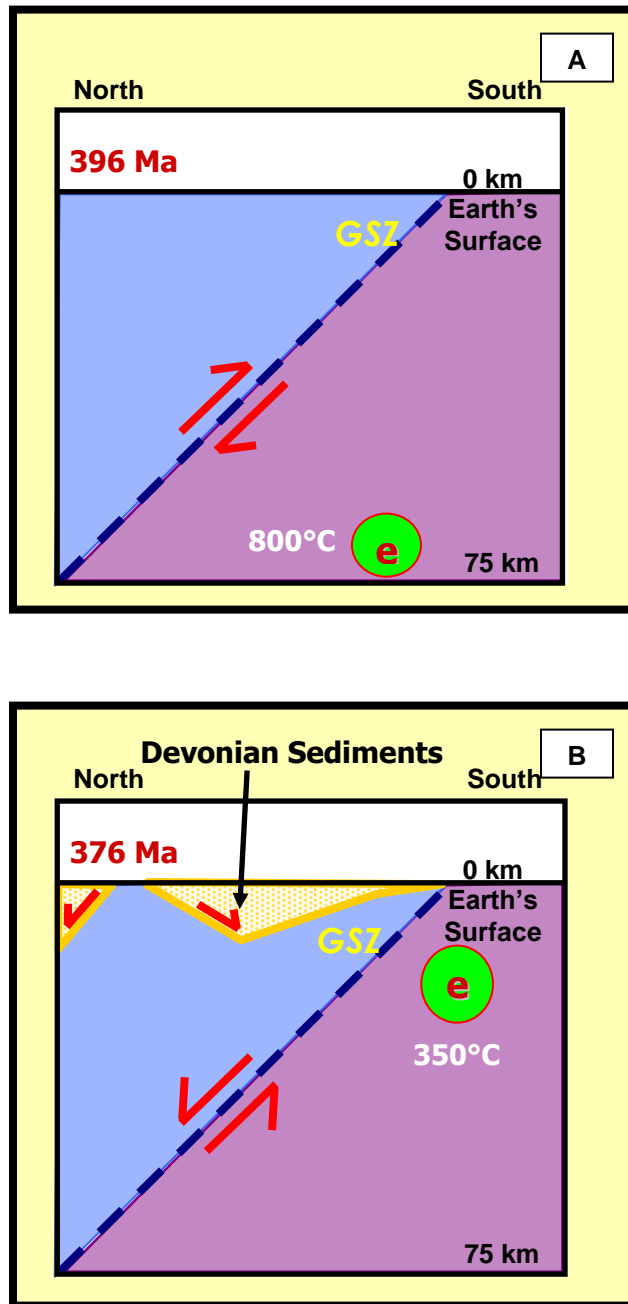


Figure 28. Cartoon illustrations of **A.** Early Devonian eclogite-facies metamorphism. **B.** Exhumation of the eclogites through the 350°C muscovite isotherm in the Middle Devonian. Blue is hanging wall block and purple is footwall block. Red “e” in green circle represents eclogitized rocks. GSZ = Gubbedalen Shear Zone.

Sample JWB-06-M28A, center of pegmatite, has an age of 386.5 ± 1.5 Ma and JWB-06-M28B, edge of pegmatite, has an age of 387.0 ± 1.2 Ma, similar to the age distribution of JWB-06-M28A. Muscovites from the pegmatite ages are older than those from surrounding country rock (JWB-06-M28C; 380.2 ± 1.6 Ma). Footwall quartzofeldspathic gneiss is cut by pegmatites and granitic dikes with U/Pb zircon crystallization ages of 388 Ma and 386 Ma, respectively (Augland, 2007). These ages are similar to the muscovite cooling ages of the hanging wall pegmatite; JWB-06-M28A and JWB-06-M28B (386.5 ± 1.5 Ma and 387.0 ± 1.2 Ma, respectively).

In summary, oldest $^{40}\text{Ar}/^{39}\text{Ar}$ age distribution at ca. 388 Ma are related to pegmatite cooling. Youngest $^{40}\text{Ar}/^{39}\text{Ar}$ age distribution at ca. 380 Ma reflects cooling near the Gubbedalen Shear Zone. Combined with field and structural observations, the $^{40}\text{Ar}/^{39}\text{Ar}$ ages indicate that the Gubbedalen Shear Zone was active during pegmatite cooling and footwall exhumation. In addition, zircon and rutile U/Pb ages in eclogites are 400 Ma and 371 Ma, respectively (Augland, 2007), indicating eclogites were cooling during fault movement, 380 Ma, and pegmatite cooling at 388 Ma. Rutile cooling is younger than the youngest muscovite cooling age (378.50 ± 0.63 Ma; DRB-06-16) in the footwall. The Gubbedalen Shear Zone thus records thermochronological eclogite exhumation from at least 388 Ma to 372 Ma.

V. DISCUSSION

In this discussion, a temperature-*time* path for Liverpool Land will first be developed, based on analytical results in the previous section. This temperature-*time* path will then be compared to paths reported for eclogites within other continental basement terranes in the Caledonides, the Western Gneiss Region, Bergen Arcs, and Lofoten, Norway, and the North-East Greenland eclogite province (NEGEP). The rationale for such a comparison is to explore for any trends that might explain how eclogite formation and exhumation in Liverpool Land relates to those along the length of the Caledonian orogen, a main objective of this thesis.

Rocks in the hanging wall block to the Gubbedalen Shear Zone are lithologically correlated to the Krummedal Sequence in more northern parts of the East Greenland Caledonides. The age of amphibolite-facies metamorphism in the Krummedal is argued from place to place to be either Neoproterozoic (900-950 Ma) and related to the Grenville orogeny (Strachen et al., 1995; Leslie and Higgins, 1999; and Henriksen et al., 2003) or Siluro-Devonian related to the Scandian phase of the Caledonian orogeny (Andresen et al., 1998, 2007; White et al., 2002). No dates are reported for this event in Krummedal rocks of the present study area. During the Caledonian, the Hurry Inlet Granite intruded in two phases, one at 445 and another at 438 Ma (Augland, 2007). A later monzodiorite pluton intruded the Krummedal at 424 Ma (Augland, 2007).

Plutonic activity at this time is widespread throughout the East Greenland Caledonides and is interpreted as the result of continental arc volcanism and plutonism during Iapetus oceanic crust subduction (Fig. 3; Haller, 1985; Gilotti and McClelland, 2005). Earliest $^{40}\text{Ar}/^{39}\text{Ar}$ cooling ages reported herein for the hanging wall are interpreted to date protracted, slow cooling following plutonism at 424 Ma to $\sim 350^\circ\text{C}$ at 381 Ma.

The footwall block to the Gubbedalen Shear Zone contains a much younger and more extreme metamorphic history than does the hanging wall block. Eclogitization at >18 kbar and 850°C (Buchanan, 2008) requires residency of these continental basement units in the lower crust (~ 75 km deep) at 395 Ma, 30 m.y. after the amphibolite-facies peak of metamorphism in the hanging wall block. In contrast to slow, prolonged cooling documented in the hanging wall block, the footwall block cooled relatively rapidly from 850°C to 350°C between 395 Ma and ~ 378 Ma, only 17 m.y.

Field observations from the Gubbedalen Shear Zone indicate it to be a tops-south thrust fault that was reactivated as a tops-north normal fault with two pulses of movement, one at 385 Ma and the latest at 378 Ma (see Buchanan, 2008 for structural data). Rheologies of the fault rocks range from mylonite ($>\sim 500^\circ\text{C}$, crystal-plastic feldspar) to breccia ($\sim 100^\circ\text{C}$, crystal-brittle quartz), documenting progressive temperature decrease as this crustal-scale shear zone was exhumed to higher crustal levels.

Amount of movement along the Gubbedalen Shear Zone is not known but exhumation and cooling rates provide some constraints to the vertical throw along it. Using footwall eclogite minimum pressure and temperature estimates (>18 kbar [~ 75 km] and 850°C ; Buchanan, 2008) together with a U/Pb zircon date on eclogitization (Augland, 2007) and $^{40}\text{Ar}/^{39}\text{Ar}$ muscovite cooling ages (reported herein; $\sim 350^\circ\text{C}$),

cooling of the footwall block occurred from 400 Ma to 376 Ma (24 m.y.) at a rate of 23°C/m.y. and an exhumation rate of >0.75 kbar/m.y. This indicates the eclogite-bearing footwall block of the Gubbedalen Shear Zone was rapidly exhumed from depths of ~ 75 km to the 350°C isotherm (~11.7 km depth conservatively using a 'standard' 30°C/km geotherm) over 24 m.y.

This thesis has new data bearing on the hypothesis of Hartz et al. (2005) that tectonic overpressures were responsible for producing eclogites in the overriding plate (i.e. Laurentian-East Greenland) of the Caledonian A-type subduction zone boundary. Hartz et al. (2005) hypothesized that during Early Devonian deep-continental subduction of Baltica, Liverpool Land collided with the Western Gneiss Region. An Early Devonian palinspastic reconstruction would make Liverpool Land the western half of a transect containing the Western Gneiss Region to the east. Data in the study of Buchanan (2008) indicate HP metamorphic conditions at >18 kbar and 850°C instead of UHP metamorphism in Liverpool Land i in the abstract by Hartz et al. (2005). During the Early Devonian collision, the Western Gneiss Region was experiencing UHP metamorphism at depths of ~120 km (~35 kbar) while Liverpool Land was under HP conditions at substantially shallower depths of ~75 km.

In the absence of fluids, tectonic overpressures might locally be achieved in resilient, anhydrous granulite-facies rocks, perhaps enough to produce local volumes of eclogitization. Unusual occurrences of localized hydrous eclogite restricted to discrete shear zones and pseudotachylite veins in otherwise anhydrous granulites in the Bergen Arcs (Austerheim, 1987) and Lofoten (Steltenpohl et al., 2006), Norway, attest to the resiliency and strength of the lower-continental crust during the Caledonian collision.

Such a mechanism is unlikely in Liverpool Land, however, because these amphibolite-facies, quartzofeldspathic gneisses clearly are hydrated and flowed plastically around extended (i.e., not contracted) boudins of eclogite. Augland (2007) describes garnet and orthopyroxene veins, interpreted as decompressional melts related to exhumation immediately following eclogitization, but there are no granulite-facies host gneisses in Liverpool Land. Furthermore, there are no eclogite-facies pseudotachylytes or eclogite shear zones in Liverpool Land that might suggest unusual conditions for eclogitization; rather, they are typical eclogite pods within felsic gneisses that look identical to those of the Western Gneiss Region. The present author, therefore, suggests that something other than tectonic overpressures were responsible for forming the Liverpool Land eclogites.

Fundamental to Hartz et al.'s (2005) hypothesis for tectonic overpressures is that both Liverpool Land and the Western Gneiss Region eclogites formed at the same time, ~395 Ma, while the former rocks resided in the upper plate to the continental subduction zone boundary directly above the latter. Various palinspastic restorations published for the collision during the Early Devonian, however, are quite varied (e.g. Ziegler, 1988; MacNiocaill and Smethrust, 1994; Hartz et al., 1997; Roberts, 2002). These differences result primarily from Late-Devonian to Carboniferous movements along major strike-slip faults in East Greenland, West Norway, and throughout the United Kingdom that have shuffled the terranes leaving their original palinspastic relations suspect (Roberts, 1983; Hutton, 1987; Hutton and McErlean, 1991).

If Liverpool Land eclogites developed above and proximal to those of the Western Gneiss terrane, then either a pattern or a common point of divergence in their respective temperature-*time* paths would be seen. With this in mind, Figure 29 was

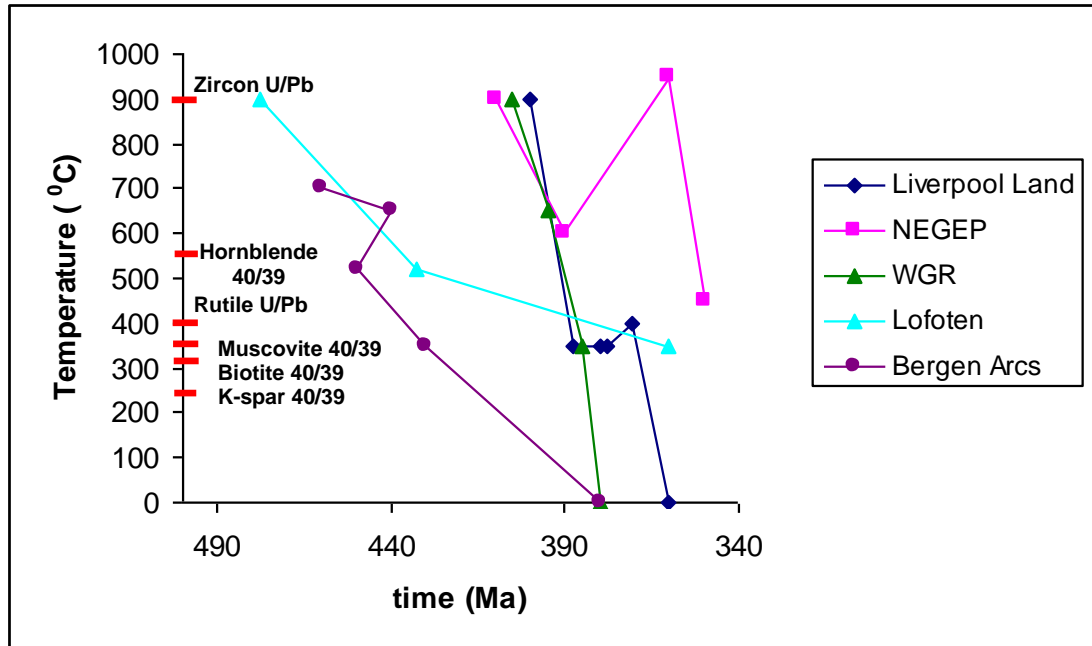


Figure 29. Temperature-time diagram comparing Liverpool Land and North-East Greenland eclogite province (NEGEP), East Greenland, with Western Gneiss Region (WGR), Lofoten, and Bergen Arcs, Norway (Strachan and tribe, 1994; Gilotti and Ragna, 2002; White and Hodges, 2003; Gilotti et al., 2004; McClelland et al., 2005; Hacker, 2007; Kassos, 2008). Red lines indicate closure temperature of corresponding minerals (Dodson, 1973; Boundy et al., 1997; von Blackenburg et al., 1989; Lee et al., 1997; Schmitz and Bowring, 2003). 0°C temperature data are Devonian basin formation (Siedlecka, 1975; Boundy et al., 1997; White et al., 2002). K-spar = potassium feldspar, 40/39 = $^{40}\text{Ar}/^{39}\text{Ar}$ age dating, U/Pb = U/Pb age dating.

compiled from information published for eclogite terranes on both sides of the orogen, including the data reported herein. The Lofoten and the Bergen Arc paths are the oldest and they indicate a long, protracted metamorphic cooling history unlike any of the other eclogite provinces. These differences further strengthen the argument made above that Liverpool Land eclogites are not unusual, unlike those exposed in Lofoten and the Bergen Arcs. Thus, a more reasonable approach toward explaining the Liverpool Land eclogites, rather than tectonic overpressures, is proposed below.

Comparison of the Liverpool Land, Western Gneiss Region, and NEGEP temperature-*time* paths in Figure 29 illustrates some intriguing patterns. The older (~400 - 390 Ma), higher-temperature parts of these paths nearly overlap for the temperature interval between 900°C and 600°C. Continuing toward younger ages, the path for the NEGEP sharply diverges from the Liverpool Land and Western Gneiss Region paths, the former taking a reheating path that peaked again at UHP conditions ~360 Ma. To explain this second pulse of UHP eclogitization in the NEGEP, Gilotti and McClelland (2007) argued for foreland-directed imbrication of the Laurentian plate to form a new, subsidiary A-type subduction zone (Laurentia beneath the previously eclogitized Laurentian fragment).

In contrast to the NEGEP, the Western Gneiss Region temperature-*time* path continues to trace the same path as Liverpool Land down to the 350°C blocking temperature of muscovite (Fig. 29). At this time, about 380 Ma, the Liverpool Land path diverges from that of the Western Gneiss Region, flattening out for a ~10 m.y. interval before climbing in temperature an estimated 100°C at ~370 Ma (rutile dates reported by Augland, 2007). The correspondence in time of this trough in the Liverpool Land path to

the more dramatic one documented for the NEGEP is unexpected and not yet understood. It should be further explored, however, as it could be related to tectonic processes/events between the two areas today separated by nearly 800 km.

Following about 380 Ma, the Western Gneiss Region was rapidly brought to the Earth's surface (0°C in Figure 29) where it was soon buried beneath Devonian sediments. Likewise, Liverpool Land followed a similarly steep temperature-*time* path, though delayed by ~10 m.y., to be buried by even younger Devonian sediments. Divergence of the two paths at ~380 Ma might indicate that the Western Gneiss Region experienced crustal-scale extensional faulting (Andersen and Jamtveit, 1990; Hacker, 2007) and was exhumed to Earth's surface while Liverpool Land remained at mid- to upper-crustal depths (near the 350°C isotherm) for another 10 m.y.

The fact that the Western Gneiss Region temperature-*time* path overlaps the one for Liverpool Land from eclogite-facies peak temperatures to the ~350°C isotherm lends support to Hartz et al.'s (2005) suggested palinspastic juxtaposition of the two terranes in the early Devonian (~395 Ma). Ultra-high pressure metamorphism recorded in rocks of the Western Gneiss Region indicate a cooling rate of >60°C/m.y. and an exhumation rate of 1.0 kbar/m.y. (Hacker, 2007) comparable to Liverpool Land rates; though Hacker (2007) suggested that this cooling rate for the Western Gneiss Region might be exaggerated, an artifact of the structural imbrication of hot UHP rocks against colder HP rocks. Numerous other similarities exist between the Liverpool Land and Western Gneiss Region eclogite provinces. Quartzofeldspathic continental basement gneisses and migmatites host pods of eclogite. Recent work by Augland (2007) and Augland et al. (2007) indicate that the host gneisses not only have similar crystallization ages, ~1.6 Ma

to 1.65 Ma, but contain xenocrystic zircon populations that overlap (Augland et al., 2007). High-pressure mafic and ultramafic veins/pods occur within the quartzofeldspathic gneissic hosts in both terranes (Dobrzhinetskaya et al., 1995, Root et al., 2004). The small data set of $^{40}\text{Ar}/^{39}\text{Ar}$ muscovite cooling ages for Liverpool Land reported herein suggest a cooling pattern of roughly east-west striking isochronal surfaces that parallel the Gubbedalen Shear Zone, perpendicular to east coastline, and youngs from 388 Ma to 379 Ma toward the south (Fig. 23). However, Western Gneiss Region $^{40}\text{Ar}/^{39}\text{Ar}$ muscovite cooling trends roughly parallel the west coastline of Norway and range from 400 to 385 Ma younging toward the west (Fossen and Dunlap, 1998). All these similarities may indicate that Liverpool Land is an ‘orphaned’ block of the Western Gneiss Region sutured onto Laurentia (Augland, 2007; Augland et al., 2007).

Alternatively, recent numerical modeling of a subduction zone channel for a continent-ocean convergent margin by Gerya and Stöckhert (2006) might also explain integration of HP and UHP rocks as is indicated in the case of Liverpool Land and the Western Gneiss Region. Their study evaluated different crustal conditions, subduction rates, and hydration to model P-T paths. Consequently, they calculated exhumation rates and modeled intermingling of sediments, continental crust, oceanic crust, and mantle. From their models, (U)HP rocks can be emplaced in the continental crust by subducting oceanic crust that intermingles with the overriding continental crust (Fig. 30). According to their simulations, continental crust can be subducted at the leading edge of an overriding plate and incorporated into the orogenic wedge. The wedge is carried deeper into the subduction channel to about 50-70 km but minor amounts may reach 100 km deep. Oceanic and continental crust intermingles creating a “marble cake” in the

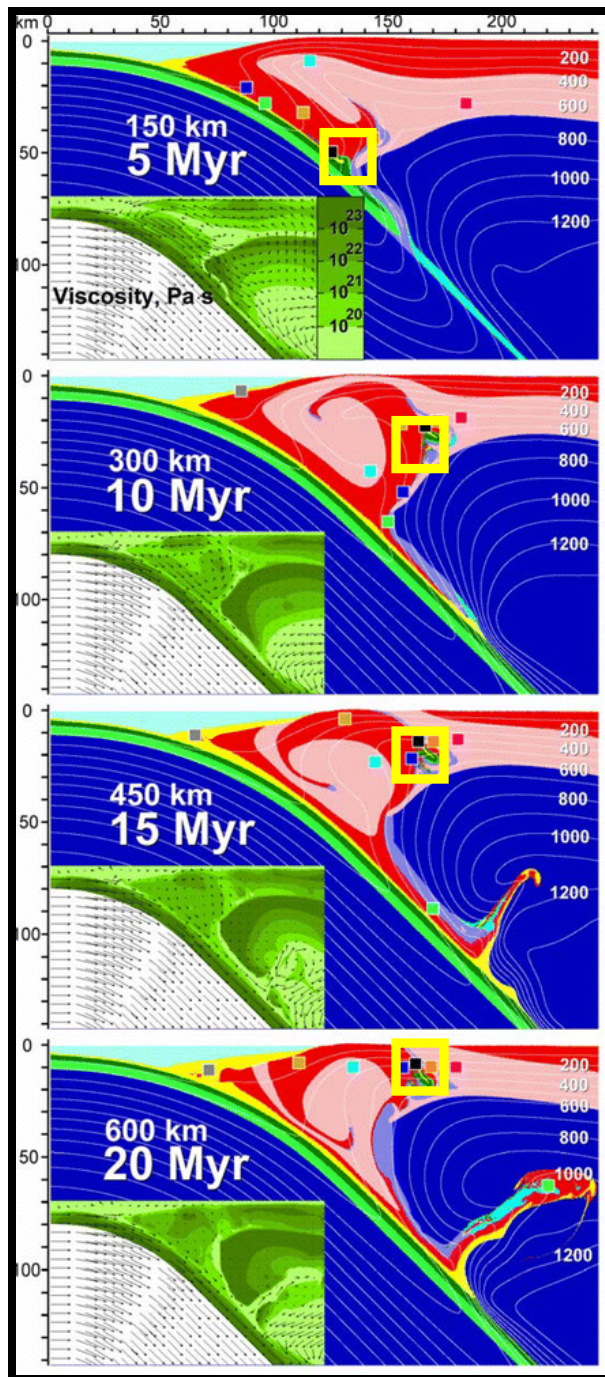


Figure 30. Numerical model of active continental margin from 150 km to 600 km of subduction. Boxed yellow area is stranded oceanic crust in continental crust. **yellow**=sediments, **red**=upper continental crust, **pink**=lower continental crust, **dark green**=upper oceanic crust, **light green**=lower oceanic crust, **dark blue**=dry mantle, **light blue**=hydrated mantle, **purple**=serpentinized mantle (Gerya and Stöckhert, 2006).

subduction channel. This is reasonable considering the small aerial extent of eclogites in Liverpool Land and that they are restricted to a small area of the footwall block (Fig. 5). Intermingling of oceanic and continental crust could have stranded HP eclogites and amphibolites in continental crust. The Gubbedalen Shear Zone may have been the thrust fault bringing minor amounts of oceanic crust into the continental crust. This pre-existing weakness later was reactivated as an extensional fault exhuming the eclogites. This interpretation would make Liverpool Land eclogites part of the deep-continental root beneath Laurentia that was exhumed along the Gubbedalen Shear Zone rather than an orphaned block of Baltica.

Figure 31 is a time-progressive series of cross-sections through Liverpool Land (W-E striking) nearly parallel to the movement direction along the Gubbedalen Shear Zone fault plane modeled after the findings of Gerya and Stöckhert (2006). Beginning at ca. 440 Ma, the first phase of Hurry Inlet Granite, 445 Ma, had already ascended to upper-crustal levels and crystallized within the Krummedal Sequence along a magmatic arc on the east Laurentian (modern geographic coordinates) continental margin (Higgins et al., 1981; Andresen et al., 1998). progressed to ~150 km in 5 m.y. of subduction at this time. An orogenic wedge has already formed beneath the Laurentian margin incorporating oceanic crust into lower continental crust. Amphibolite-facies metamorphism in the middle crust affected the entire east margin of Laurentia at 425 Ma (see Figure 30 for progression from 5-20 m.y.) as Baltica collides with Laurentia (~450 km in 20 m.y. of subduction). The Hurry Inlet Granite and its host units might already have begun being emplaced upon Liverpool Land along the Gubbedalen Shear Zone at this time (Dewey and Strachan, 2003; Augland, 2007). In the orogenic wedge, mafic

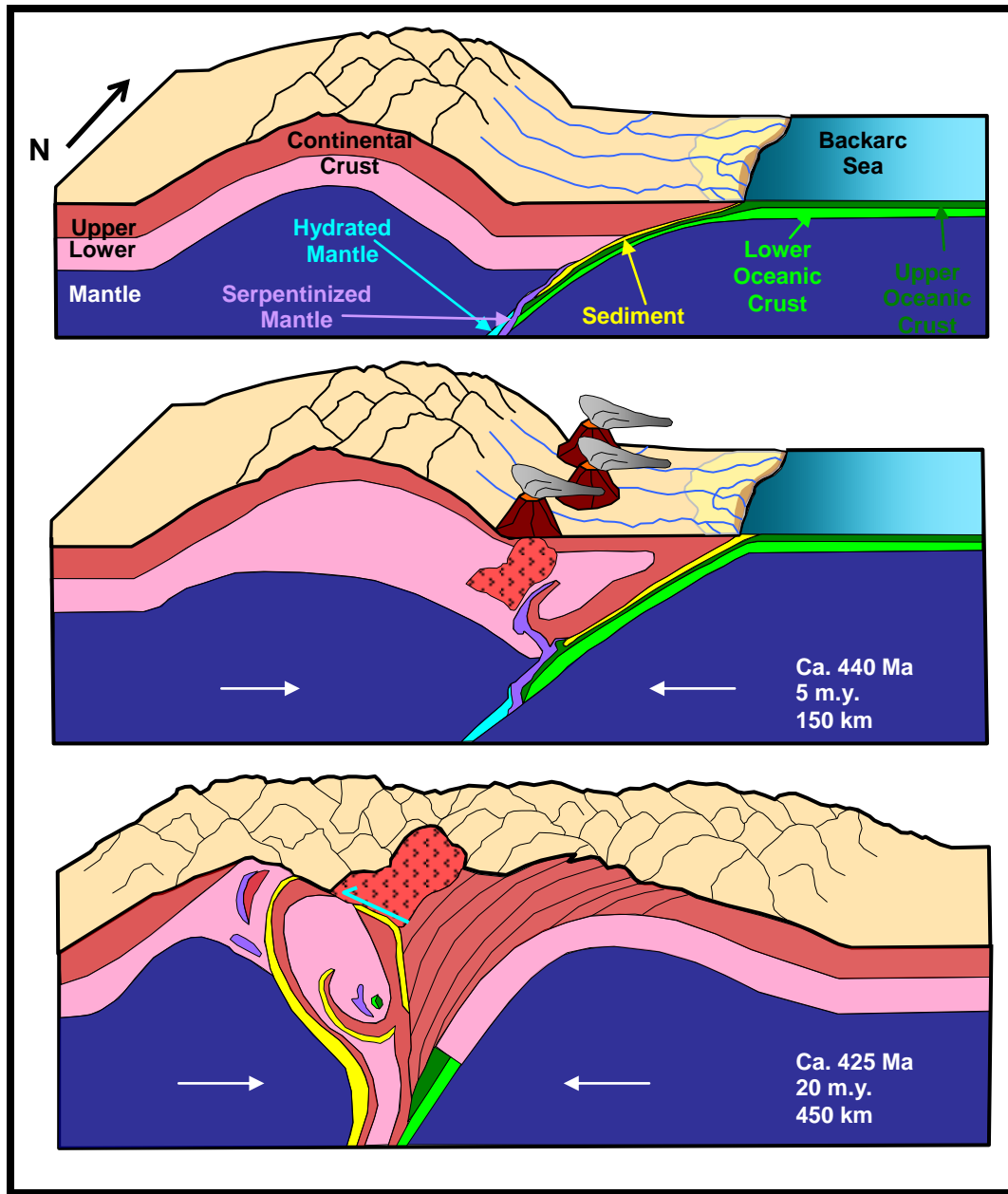


Figure 31. Series of time-progressive cross sections through Liverpool Land illustrating possible origin and exhumation of eclogites. Approximately 440 Ma, 5 million years after volcanic island arc (just east of cross-section) and Baltica collide, intrusion of Hurry Inlet Granite at 445 and 438 Ma. Approximately 150 km of subduction, formational rotation of orogenic flow channel in Laurentian plate. Approximately 425 Ma, 20 million years after collision, ~450 km of subduction; oceanic crust and mantle material ascend through lower continental crust; Baltic continental crust is subducted. Light blue arrow is contractional movement (into plane of model) along Gubbedalen Shear Zone. Distances not to scale.

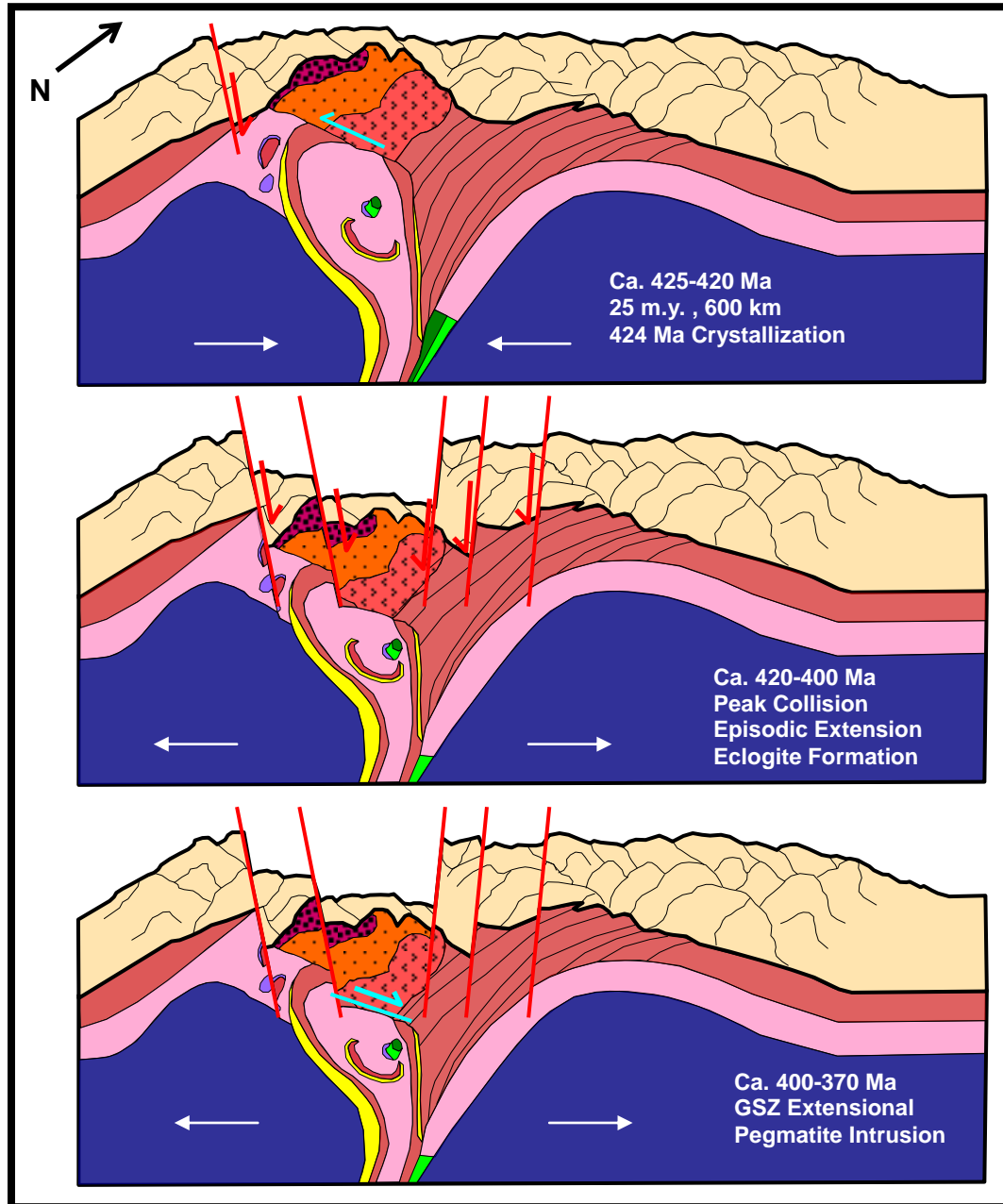


Figure 31 (cont'd). Approximately 425-420 Ma, ~25 million years after collision, ~600 km of subduction. The Hurry Inlet Granite continues thrusting (into plane of model) west across Liverpool Land and Krummedal Sequence and monzodiorite crystallize. Fjord Region Detachment initiated as extensional. Approximately 420-400 Ma, peak collision of Caledonian orogen with episodic extension initiating Western Fault Zone. Approximately 400-370 Ma, GSZ becomes extensional and pegmatites intrude hanging wall and footwall 388-386 Ma. Distances not to scale.

oceanic crust is stranded in lower continental crust and gradually ascends due to rotational flow within the wedge. Upper continental crust, subducted sediments, and serpentized mantle are also intermingled with the lower crust. From 425-420 Ma Baltica continued to collide with Laurentia. At 424 Ma the monzodiorite in the northern field area in Liverpool Land intruded into the Krummedal Sequence and crystallized. Rotation within the orogenic wedge strands additional upper crustal material and subducted sediments.

The Fjord Region Detachment (Fig. 4) changes fault motion from a tops-west thrust to a tops-east extensional shear zone between 424 and 357 Ma (White et al., 2002), marking the beginning of episodic gravitational collapse throughout Central East Greenland and affecting areas as far south as Liverpool Land. Several other major N-S striking normal faults became active between 420-370 Ma in Greenland and Norway down dropping younger Paleozoic rocks adjacent Caledonian crystalline basement (Hartz and Andresen, 1995; Marshall and Stephenson, 1997; Roberts, 2002; White and Hodges, 2003). Central East Greenland faults indicate middle to upper crustal extension at this time dissecting the orogenic wedge and progressively uplifting blocks to the surface (White et al., 2002). Between 400 and 385 Ma, the Gubbedalen Shear Zone shifted from a tops-south thrust to a tops-north extensional fault while pegmatites intruded the surrounding country rock. This timing is compatible with initial movement along the Western Fault Zone (i.e., Middle Devonian) in Central East Greenland (Fig. 4), which has been interpreted to be the result of synorogenic gravitational collapse (Hartz and Andresen, 1995). Periods of gravitational collapse in East Greenland are reminiscent of

those documented in the active Himalayas where they form contemporaneous thrusts and normal faults (White et al., 2002).

Figure 32 is a cartoon diagram illustrating the present-day geological relationships between the Fjord Region Detachment, the Western Fault Zone, and the Gubbedalen Shear Zone. $^{40}\text{Ar}/^{39}\text{Ar}$ muscovite cooling ages are superimposed upon the diagram to illustrate local cooling trends. Middle Devonian movement along the Western Fault Zone likely cuts out the earlier-thrust history associated with the Gubbedalen Shear Zone (i.e., ~395 – 385 Ma) and the Fjord Region Detachment in the subsurface beneath the Jameson Land basin, juxtaposing the Stauning Alper terrane against Liverpool Land. Subsequently, around 378 Ma, latest extensional reactivation of the Gubbedalen Shear Zone exhumed the footwall block through upper-crustal levels eventually exposing lower continental crust with its stranded mafic material (i.e., oceanic crust in this interpretation) that has been variably eclogitized.

The hypothesis that Liverpool Land eclogites originated as blebs of subducted oceanic crust that had intermingled with lower Laurentian crust within a “marble-caked” subduction flow channel provides plausible explanation for a host of observations that do not fit the hypothesis for tectonic overpressures. Both hypotheses suggest proximity of Liverpool Land to the Western Gneiss Region within the Early Devonian Caledonian A-type subduction zone. Intermingling accounts for the presence of ultramafic bodies and the intense plastic style of deformation observed within the well-hydrated quartzo-feldspathic gneisses hosting the eclogites whereas tectonic overpressures do not. The generation of HP eclogites, not UHP ones as suggested earlier, in the overriding plate subduction channel is consistent with UHP metamorphism in subducting Baltic

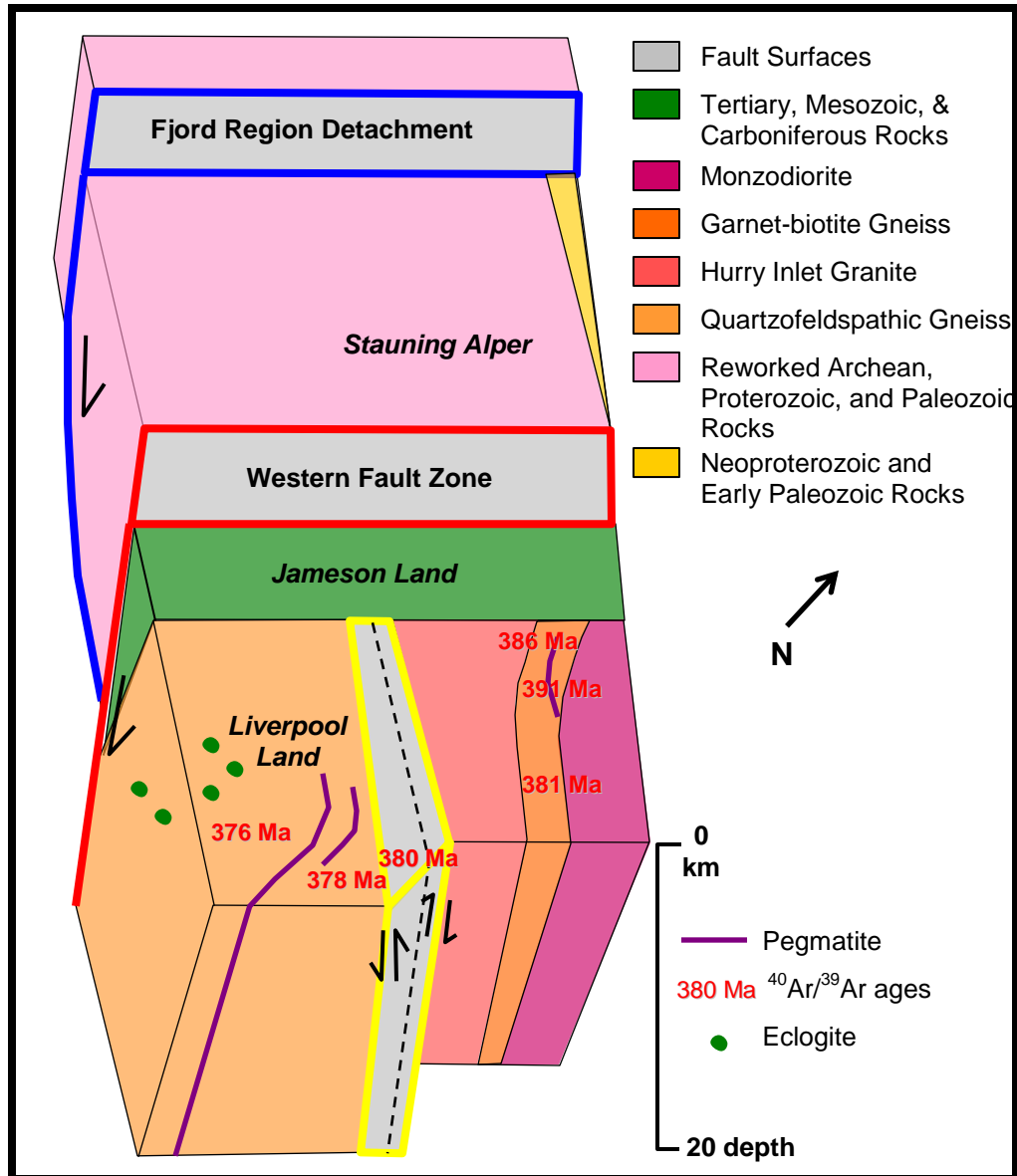


Figure 32. Present day close-up cross section parallel to Greenland coastline (e.g. perpendicular to Liverpool Land). Red fault lines are high angle normal faults ca. 425 Ma -<Tertiary. Blue fault line is listric detachment of Fjord Region Detachment, respectively. Yellow fault line is extensional Gubbedalen Shear Zone. Dashed black line is approximate location between upper thrust and lower extension. Pegmatites intruded during extension from 388-386 Ma. Longitudinal distance is not to scale.

lithosphere (i.e., the Western Gneiss Region). Intermingling also is consistent with established $^{40}\text{Ar}/^{39}\text{Ar}$ muscovite cooling patterns and temperature-*time* paths from Liverpool Land and the Western Gneiss Region. As the Baltic crust was exhumed from underneath Laurentia, tops-westward motion along the Sogn-Nordfjord detachment, muscovite cooling progressed from east to west (seaward) (Dallmeyer et al., 1992; Fossen and Dunlap, 1998; Carswell et al., 2003; Hacker, 2007; Walsh et al., 2007). Cooling of muscovite in Liverpool Land was ~10 m.y. later and slightly reheated before final exhumation to Earth's surface.

Very few studies explain interactions of subducted material in an orogenic wedge, particularly effect on basement rock, in continent-continent collisions (e.g. Beaumont et al., 2006; Culshaw et al., 2006). Significant basement U/Pb zircon age difference between North-East Greenland eclogite province (1.89-1.98 Ga; Brueckner et al., 1998) and Liverpool Land (1.6 Ga; Augland et al., 2007) indicate dissimilar basement origins. A possible interpretation for this difference and similarity of basement gneiss data for the Western Gneiss Region (1.5-1.7 Ga; Gebauer et al., 1985) to Liverpool Land is intermingling of subducted Baltic crust within lower Laurentian continental crust. Thus, zircon would be transferred from the subducted crust to the lower continental crust.

VI. SUMMARY

From the above investigation of rocks in Liverpool Land, the following conclusions have been assessed.

1. For each sample, $^{40}\text{Ar}/^{39}\text{Ar}$ incrementally heated single grains yield plateau ages within the age distribution from single crystal total fusion analyses.
2. The Gubbedalen Shear Zone records thermochronological eclogite exhumation from at least 388 Ma to 372 Ma.
3. Hanging wall block $^{40}\text{Ar}/^{39}\text{Ar}$ muscovite ages indicate pegmatite intrusion cooling from 387.0 Ma to 386.5 Ma, well before cooling of the footwall block from 380.7 Ma to 376.1 Ma.
4. HP Liverpool Land eclogites may have formed by the intermingling of subducted oceanic crust with lower Laurentian continental crust in the subduction zone channel, providing a mechanism that might be applicable to other lower-crustal continental basement terranes formed through continent-continent collision.
5. Liverpool Land and Western Gneiss Region exhumation rates, cooling rates, and cooling ages are similar and support proximal positions on either side of the Caledonian A-type subduction zone boundary as an overriding plate and subducting plate, respectively.

6. A trough in the temperature-*time* path determined for Liverpool Land corresponds in time to a much more dramatic one documented for the NEGEP that is not yet understood.

Future investigations should include additional sampling throughout the Liverpool Land area to add to the initial dataset reported herein. A more detailed dataset would add to our ability to further characterize the tectonothermal evolution of rocks and structures in this important setting. Further analysis should include in-situ dating of a grain from each sample to cylindrical diffusion of muscovite grains from core to rim (Hames and Bowring, 1994). The thermal evolution of the hanging wall block is largely unconstrained in Liverpool Land, and needs further characterization to understand the earlier, pre-~400 Ma Caledonian evolution of this region. Additional information concerning the formation and exhumation of eclogites throughout the Caledonides is needed to better understand their significance for continental dynamics. Finally, future work needs to better explore the details of the architecture of the troughs in the temperature-*time* paths determined for Liverpool Land and the NEGEP eclogite terranes. Why the eclogites cooled substantially and then reheated in these two areas that are today separated by nearly 800 km may be related tectonic processes/events that we do not yet understand.

REFERENCES

- Andresen, A., Hartz, E., and Vold, J., 1998, A late orogenic extensional origin for the infracrustal gneiss domes of the East Greenland Caledonides (72-72°N): *Tectonophysics*, v. 285, p. 353-369.
- Andresen, A., Rehnström, E., and Holte, M., 2007, Evidence for simultaneous contraction and extension at different crustal levels during the Caledonian orogeny in NE Greenland: *Journal of the Geological Society of London*, v. 164, p. 1-12.
- Andersen, T.B., and Jamtveit, B., 1990, Uplift of deep crust during orogenic extensional collapse: A model based on field studies in the Sogn-Sunnfjord region of western Norway: *Tectonics*, v. 9, p. 1097-1112.
- Augland, L.E., 2007, The Gubbedalen Shear zone; a terrane boundary in the East Greenland Caledonides: A structural and Geochronological study [M.S. thesis]: Oslo, Norway, University of Oslo, 126 p.
- Augland, L.E., Andresen, A., Corfu, F., Buchanan, J.W., and Steltenpohl, M.G., 2007, The Liverpool Land eclogite terrane: A piece of Baltica within the east Greenland Caledonides?: *Geological Society of America Abstracts with Programs*, v. 39, no. 6.
- Austerheim, H., 1987, Eclogitisation of lower crustal granulites by fluid migration through shear zones: *Earth and Planetary Science Letters*, v. 81, p. 221-232.
- Beaumont, C., Nguyen, M. H., Jamieson, R. A., and Ellis, S., 2006, Crustal flow modes in large hot orogens, *in* Law, R. D., Searle, M. P. and Godin, L., eds, *Channel Flow, Ductile Extrusion and Exhumation in Continental Collision Zones*, Special Publication 268: Geological Society, London, p. 91-145.
- Boundy, T.M, Mezger, K., and Essen, E.J., 1997, Temporal and tectonic evolution of the granulite-eclogite association from the Bergen Arcs, western Norway: *Lithos*, v. 39, p. 159-178.
- Brueckner, H.K., Gilotti, J.A., and Nutman, A.P., 1998, Caledonian eclogite facies metamorphism of Early Proterozoic protoliths from the North-East Greenland Eclogite Province: *Contributions to Mineralogy and Petrology*, v. 130, p. 103-120.

- Buchanan, J.W., 2008, Tectonic evolution of a Caledonian-aged continental basement eclogite terrane in Liverpool Land, East Greenland, [M.S. thesis]: Auburn, Alabama, Auburn University, 121 p.
- Buchanan, J.W., Augland, L.E., Steltenpohl, M.G., and Andresen, A., 2007, Structural and petrologic framework of a Caledonian eclogite terrane within southern Liverpool Land, east Greenland: *Geological Society of America Abstracts with Programs*, v. 39, no. 6.
- Carswell, D.A., Brueckner, H.K., Cuthbert, S.J., Mehta, K., and O'Brien, P.J., 2003, The timing of stabilization and the exhumation rate for ultrahigh-pressure rocks in the Western Gneiss Region of Norway: *Journal of Metamorphic Geology*, v. 21, p. 601-612.
- Cross, W.G., 1951, Two-directional focusing of charged particles with a sector-shaped, uniform magnetic field: *Reviews of Scientific Instruments*, v. 22, p. 717-722.
- Culshaw, N.G., Beaumont, C., and Jamieson, R.A., 2006, The orogenic superstructure–infrastructure concept: revisited, quantified, and revived: *Geology*, v. 34, p. 733–736.
- Dallmeyer, R.D., Johansson, L., and Möller, C., 1992, Chronology of Caledonian high-pressure granulite-facies metamorphism, uplift, and deformation within northern parts of the Western Gneiss Region, Norway: *Geological Society of America Bulletin*, v. 104, p. 444-455.
- Dewey, J. F. and Strachan, R. A., 2003, Changing Silurian-Devonian relative plate motion in the Caledonides: sinistral transpression to sinistral transtension: *Journal of the Geological Society*, v. 160, p. 219-229.
- Dobrzhinetskaya, L.F., Eide, E.A., Larsen, R.B., Sturt, B.A., Tronnes, R.G., Smith, D.C., Taylor, W.R., and Posukhova, T.V., 1995, Microdiamonds in high-grade metamorphic rocks of the Western Gneiss region, Norway: *Geology*, v. 23, p. 597-600.
- Dodson, M.H., 1973, Closure temperature in cooling geochronological and petrological systems: *Contributions to Mineralogy and Petrology*, v. 81, p. 340-349.
- Fossen, H., and Dunlap, W.J., 1998, Timing and kinematics of Caledonian thrusting and extension collapse, south Norway: Evidence from $^{40}\text{Ar}/^{39}\text{Ar}$ thermochronology: *Journal of Structural Geology*, v. 20, p. 765-781.
- Gebauer, D., Lappin, M.A., Grünenfelder, M., and Wytttenbach, A., 1985, The age and origin of some Norwegian eclogites: A U-Pb zircon and REE study: *Chemical Geology*, v. 52, p. 227-247.

- Gerya, T and Stöckhert, B, 2006, Two-dimensional numerical modeling of tectonic and metamorphic histories at active continental margins: *International Journal Earth Science*, v. 95, p. 250-274.
- Gilotti, J.A., and Krogh Ravn, E.J., 2002, First evidence for ultrahigh-pressure metamorphism in the north-east Greenland Caledonides: *Geology*, v. 30, p. 551-554.
- Gilotti, J.A., and McClelland, W.C., 2005, Leucogranites and the time of extension in the east Greenland Caledonides: *Journal of Geology*, v. 113, p. 399-417.
- Gilotti, J.A., and McClelland, W.C., 2007, Characteristics of, and a tectonic model for, Ultrahigh-Pressure metamorphism in the overriding plate of the Caledonian orogen: *International Geology Review*, v. 49, p. 777-797.
- Gilotti, J.A., Nutman, A.P., and Brueckner, H.K., 2004, Devonian to Carboniferous collision in the Greenland Caledonides: U-Pb zircon and Sm-Nd ages of high-pressure and ultrahigh-pressure metamorphism: *Contributions to Mineral Petrology*, v. 148, p. 216-235.
- Griffin, W.L., Taylor, P.N., Hakkinen, J.W., Heiser, K.S., Iden, I.K., Krogh, E.J., Malm, O., Olsen, K.I., Ormassen, D.E., and Tveten, E., 1978, Archean and Proterozoic crustal evolution of Lofoten-Vesterålen, north Norway: *Geological Society [London] Journal*, v. 135, p. 629-647.
- Hacker, B.R., 2007, Ascent of the ultrahigh-pressure Western Gneiss Region, Norway, *in* Cloos, M., et al. eds., *Convergent Margin Terranes and Associated Regions: A Tribute to W.G. Ernst*: Geological Society of America Special Paper 419, 14 p.
- Haller, J., 1985, The East Greenland Caledonides—reviewed, *in* Gee, D.G. and Sturt, B.A., eds., *The Caledonide Orogen—Scandinavia and Related Areas*: Wiley & Sons Ltd., p. 1031-1046.
- Hames, W.E. and Bowring, S.A., 1994, An empirical evaluation of the argon diffusion geometry in muscovite: *Earth and Planetary Science Letters*, v. 124, p. 161-167.
- Hartz, E., and Andresen, A., 1995, Caledonian sole thrust of central East Greenland: A crustal-scale Devonian extensional detachment?: *Geology*, v. 23, p. 637-640.
- Hartz, E.H., Torsvik, T.H., and Andresen, A., 1997, Carboniferous age for the East Greenland "Devonian" basin: Paleomagnetic and isotopic constraints on age, stratigraphy, and plate reconstructions: *Geology*, v. 25, p. 675-678.

- Hartz, E.H., Condon, D. Austerheim, H., and Erambert, M., 2005, Rediscovery of the Liverpool Land eclogites (Central East Greenland): A post and supra-subduction UHP province: *Mitt. Osterr. Miner. Ges.*, v. 150, abstract.
- Henriksen, N., Higgins, A.K., and Christoffersen, M., 2003, Caledonian Orogen East Greenland 70–82 N, a compilation of lithostructural data: The Geological Society of Denmark and Greenland, Copenhagen.
- Higgins, A. K., Friderichsen, J. D., and Thyrted, T., 1981, Precambrian metamorphic complexes in the East Greenland Caledonides (72-74 ° N) - their relationships to the Eleonore Bay Group, and Caledonian orogenesis: *Rapport Grønlands Geologiske Undersøgelse*, v. 104, p. 5-46.
- Hodges, K.V, Bartley, J.M, and Burchfiel, B.C, 1982, Structural evolution of an A-type subduction zone, Lofoten-Rombak area, northern Scandinavian Caledonides: *Tectonics*, v. 1, p. 441-462.
- Hodges, K.V., Burchfiel, B.C., Royden, L.H., Chen, Z., and Liu, Y., 1993, The metamorphic signature of contemporaneous extension and shortening in the central Himalayan orogen-data from the Nyalam transect, southern Tibet: *Journal of Metamorphic Petrology*, v. 11, p. 721-737.
- Hutton, D.H.W., 1987, Strike-slip terranes and a model for the evolution of the British and Irish Caledonides: *Geological Magazine*, v. 124, p. 405-500.
- Hutton, D.H.W. and McErlean, M., 1991, Silurian and Early Devonian sinistral deformation of the Ratagain granite, Scotland: constraints on the age of Caledonian movements on the Great Glen fault system: *Journal of the Geological Society*, London, v. 148, p. 1-4.
- Kassos, G., 2008, Structural, isotopic, and kinematic analysis of eclogite-facies shear zones and associated structures, Lofoten, north Norway: M.S. Thesis, Auburn University, Auburn, Alabama, 205 p.
- Lee, J.K.W., Williams, F.S., and Ellis, D.J., 1997, Pb, U and Th diffusion in natural zircon: *Nature*, v. 390, p. 159-162.
- Larsen, P.H. and Bengaard, H.J., 1991, Devonian basin initiation in East Greenland: a result of sinistral wrench faulting and Caledonian extensional collapse: *Journal of the Geological Society of London*, v. 148, p. 355-368.
- Leslie, A. G. and Higgins, A. K., 1999, Granitic signposts to Grenvillian deformation in the Caledonian fold and thrust belt of eastern Greenland: *Irish Journal of Earth Sciences*, v. 17, p. 131.

- Ludwig, K.R., 2003, User's manual for Isoplot, v. 3.0, a geochronological toolkit for Microsoft Excel: Berkeley Geochronological Center, Special Publication no. 4.
- MacKenzie, W.S. and Adams, A.E., 2001, A colour atlas of rocks and minerals in thin section: Manson Publishing, 192 p.
- Marshall, J.E.A., and Stephenson, B.J., 1997, Sedimentological responses to basin initiation in the Devonian of East Greenland: *Sedimentology*, v. 44, p. 407-419.
- McClelland, W.C., and Gilotti, J.A., 2003, Late-stage extensional exhumation of high-pressure granulites in the Greenland Caledonides: *Geology*, v. 31, p. 259-262.
- McClelland, W.C., Gilotti, J.A., Power, S.E, and Mazdab, F.K., 2005, Dating of UHP metamorphism, NE Greenland Caledonides: *Mitteilunge der Österreichischen Mineralogischen Gesellschaft*, v. 150, p. 107.
- MacNiocaill, C. and Smethrust, M.A., 1994, Paleozoic paleogeography of Laurentia and its margins-A reassessment of paleomagnetic data: *Geophysical Journal International*, v. 116, p. 715-725.
- Mosar, J. Eide, E.A., Osmundsen, P.T., Sommaruga, A., and torsvik, T.H., 2002, Greenland-Norway separation: A geodynamic model for the North Atlantic: *Norwegian Journal of Geology*, v. 82, p. 282-299.
- Passchier, C.W., and Trouw, R.A., 2005, Natural Microgauges, *in* *Microtectonics*: Springer, p. 247-262.
- Renne, P.R., Swisher, C.C., Deino, A.L., Karner, D.B., Owens, T.L., and DePaolo, D.J., 1998, Intercalibration of standards, absolute ages, and uncertainties in $^{40}\text{Ar}/^{39}\text{Ar}$ dating: *Chemical Geology*, v. 145, p. 117-152.
- Roberts, D., 1983, Devonian tectonic deformation in the Norwegian Caledonides and its regional perspectives: *Norges Geologiske Undersøkelse*, v. 380, p. 85-96.
- Roberts, D., 2002, The Scandianavian Caledonides: event chronology, palaeogeographic settings and likely modern analogues: *Tectonophysics*, v. 365, p. 283-299.
- Roberts, D. and Gee, D.G., 1985, An introduction to the structure of the Scandinavian Caledonides: *in* Gee, D.G. and Sturt, B.A., eds., *The Caledonide Orogen—Scandinavia and Related Areas*: Wiley & Sons Ltd., p. 55-68.
- Root, D.B., Hacker, B.R., Mattinson, J.M., and Wooden, J.L., 2004, Zircon geochronology and ca. 400 Ma exhumation of Norwegian ultrahigh pressure rocks; an ion microprobe and chemical abrasion study: *Earth and Planetary Science Letter*, v. 228, p. 325-341.

- Sartini-Rideout, C., Gilotti, J.A., and McClelland, W.C., 2006, Geology and timing of dextral strike-slip shear zones in Danmarkshavn, north-east Greenland Caledonides: *Geological Magazine*, v. 143, p. 431-446.
- Schmitz, M.D., and Bowring, S.A., 2003, Constraints on the thermal evolution of continental lithosphere from U-Pb accessory mineral thermochronometry of lower crustal xenoliths, southern Africa: *Contributions to Mineralogy and Petrology*, v. 140, p. 559-567.
- Siedlecka, A., 1975, Old Red sandstone lithostratigraphy and sedimentation of the outer Fossen area, Trondheim region: *Norges Geologiske Undersøkelse*, v. 321, p. 1-35.
- Steltenpohl, M.G., Hames, W.E., Andresen, A., and Markl, G., 2003, New Caledonian eclogite province in Norway and potential Laurentian (Taconic) and Baltic links: *Geology*, v. 31, p. 985-988.
- Steltenpohl, M.G., Hames, W.E., and Andresen, A., 2004, The Silurian to Permian history of a metamorphic core complex in Lofoten, northern Scandinavian Caledonides: *Tectonics*, v. 23, p. 1-23.
- Steltenpohl, M.G., Kassos, G., and Andresen, A., 2006, Retrograded eclogite-facies pseudotachylytes as deep-crustal paleoseismic faults within continental basement of Lofoten, north Norway: *Geosphere*, v. 2, p. 61-72.
- Strachan, R.A., Nutman, A.P., and Friderichsen, J.D., 1995, SHRIMP U-Pb geochronology and metamorphic history of the Smallefjord sequence, NE Greenland Caledonides: *Journal of the Geological Society*, London, v. 152, p. 779-784.
- Strachan, R.A., and Tribe, I.R., 1994, Structure of the Storstrømmen shear zone, eastern Hertugen af Orleans Land, North-East Greenland: *Rapport Grønlands Geologiske Undersøgelse*, v. 148, p. 1861-1884.
- von Blackenburg, F., Villa, I.M., Haur, H., Morteani, G., and Steiger, R.H., 1989, Time calibration of a PT-path from the western Tauern Window, eastern Alps: the problem of closure temperatures: *Contributions to Mineralogy and Petrology*, v. 101, p. 1-11.
- Walsh, E.O., Hacker, B.R., Gans, P.B., Grove, M., and Gehrels, G., 2007, Protolith ages and exhumation histories of (ultra)high-pressure rocks across the Western Gneiss Region, Norway: *Geological Society of America Bulletin*, v. 119, p. 289-301.

- White, A.P. and Hodges, K.V., 2003, Pressure-temperature-time evolution of the central East Greenland Caledonides; quantitative constraints on crustal thickening and synorogenic extension: *Journal of Metamorphic Geology*, v. 21, p. 875-897.
- White, A.P., Hodges, K.V., Martin, M.W., and Andresen, A., 2002, Geologic constraints on middle-crustal behavior during broadly synorogenic extension in the central East Greenland Caledonides: *International Journal of Earth Science*, v. 91, p. 187-208.
- Winter, J.D., 2001, *An Introduction to Igneous and Metamorphic Petrology*: Prentice Hall, 699 p.
- Ziegler, P., 1988, Evolution of the Arctic-North Atlantic and the Western Tethys: *American Association of Petroleum Geologists Memoir 43*, p. 164-196.

APPENDIX A

Raw data for:

1. monitor minerals (p.80)
2. muscovite single crystal total fusion (p.81)
3. muscovite incrementally heated (p.83)

Below is a table of muscovite grain size according to sieve screen size and coordinates of sample location.

Sample	Sieve Size	Latitude	Longitude
DRB-06-16	425 μm – 180 μm	N: 70 34.022	W: 22 11.621
DRB-06-22	600 μm – 425 μm	N: 70 36.025	W: 22 9.891
JWB-06-CP73	600 μm – 425 μm	N: 70 36.039	W: 22 12.995
JWB-06-M28A	600 μm – 425 μm	N: 70 52.139	W: 22 19.777
JWB-06-M28B	600 μm – 425 μm	N: 70 52.139	W: 22 19.777
JWB-06-M28C	600 μm – 425 μm	N: 70 52.139	W: 22 19.777

DATA FOR MONITOR MINERAL FC-2 (New Mexico Tech)

	⁴⁰ Ar (*, atm)	³⁹ Ar (K-derived)	³⁹ Ar (Cl-derived, atm)	³⁷ Ar (Ca-derived)	³⁶ Ar (*)	%Rad	R	J-value	%-sd
au9.4i.san	76 1.1E-13 ± 5.9E-17	9.6E-14 ± 3.1E-17	2.1E-16 ± 7.1E-19	4.8E-16 ± 4.3E-18	1.5E-18 ± 1.0E-19	100%	1.15	0.0137 ± 0.00001	0.0007
	77 5.7E-14 ± 3.7E-17	4.9E-14 ± 3.6E-17	1.2E-16 ± 6.8E-19	2.9E-16 ± 3.2E-18	1.2E-18 ± 8.4E-20	96%	1.15	0.0136 ± 0.00001	0.0011
	78 9.6E-14 ± 7.3E-17	8.0E-14 ± 3.0E-17	2.3E-16 ± 1.4E-18	4.2E-16 ± 3.9E-18	1.2E-17 ± 2.0E-19	99%	1.15	0.0136 ± 0.00001	0.0011
	79 7.6E-14 ± 3.0E-17	6.5E-14 ± 5.0E-17	1.7E-16 ± 1.1E-18	3.3E-16 ± 5.1E-18	1.5E-18 ± 1.1E-19	99%	1.16	0.0135 ± 0.00001	0.0010
	80 6.0E-14 ± 4.8E-17	5.2E-14 ± 3.6E-17	1.2E-16 ± 5.4E-19	2.8E-16 ± 2.7E-18	3.9E-19 ± 6.9E-20	100%	1.16	0.0135 ± 0.00002	0.0011
								0.0136 ± 0.00003	0.0021
au9.3i.san	86 1.3E-13 ± 1.6E-16	1.1E-13 ± 1.8E-16	2.8E-16 ± 1.2E-18	6.8E-16 ± 9.9E-18	1.6E-18 ± 1.3E-19	100%	1.15	0.0136 ± 0.00003	0.0021
	87 7.4E-14 ± 6.4E-17	6.4E-14 ± 7.3E-17	1.6E-16 ± 8.9E-19	3.6E-16 ± 3.6E-18	6.9E-19 ± 1.0E-19	100%	1.16	0.0135 ± 0.00002	0.0015
	88 9.4E-14 ± 4.2E-17	8.1E-14 ± 6.8E-17	2.1E-16 ± 9.8E-19	4.5E-16 ± 3.9E-18	2.7E-18 ± 1.3E-19	99%	1.15	0.0136 ± 0.00001	0.0011
	89 1.2E-13 ± 9.1E-17	1.0E-13 ± 5.1E-17	2.7E-16 ± 1.0E-18	6.2E-16 ± 7.0E-18	4.9E-18 ± 1.3E-19	99%	1.16	0.0135 ± 0.00001	0.0010
	90 1.3E-13 ± 6.8E-17	1.1E-13 ± 3.4E-17	2.9E-16 ± 1.6E-18	6.4E-16 ± 4.5E-18	4.2E-18 ± 1.4E-19	99%	1.15	0.0136 ± 0.00001	0.0007
								0.0135 ± 0.00002	0.0016
au9.2i.san	91 3.5E-14 ± 2.3E-17	2.8E-14 ± 1.5E-17	6.5E-17 ± 3.1E-19	1.7E-16 ± 2.8E-18	8.5E-18 ± 1.8E-19	93%	1.16	0.0135 ± 0.00003	0.0019
	92 8.5E-14 ± 5.0E-17	7.2E-14 ± 3.1E-17	1.7E-16 ± 6.9E-19	4.0E-16 ± 4.2E-18	5.7E-18 ± 1.8E-19	98%	1.15	0.0136 ± 0.00001	0.0010
	93 7.6E-14 ± 6.3E-17	6.4E-14 ± 3.0E-17	1.5E-16 ± 9.8E-19	5.0E-16 ± 1.1E-17	7.1E-18 ± 2.0E-19	97%	1.15	0.0136 ± 0.00002	0.0013
	94 8.0E-14 ± 5.1E-17	6.9E-14 ± 5.7E-17	1.6E-16 ± 8.5E-19	3.9E-16 ± 6.4E-18	3.4E-18 ± 2.2E-19	99%	1.16	0.0135 ± 0.00002	0.0014
	95 7.2E-14 ± 5.1E-17	6.2E-14 ± 5.2E-17	1.4E-16 ± 5.9E-19	3.4E-16 ± 2.6E-18	1.1E-18 ± 1.3E-19	100%	1.15	0.0136 ± 0.00002	0.0013
								0.0136 ± 0.00003	0.0021
au9.1j.san	96 5.2E-14 ± 3.1E-17	4.4E-14 ± 3.5E-17	1.1E-16 ± 7.3E-19	3.3E-16 ± 4.6E-18	1.7E-18 ± 8.8E-20	99%	1.17	0.0134 ± 0.00002	0.0011
	97 5.5E-14 ± 3.3E-17	4.6E-14 ± 2.3E-17	1.3E-16 ± 8.1E-19	4.5E-16 ± 2.8E-18	2.3E-18 ± 9.7E-20	99%	1.16	0.0135 ± 0.00001	0.0010
	98 6.6E-14 ± 7.5E-17	5.4E-14 ± 5.2E-17	1.8E-16 ± 1.2E-18	6.8E-16 ± 4.2E-18	7.6E-18 ± 1.1E-19	97%	1.17	0.0134 ± 0.00002	0.0016
	99 1.1E-13 ± 1.1E-16	9.1E-14 ± 6.8E-17	2.4E-16 ± 6.8E-19	5.6E-16 ± 6.2E-18	9.6E-18 ± 1.5E-19	97%	1.16	0.0135 ± 0.00002	0.0013
	100 1.1E-13 ± 3.5E-17	9.3E-14 ± 4.1E-17	2.4E-16 ± 1.0E-18	5.8E-16 ± 5.4E-18	9.9E-18 ± 2.1E-19	97%	1.18	0.0133 ± 0.00001	0.0008
								0.0134 ± 0.00003	0.0026
au9.3g.san	71 1.6E-13 ± 4.2E-17	1.4E-13 ± 4.1E-17	3.8E-16 ± 8.7E-19	8.2E-16 ± 5.1E-18	2.5E-18 ± 1.0E-19	100%	1.17	0.0134 ± 0.00001	0.0005

Data are in moles

(*, atm) radiogenic and atmospheric derived argon

J-values calculated assuming an age of 28.02 Ma (after Renne et al., 1998)

Errors are the standard deviation

FC-2 sample prepared by New Mexico Tech; 20-28 mesh size

Raw data for monitor minerals.

JWB-06-M28A MUSCOVITE (single crystal total fusion) au9.1e.mus.sf									
grain size = 0.5-1.0 mm diameter									
J = 0.0136 ± 0.00003	⁴⁰ Ar (*, atm)	³⁹ Ar (K-derived)	³⁹ Ar (Cl-derived, atm)	³⁷ Ar (Ca-derived)	³⁶ Ar (*, *)	%Rad	R	Age (Ma)	%-sd
71	9.044E-14 ± 1.1E-15	4.661E-15 ± 1.3E-16	1.945E-17 ± 3.9E-19	7.226E-19 ± 8.7E-19	2.627E-18 ± 1.4E-19	99%	19.24	414.1 ± 12.6	3.0%
73	1.237E-13 ± 6.4E-16	6.838E-15 ± 2.7E-17	1.735E-17 ± 3.0E-19	6.148E-19 ± 1.2E-18	2.947E-18 ± 1.4E-19	99%	17.96	389.3 ± 2.5	0.7%
74	1.673E-13 ± 4.8E-16	9.029E-15 ± 3.8E-17	2.121E-17 ± 2.9E-19	3.944E-18 ± 1.4E-18	1.452E-17 ± 2.1E-19	97%	18.06	391.2 ± 2.1	0.5%
75	1.210E-13 ± 1.6E-16	6.749E-15 ± 1.1E-17	1.536E-17 ± 1.1E-19	2.383E-18 ± 9.6E-19	3.415E-18 ± 1.0E-19	99%	17.78	385.9 ± 0.8	0.2%
76	1.616E-13 ± 2.8E-16	8.862E-15 ± 2.1E-17	2.835E-17 ± 2.8E-19	2.855E-18 ± 1.2E-18	9.298E-18 ± 1.9E-19	98%	17.93	388.8 ± 1.2	0.3%
77	3.396E-13 ± 2.0E-16	1.862E-14 ± 4.1E-17	5.148E-17 ± 6.0E-19	9.135E-18 ± 1.8E-18	3.078E-17 ± 4.9E-19	97%	17.75	385.3 ± 0.9	0.2%
78	2.281E-13 ± 1.0E-16	1.271E-14 ± 3.2E-17	3.231E-17 ± 2.9E-19	9.137E-18 ± 1.6E-18	7.290E-18 ± 1.7E-19	99%	17.77	385.6 ± 1.0	0.3%
79	7.815E-16 ± 4.0E-18	4.337E-17 ± 9.8E-19	6.793E-20 ± 3.8E-20	1.047E-18 ± 9.8E-19	2.989E-20 ± 6.9E-20	99%	17.81	386.5 ± 13.8	3.6%
80	5.910E-14 ± 2.6E-16	3.249E-15 ± 1.9E-17	9.538E-18 ± 1.3E-19	1.670E-18 ± 1.2E-18	2.688E-18 ± 1.2E-19	99%	17.94	388.1 ± 2.9	0.7%
	1.292E-12	7.076E-14			7.357E-17				
							Total Gas Age:	390.7	
							Weighted Average Age:	386.5 ± 1.5	

Data are in moles

(*, atm) radiogenic and atmospheric derived argon

Highlighted area is outlying data point not used in age calculations

JWB-06-M28B MUSCOVITE (single crystal total fusion) au9.4a.mus.sf									
grain size = 0.5-1.0 mm diameter									
J = 0.0136 ± 0.00003	⁴⁰ Ar (*, atm)	³⁹ Ar (K-derived)	³⁹ Ar (Cl-derived, atm)	³⁷ Ar (Ca-derived)	³⁶ Ar (*, *)	%Rad	R	Age (Ma)	%-sd
61	1.367E-13 ± 3.3E-17	7.721E-15 ± 1.6E-17	2.075E-17 ± 2.0E-19	1.228E-17 ± 1.3E-18	6.100E-18 ± 1.8E-19	99%	17.48	384.2 ± 0.9	0.2%
62	0.201E-14 ± 1.7E-16	4.629E-15 ± 7.4E-18	1.388E-17 ± 8.7E-20	8.605E-18 ± 8.8E-19	1.370E-18 ± 1.3E-19	100%	17.63	387.2 ± 1.0	0.3%
63	1.274E-13 ± 4.7E-16	7.169E-15 ± 2.3E-17	1.969E-17 ± 2.1E-19	1.075E-17 ± 1.0E-18	3.493E-18 ± 1.4E-19	99%	17.63	387.3 ± 1.9	0.5%
64	1.447E-13 ± 2.0E-16	8.189E-15 ± 1.8E-17	2.108E-17 ± 9.8E-20	1.023E-17 ± 1.2E-18	2.821E-18 ± 1.4E-19	99%	17.57	386.0 ± 1.0	0.3%
65	8.216E-14 ± 2.1E-16	4.645E-15 ± 7.9E-18	1.294E-17 ± 1.4E-19	8.588E-18 ± 1.5E-18	1.370E-18 ± 9.5E-20	100%	17.60	386.7 ± 1.2	0.2%
66	1.247E-13 ± 4.2E-17	7.015E-15 ± 1.0E-17	1.748E-17 ± 1.8E-19	1.782E-17 ± 9.0E-19	2.167E-18 ± 1.0E-19	99%	17.68	388.3 ± 0.6	0.2%
67	1.372E-13 ± 4.3E-16	7.908E-15 ± 1.9E-17	2.408E-17 ± 2.2E-19	8.266E-18 ± 1.1E-18	1.424E-17 ± 2.0E-19	97%	17.72	389.0 ± 1.6	0.4%
68	1.020E-14 ± 2.0E-17	5.786E-16 ± 1.3E-18	1.773E-18 ± 4.8E-20	-4.199E-20 ± 6.4E-19	7.208E-20 ± 6.6E-20	100%	17.59	386.5 ± 1.4	0.4%
69	1.214E-13 ± 3.1E-16	6.795E-15 ± 2.1E-17	1.940E-17 ± 1.3E-19	1.388E-17 ± 1.6E-18	5.331E-18 ± 1.3E-19	99%	17.54	387.5 ± 1.6	0.4%
	9.665E-13	5.425E-14			3.696E-17				
							Total Gas Age:	387.5	
							Weighted Average Age:	387.0 ± 1.2	

Data are in moles

(*, atm) radiogenic and atmospheric derived argon

JWB-06-M28C MUSCOVITE (single crystal total fusion) au9.1h.mus.sf									
grain size = 0.5-1.0 mm diameter									
J = 0.0136 ± 0.00003	⁴⁰ Ar (*, atm)	³⁹ Ar (K-derived)	³⁹ Ar (Cl-derived, atm)	³⁷ Ar (Ca-derived)	³⁶ Ar (*, *)	%Rad	R	Age (Ma)	%-sd
91	8.772E-14 ± 2.2E-16	4.987E-15 ± 1.0E-17	1.106E-17 ± 1.4E-19	4.112E-18 ± 1.3E-18	2.847E-18 ± 1.3E-19	99%	17.42	378.8 ± 1.2	0.3%
92	1.092E-13 ± 1.5E-16	6.121E-15 ± 7.5E-18	1.611E-17 ± 1.6E-19	2.691E-18 ± 1.3E-18	6.176E-18 ± 1.4E-19	99%	17.59	382.2 ± 0.7	0.2%
93	8.744E-14 ± 1.3E-16	4.995E-15 ± 1.0E-17	1.178E-17 ± 1.2E-19	4.439E-18 ± 1.4E-18	1.053E-18 ± 8.6E-20	100%	17.44	379.3 ± 1.0	0.3%
94	5.212E-14 ± 3.5E-17	2.968E-15 ± 1.2E-17	6.855E-18 ± 1.0E-19	1.163E-18 ± 1.3E-18	1.859E-18 ± 1.2E-19	99%	17.38	378.0 ± 1.6	0.4%
95	9.812E-14 ± 7.4E-17	5.895E-15 ± 1.4E-17	1.491E-17 ± 3.2E-19	1.715E-18 ± 9.5E-19	2.064E-18 ± 1.1E-19	99%	17.43	379.0 ± 1.0	0.3%
96	1.394E-13 ± 1.7E-16	7.881E-15 ± 2.0E-17	2.465E-17 ± 3.7E-19	2.816E-18 ± 1.0E-18	1.852E-18 ± 9.2E-20	100%	17.62	382.8 ± 1.1	0.3%
97	1.184E-13 ± 1.7E-16	6.836E-15 ± 2.0E-17	1.692E-17 ± 2.2E-19	2.567E-18 ± 1.2E-18	1.093E-18 ± 9.7E-20	100%	17.27	375.9 ± 1.3	0.3%
98	1.259E-13 ± 2.1E-16	7.183E-15 ± 1.7E-17	1.548E-17 ± 1.2E-19	2.085E-18 ± 1.3E-18	2.031E-18 ± 1.1E-19	100%	17.45	379.4 ± 1.1	0.3%
99	2.070E-13 ± 1.3E-16	1.172E-14 ± 2.8E-17	3.450E-17 ± 5.1E-19	2.150E-17 ± 2.4E-18	4.971E-18 ± 2.1E-19	99%	17.53	381.0 ± 1.0	0.3%
	1.025E-12	5.629E-14			2.265E-17				
							Total Gas Age:	384.7	
							Weighted Average Age:	380.2 ± 1.6	

Data are in moles

(*, atm) radiogenic and atmospheric derived argon

Raw data for muscovite single crystal total fusion analyses.

JWB-06-M28A MUSCOVITE (single crystal total fusion) au9.1e.mus.sf

J = 0.0136 ± 0.00003 grain size = 0.5-1.0 mm diameter

	⁴⁰ Ar (*, atm)	³⁹ Ar (K-derived)	³⁸ Ar (Cl-derived, atm)	³⁷ Ar (Ca-derived)	³⁶ Ar (*, *)	%Rad	R	Age (Ma)	%-sd
71	9.044E-14 ± 1.1E-15	4.861E-15 ± 1.3E-16	1.645E-17 ± 3.9E-19	7.226E-19 ± 6.7E-19	2.627E-18 ± 1.4E-19	99%	19.24	414.1 ± 12.6	3.0%
73	1.237E-13 ± 6.4E-16	6.839E-15 ± 2.7E-17	1.735E-17 ± 3.0E-19	6.148E-19 ± 1.2E-18	2.947E-18 ± 1.4E-19	99%	17.96	389.3 ± 2.5	0.7%
74	1.673E-13 ± 4.8E-16	9.029E-15 ± 3.9E-17	2.121E-17 ± 2.9E-19	3.944E-18 ± 1.4E-18	1.452E-17 ± 2.1E-19	97%	18.06	391.2 ± 2.1	0.5%
75	1.210E-13 ± 1.6E-16	6.745E-15 ± 1.1E-17	1.539E-17 ± 1.1E-19	2.393E-18 ± 9.6E-19	3.415E-18 ± 1.0E-19	99%	17.78	385.9 ± 0.8	0.2%
76	1.616E-13 ± 2.8E-16	8.862E-15 ± 2.1E-17	2.635E-17 ± 2.8E-19	2.855E-18 ± 1.2E-18	9.298E-18 ± 1.9E-19	98%	17.93	388.8 ± 1.2	0.3%
77	3.396E-13 ± 2.0E-16	1.862E-14 ± 4.1E-17	5.148E-17 ± 6.0E-19	9.135E-18 ± 1.8E-18	3.076E-17 ± 4.9E-19	97%	17.75	385.3 ± 0.9	0.2%
78	2.281E-13 ± 1.0E-16	1.271E-14 ± 3.2E-17	3.231E-17 ± 2.9E-19	9.137E-18 ± 1.6E-18	7.290E-18 ± 1.7E-19	99%	17.77	385.6 ± 1.0	0.3%
79	7.815E-16 ± 4.0E-18	4.337E-17 ± 9.9E-19	6.798E-20 ± 3.6E-20	1.047E-18 ± 9.8E-19	2.968E-20 ± 6.9E-20	99%	17.81	386.5 ± 1.3	3.6%
80	5.910E-14 ± 2.6E-16	3.249E-15 ± 1.9E-17	9.638E-18 ± 1.5E-19	1.670E-18 ± 1.2E-18	2.686E-18 ± 1.2E-19	99%	17.94	399.1 ± 2.9	0.7%
	1.292E-12	7.076E-14			7.357E-17				

Total Gas Age: 390.7
Weighted Average Age: 385.5 ± 1.5

Data are in moles
(*, atm) radiogenic and atmospheric derived argon
Highlighted area is outlying data point not used in age calculations

JWB-06-M28B MUSCOVITE (single crystal total fusion) au9.4a.mus.sf

J = 0.0136 ± 0.00003 grain size = 0.5-1.0 mm diameter

	⁴⁰ Ar (*, atm)	³⁹ Ar (K-derived)	³⁸ Ar (Cl-derived, atm)	³⁷ Ar (Ca-derived)	³⁶ Ar (*, *)	%Rad	R	Age (Ma)	%-sd
61	1.387E-13 ± 3.3E-17	7.721E-15 ± 1.8E-17	2.075E-17 ± 2.0E-19	1.228E-17 ± 1.3E-18	6.100E-18 ± 1.8E-19	99%	17.48	384.2 ± 0.9	0.2%
62	8.201E-14 ± 1.7E-16	4.629E-15 ± 7.4E-18	1.386E-17 ± 8.7E-20	8.605E-18 ± 8.8E-19	1.370E-18 ± 1.3E-19	100%	17.63	387.2 ± 1.0	0.3%
63	1.274E-13 ± 4.7E-16	7.168E-15 ± 2.3E-17	1.969E-17 ± 2.1E-19	1.075E-17 ± 4.0E-18	3.493E-18 ± 1.4E-19	99%	17.63	387.3 ± 1.9	0.5%
64	1.447E-13 ± 2.0E-16	8.189E-15 ± 1.8E-17	2.109E-17 ± 9.6E-20	1.023E-17 ± 4.2E-18	2.821E-18 ± 1.4E-19	99%	17.57	386.0 ± 1.0	0.3%
65	8.216E-14 ± 2.1E-16	4.645E-15 ± 7.9E-18	1.294E-17 ± 1.4E-19	8.589E-18 ± 1.5E-18	1.370E-18 ± 9.5E-20	100%	17.60	388.3 ± 1.2	0.3%
66	1.247E-13 ± 4.2E-17	7.015E-15 ± 1.0E-17	1.748E-17 ± 1.8E-19	1.782E-17 ± 1.5E-18	2.167E-18 ± 1.0E-19	99%	17.68	388.3 ± 0.6	0.2%
67	1.372E-13 ± 4.3E-16	7.505E-15 ± 1.9E-17	2.409E-17 ± 2.2E-19	8.286E-18 ± 1.1E-18	1.424E-17 ± 2.0E-19	97%	17.72	389.0 ± 1.6	0.4%
68	1.020E-14 ± 2.0E-17	5.786E-16 ± 1.3E-18	1.773E-18 ± 4.6E-20	-4.199E-20 ± 6.4E-19	7.208E-20 ± 6.8E-20	100%	17.59	388.5 ± 1.4	0.4%
69	1.214E-13 ± 3.1E-16	6.795E-15 ± 2.1E-17	1.940E-17 ± 1.3E-19	1.388E-17 ± 1.6E-18	5.331E-18 ± 1.3E-19	99%	17.64	387.5 ± 1.5	0.4%
	9.665E-13	5.425E-14			3.699E-17				

Total Gas Age: 387.5
Weighted Average Age: 387.0 ± 1.2

Data are in moles
(*, atm) radiogenic and atmospheric derived argon

JWB-06-M28C MUSCOVITE (single crystal total fusion) au9.1h.mus.sf

J = 0.0136 ± 0.00003 grain size = 0.5-1.0 mm diameter

	⁴⁰ Ar (*, atm)	³⁹ Ar (K-derived)	³⁸ Ar (Cl-derived, atm)	³⁷ Ar (Ca-derived)	³⁶ Ar (*, *)	%Rad	R	Age (Ma)	%-sd
91	8.772E-14 ± 2.2E-16	4.987E-15 ± 1.0E-17	1.105E-17 ± 1.4E-19	4.112E-18 ± 1.3E-18	2.847E-18 ± 1.3E-19	96%	17.42	378.6 ± 1.2	0.3%
92	1.092E-13 ± 1.5E-16	6.121E-15 ± 7.5E-18	1.611E-17 ± 1.3E-19	2.691E-18 ± 1.3E-18	5.176E-18 ± 1.4E-19	96%	17.59	382.2 ± 0.7	0.2%
93	8.744E-14 ± 1.3E-16	4.965E-15 ± 1.0E-17	1.178E-17 ± 1.2E-19	4.439E-18 ± 1.4E-18	1.053E-18 ± 8.6E-20	100%	17.44	378.3 ± 1.0	0.3%
94	5.212E-14 ± 3.5E-17	2.988E-15 ± 1.2E-17	6.655E-18 ± 1.0E-19	1.163E-18 ± 1.3E-18	1.859E-18 ± 1.2E-19	99%	17.38	379.0 ± 1.6	0.4%
95	9.812E-14 ± 7.4E-17	5.595E-15 ± 1.4E-17	1.491E-17 ± 3.2E-19	1.715E-18 ± 9.9E-19	2.084E-18 ± 1.1E-19	99%	17.43	379.0 ± 1.0	0.3%
96	1.394E-13 ± 1.7E-16	7.881E-15 ± 2.0E-17	2.465E-17 ± 3.7E-19	2.816E-18 ± 1.0E-18	1.552E-18 ± 9.2E-20	100%	17.62	382.8 ± 1.1	0.3%
97	1.194E-13 ± 1.7E-16	6.838E-15 ± 2.0E-17	1.892E-17 ± 2.2E-19	2.567E-18 ± 1.2E-18	1.093E-18 ± 9.7E-20	100%	17.27	375.9 ± 1.3	0.3%
98	1.259E-13 ± 2.1E-16	7.183E-15 ± 1.7E-17	1.548E-17 ± 1.2E-19	2.085E-18 ± 1.3E-18	2.031E-18 ± 1.1E-19	100%	17.45	379.4 ± 1.1	0.3%
99	2.070E-13 ± 1.3E-16	1.172E-14 ± 2.8E-17	3.450E-17 ± 5.1E-19	2.150E-17 ± 2.4E-18	4.971E-18 ± 2.1E-19	99%	17.53	381.0 ± 1.0	0.3%
	1.025E-12	5.829E-14			2.265E-17				

Total Gas Age: 384.7
Weighted Average Age: 380.2 ± 1.6

Data are in moles
(*, atm) radiogenic and atmospheric derived argon

Raw data for muscovite single crystal total fusion analyses (continued).

DRB-06-22 MUSCOVITE (incrementally heated) au9.1c.mus.ih

90.5% gas released in steps 0.3 to 0.33 grain size = 0.5 - 1.0 mm diameter

%P	⁴⁰ Ar (*, atm)	³⁹ Ar (K-derived)	³⁸ Ar (Cl-derived, atm)	³⁷ Ar (Ca-derived)	³⁶ Ar (*, °)	%Rad	R	Age (Ma)	%-sd
0.3	4.515E-15 ± 7.4E-18	2.175E-16 ± 9.1E-19	8.751E-19 ± 6.4E-20	-1.320E-18 ± 8.9E-19	2.402E-18 ± 8.2E-20	84%	17.49	380.2 ± 3.2	0.8%
0.33	3.210E-14 ± 7.6E-17	1.811E-15 ± 4.9E-18	4.909E-18 ± 7.5E-20	-9.336E-19 ± 6.9E-19	1.213E-18 ± 1.3E-19	99%	17.53	381.0 ± 1.5	0.4%
0.36	8.289E-14 ± 1.3E-16	4.756E-15 ± 1.4E-17	1.200E-17 ± 1.3E-19	6.926E-18 ± 1.2E-18	1.154E-18 ± 8.4E-20	100%	17.36	377.6 ± 1.3	0.3%
0.38	9.201E-14 ± 1.0E-16	5.279E-15 ± 1.0E-17	1.394E-17 ± 1.5E-19	4.408E-18 ± 1.6E-18	9.315E-19 ± 7.2E-20	100%	17.38	378.0 ± 0.9	0.2%
0.4	1.604E-15 ± 3.7E-18	9.177E-17 ± 1.2E-18	4.538E-19 ± 6.5E-20	8.045E-20 ± 9.0E-19	9.568E-20 ± 5.4E-20	98%	17.17	373.9 ± 6.4	1.7%
0.43	1.620E-15 ± 3.8E-18	9.117E-17 ± 6.7E-19	3.448E-19 ± 5.7E-20	-2.493E-19 ± 1.0E-18	-5.048E-20 ± -5.4E-20	101%	17.93	388.8 ± 4.8	1.2%
0.45	6.726E-15 ± 7.4E-18	3.793E-16 ± 1.8E-18	7.020E-19 ± 2.9E-20	-3.312E-19 ± 8.8E-19	5.746E-20 ± 5.5E-20	100%	17.69	384.0 ± 2.1	0.5%
0.5	7.398E-16 ± 4.5E-18	4.153E-17 ± 4.4E-19	1.559E-19 ± 5.1E-20	-9.545E-19 ± 1.0E-18	-3.512E-20 ± -5.9E-20	101%	18.06	391.4 ± 10.2	2.6%
0.55	7.979E-16 ± 3.1E-18	4.284E-17 ± 3.4E-19	3.181E-19 ± 8.7E-20	-5.808E-19 ± 1.0E-18	-3.728E-21 ± -5.4E-20	100%	18.23	394.6 ± 8.8	2.2%
0.6	1.96E-14 ± 1.7E-16	7.249E-16 ± 1.0E-17	2.050E-18 ± 6.0E-20	-9.306E-19 ± 1.0E-18	-7.595E-20 ± -5.5E-20	100%	16.52	361.2 ± 7.1	2.0%
0.65	1.231E-16 ± 2.3E-18	6.300E-18 ± 3.8E-19	2.873E-20 ± 5.2E-20	8.894E-19 ± 7.5E-19	1.199E-19 ± 8.8E-20	71%	13.91	308.7 ± 95.6	31.0%
0.75	1.972E-16 ± 2.3E-18	1.094E-17 ± 5.1E-19	-1.976E-20 ± -2.8E-20	-5.239E-19 ± 8.9E-19	1.478E-19 ± 8.8E-20	78%	14.03	311.1 ± 56.0	18.0%
0.8	1.904E-16 ± 2.5E-18	1.090E-17 ± 3.9E-19	2.173E-19 ± 9.6E-20	-2.518E-19 ± 8.1E-19	3.022E-20 ± 9.6E-20	95%	16.65	363.6 ± 58.5	16.1%
0.85	1.209E-15 ± 4.3E-18	6.840E-17 ± 4.7E-19	3.040E-19 ± 4.7E-20	1.021E-19 ± 6.0E-19	1.839E-19 ± 8.8E-20	96%	16.88	368.1 ± 8.8	2.4%
2.367E-13	1.353E-14				6.171E-18				
Total Gas Age: 382.3									
Weighted Average Age: 379.1 ± 2.3									
Plateau Age: 378.5 ± 0.63									

Data are in moles
(*, atm) radiogenic and atmospheric derived argon
%P = laser power percent

JWB-06-CPT3 MUSCOVITE (incrementally heated) au9.1g.mus.ih

99.53% gas released in steps 0.3 to 0.7 grain size = 0.5 - 1.0 mm diameter

%P	⁴⁰ Ar (*, atm)	³⁹ Ar (K-derived)	³⁸ Ar (Cl-derived, atm)	³⁷ Ar (Ca-derived)	³⁶ Ar (*, °)	%Rad	R	Age (Ma)	%-sd
0.3	8.587E-16 ± 1.8E-18	4.681E-17 ± 6.9E-19	5.924E-19 ± 6.9E-20	1.709E-18 ± 7.9E-19	2.682E-19 ± 5.2E-20	91%	16.65	363.7 ± 9.4	2.6%
0.4	6.398E-14 ± 6.2E-17	3.611E-15 ± 6.0E-18	1.116E-17 ± 2.2E-19	1.365E-18 ± 7.2E-19	3.273E-18 ± 8.8E-20	98%	17.45	379.4 ± 0.7	0.2%
0.5	1.112E-13 ± 3.9E-17	6.345E-15 ± 7.4E-18	1.791E-17 ± 1.3E-19	9.647E-18 ± 1.3E-18	8.062E-19 ± 9.7E-20	100%	17.49	380.1 ± 0.5	0.1%
0.6	1.061E-14 ± 7.4E-18	6.082E-16 ± 4.5E-18	2.276E-18 ± 4.9E-20	8.188E-19 ± 8.9E-19	1.113E-19 ± 5.8E-20	100%	17.38	378.1 ± 2.9	0.8%
0.7	1.117E-14 ± 1.5E-17	6.391E-16 ± 1.2E-18	2.253E-18 ± 6.0E-20	2.513E-18 ± 8.4E-19	6.280E-20 ± 6.5E-20	100%	17.45	379.3 ± 1.1	0.3%
0.8	8.817E-16 ± 3.8E-18	5.329E-17 ± 6.7E-19	8.545E-19 ± 8.7E-20	1.246E-18 ± 9.0E-19	3.145E-20 ± 5.8E-20	99%	16.37	358.2 ± 8.4	2.3%
1.0	3.944E-16 ± 2.3E-18	2.435E-17 ± 5.1E-19	4.500E-19 ± 9.4E-20	1.865E-18 ± 1.1E-18	1.071E-20 ± 5.7E-20	99%	16.07	352.1 ± 17.8	5.1%
1.991E-13	1.133E-14				4.563E-18				
Total Gas Age: 384.3									
Weighted Average Age: 379.7 ± 1.4									
Plateau Age: 379.8 ± 0.37									

Data are in moles
(*, atm) radiogenic and atmospheric derived argon
%P = laser power percent

Raw data for muscovite incrementally heated.

JWB-06-M28A MUSCOVITE (incrementally heated) au9.1e.mus.ih									
67.3% gas released in steps 0.36 to 0.43									
grain size = 0.5 - 1.0 mm diameter									
%P	⁴⁰ Ar (°, atm)	³⁹ Ar (K-derived)	³⁹ Ar (Cl-derived, atm)	³⁷ Ar (Ca-derived)	³⁶ Ar (°, °)	%Rad	R	Age (Ma)	%-sd
0.30	2.841E-15 ± 6.2E-18	1.401E-16 ± 1.0E-18	4.192E-19 ± 2.7E-20	-2.601E-18 ± 1.1E-18	8.847E-19 ± 6.3E-20	91%	18.41	398.2 ± 4.4	1.1%
0.33	2.866E-14 ± 1.2E-17	1.425E-15 ± 3.0E-18	4.865E-18 ± 1.8E-19	-1.608E-18 ± 1.1E-18	2.572E-18 ± 6.0E-20	97%	18.18	393.7 ± 0.9	0.2%
0.36	3.794E-14 ± 2.7E-17	2.078E-15 ± 5.9E-18	5.939E-18 ± 4.3E-20	-1.869E-18 ± 1.1E-18	1.321E-18 ± 6.9E-20	99%	18.07	391.4 ± 1.2	0.3%
0.38	2.320E-14 ± 2.1E-17	1.262E-15 ± 4.5E-18	3.350E-18 ± 6.2E-20	-2.058E-18 ± 1.5E-18	6.875E-19 ± 6.4E-20	99%	18.22	394.4 ± 1.5	0.4%
0.40	5.239E-14 ± 4.5E-17	2.896E-15 ± 4.4E-18	8.054E-18 ± 1.3E-19	-4.531E-19 ± 1.1E-18	4.943E-19 ± 5.8E-20	100%	18.02	390.6 ± 0.7	0.2%
0.43	1.385E-14 ± 2.4E-17	7.652E-16 ± 4.1E-18	1.435E-18 ± 3.6E-20	1.653E-18 ± 1.0E-18	2.451E-19 ± 1.1E-19	99%	18.00	390.2 ± 2.4	0.6%
0.45	1.641E-14 ± 8.9E-18	8.952E-16 ± 3.5E-18	2.311E-18 ± 7.1E-20	9.567E-19 ± 9.7E-19	2.323E-19 ± 1.1E-19	100%	18.26	395.2 ± 1.8	0.4%
0.50	1.321E-15 ± 2.2E-18	7.183E-17 ± 8.5E-19	-8.560E-20 ± -1.7E-20	-2.364E-19 ± 1.0E-18	1.518E-19 ± 1.1E-19	97%	17.77	385.7 ± 10.8	2.8%
0.55	7.731E-15 ± 1.0E-17	4.282E-16 ± 3.3E-18	5.572E-19 ± 2.3E-20	-1.883E-19 ± 1.0E-18	2.124E-19 ± 1.1E-19	99%	17.91	388.4 ± 3.4	0.9%
0.60	8.184E-15 ± 9.0E-18	4.491E-16 ± 1.4E-18	7.624E-19 ± 3.6E-20	3.716E-19 ± 1.0E-18	-2.202E-20 ± -8.2E-20	100%	18.23	394.6 ± 1.6	0.4%
0.65	1.373E-16 ± 1.9E-18	8.190E-18 ± 5.4E-19	1.348E-19 ± 6.0E-20	1.445E-19 ± 8.1E-19	2.210E-19 ± 1.1E-19	52%	8.79	201.2 ± 97.9	48.7%
0.75	8.657E-16 ± 3.7E-18	4.887E-17 ± 7.2E-19	1.691E-20 ± 4.5E-21	-7.789E-19 ± 9.5E-19	1.771E-19 ± 1.1E-19	94%	17.05	371.6 ± 15.9	4.3%
0.80	1.301E-16 ± 1.7E-18	8.355E-18 ± 5.0E-19	3.605E-22 ± 7.4E-22	8.338E-19 ± 8.7E-19	1.045E-19 ± 1.1E-19	76%	11.88	266.7 ± 89.4	33.5%
0.85	3.686E-16 ± 2.6E-18	2.078E-17 ± 6.8E-19	1.219E-19 ± 5.4E-20	2.212E-19 ± 7.1E-19	2.076E-19 ± 1.1E-19	83%	14.64	323.5 ± 38.1	11.8%
	1.920E-13	1.050E-14			7.499E-18			Total Gas Age:	396.6
								Weighted Average Age:	392.3 ± 1.4
								Plateau Age:	391.2 ± 0.54

Data are in moles
(°, atm) radiogenic and atmospheric derived argon
%P = laser power percent

JWB-06-M28B MUSCOVITE (incrementally heated) au8.4a.mus.ih									
No Plateau									
grain size = 0.5 - 1.0 mm diameter									
%P	⁴⁰ Ar (°, atm)	³⁹ Ar (K-derived)	³⁹ Ar (Cl-derived, atm)	³⁷ Ar (Ca-derived)	³⁶ Ar (°, °)	%Rad	R	Age (Ma)	%-sd
a	3.255E-14 ± 1.2E-16	1.802E-15 ± 4.2E-18	4.862E-18 ± 5.4E-20	-1.344E-18 ± 1.0E-18	1.128E-18 ± 7.2E-20	99%	17.88	392.3 ± 1.8	0.5%
b	2.294E-14 ± 2.6E-17	1.285E-15 ± 4.4E-18	3.254E-18 ± 5.6E-20	1.800E-19 ± 8.1E-19	5.528E-19 ± 7.1E-20	99%	17.72	389.1 ± 1.5	0.4%
c	3.468E-14 ± 2.9E-17	1.955E-15 ± 4.9E-18	4.444E-18 ± 4.4E-20	-3.021E-19 ± 7.1E-19	7.836E-19 ± 7.2E-20	99%	17.62	387.1 ± 1.1	0.3%
d	3.733E-14 ± 3.6E-17	2.195E-15 ± 6.2E-18	7.985E-18 ± 1.2E-19	1.874E-19 ± 8.6E-19	3.639E-19 ± 6.5E-20	100%	16.95	373.8 ± 1.1	0.3%
e	6.127E-15 ± 9.6E-18	3.460E-16 ± 1.7E-18	8.821E-19 ± 5.0E-20	9.495E-19 ± 9.7E-19	3.686E-20 ± 7.3E-20	100%	17.68	388.2 ± 2.4	0.6%
f	4.385E-16 ± 1.9E-18	2.364E-17 ± 5.7E-19	-8.378E-20 ± -9.4E-20	-5.414E-19 ± 8.3E-19	8.706E-20 ± 7.5E-20	94%	17.46	383.9 ± 22.9	6.0%
g	7.122E-15 ± 8.6E-18	3.993E-16 ± 3.3E-18	2.789E-21 ± 2.4E-22	-2.639E-19 ± 7.2E-19	-9.662E-21 ± -6.9E-20	100%	17.84	391.5 ± 3.4	0.9%
h	1.536E-16 ± 2.4E-18	7.486E-18 ± 5.6E-19	-6.605E-19 ± -2.6E-19	-1.114E-19 ± 1.2E-18	1.994E-19 ± 1.1E-19	62%	12.65	286.0 ± 104.1	36.4%
i	3.859E-16 ± 2.1E-18	2.196E-17 ± 4.0E-19	-3.095E-19 ± -4.9E-19	-6.960E-19 ± 8.2E-19	8.474E-20 ± 7.6E-20	94%	16.44	363.5 ± 23.8	6.5%
j	8.537E-16 ± 4.0E-18	4.269E-17 ± 5.2E-19	-1.265E-20 ± -4.4E-21	-2.462E-19 ± 7.7E-19	1.365E-19 ± 7.6E-20	95%	19.05	415.1 ± 12.7	3.1%
k	2.256E-16 ± 1.7E-18	1.297E-17 ± 3.7E-19	3.349E-20 ± 4.8E-20	-7.524E-20 ± 8.0E-19	2.459E-20 ± 6.5E-20	97%	16.83	371.4 ± 34.7	9.3%
	1.428E-13	8.091E-15			3.388E-18			Total Gas Age:	385.7
								Weighted Average Age:	387 ± 1.2
								No Plateau	

Data are in moles
(°, atm) radiogenic and atmospheric derived argon
%P = laser power percent

Raw data for muscovite incrementally heated (continued).

JWB-06-M28C MUSCOVITE (incrementally heated) au9.1h.mus.ih

J = 0.0136 ± 0.00003		68.2% gas released in steps 0.36 to 0.55				grain size = 0.5 - 1.0 mm diameter			
%P	⁴⁰ Ar (*, atm)	³⁹ Ar (K-derived)	³⁹ Ar (Cl-derived, atm)	³⁷ Ar (Ca-derived)	³⁶ Ar (*)	%Rad	R	Age (Ma)	%-sd
0.30	2.192E-16 ± 2.4E-18	1.089E-17 ± 5.0E-19	-1.209E-19 ± -1.3E-18	-9.073E-19 ± 5.7E-19	-5.030E-20 ± -5.5E-20	107%	21.50	457.1 ± 37.6	8.2%
0.33	9.777E-15 ± 1.3E-17	5.032E-16 ± 2.4E-18	1.888E-18 ± 3.8E-20	4.403E-19 ± 6.8E-19	3.902E-18 ± 9.8E-20	88%	17.14	373.3 ± 2.4	0.7%
0.36	9.021E-14 ± 4.5E-17	5.019E-15 ± 8.2E-18	1.311E-17 ± 1.5E-19	8.198E-18 ± 1.0E-18	9.649E-18 ± 1.4E-19	97%	17.41	378.6 ± 0.7	0.2%
0.38	1.451E-14 ± 2.4E-17	8.215E-16 ± 5.0E-18	1.930E-18 ± 5.5E-20	9.481E-19 ± 9.6E-19	8.051E-20 ± 5.0E-20	100%	17.64	383.0 ± 2.4	0.6%
0.40	3.878E-14 ± 3.7E-17	2.222E-15 ± 5.0E-18	4.978E-18 ± 5.6E-20	6.709E-19 ± 7.3E-19	1.121E-19 ± 5.7E-20	100%	17.44	379.2 ± 0.9	0.2%
0.43	4.248E-14 ± 5.4E-17	2.413E-15 ± 5.5E-18	7.192E-18 ± 1.8E-19	-1.142E-19 ± 6.2E-19	2.201E-19 ± 1.2E-19	100%	17.58	381.9 ± 1.0	0.3%
0.45	7.427E-14 ± 5.9E-17	4.223E-15 ± 7.0E-18	8.746E-18 ± 1.1E-19	1.780E-19 ± 1.0E-18	3.483E-19 ± 1.2E-19	100%	17.56	381.7 ± 0.7	0.2%
0.50	3.001E-14 ± 6.9E-17	1.694E-15 ± 4.8E-18	3.416E-18 ± 3.1E-20	-1.694E-19 ± 1.1E-18	2.100E-19 ± 1.2E-19	100%	17.68	384.0 ± 1.5	0.4%
0.55	1.148E-14 ± 9.9E-18	6.522E-16 ± 3.2E-18	7.488E-19 ± 2.8E-20	-1.059E-18 ± 1.2E-18	1.982E-19 ± 1.2E-19	99%	17.50	380.5 ± 2.2	0.6%
0.60	3.967E-14 ± 1.8E-17	2.260E-15 ± 5.1E-18	6.857E-18 ± 2.3E-19	-6.397E-19 ± 7.0E-19	2.075E-19 ± 1.2E-19	100%	17.52	380.9 ± 0.9	0.2%
0.65	6.261E-15 ± 1.1E-17	3.543E-16 ± 3.1E-18	7.552E-19 ± 3.8E-20	-2.039E-18 ± 9.8E-19	1.064E-19 ± 9.7E-20	99%	17.58	382.0 ± 3.9	1.0%
0.75	2.349E-14 ± 2.4E-17	1.309E-15 ± 8.0E-18	3.139E-18 ± 5.2E-20	-7.463E-19 ± 9.9E-19	1.925E-19 ± 9.9E-20	100%	17.91	386.3 ± 2.5	0.6%
0.80	4.368E-16 ± 2.8E-18	2.411E-17 ± 4.9E-19	1.759E-20 ± 1.1E-20	-1.456E-18 ± 8.0E-19	1.057E-19 ± 9.5E-20	93%	16.82	367.1 ± 26.8	7.3%
	3.816E-13	2.151E-14			1.528E-17			Total Gas Age:	385.8
								Weighted Average Age:	380.6 ± 1.5
								Plateau Age:	381.3 ± 0.41

Data are in moles
 (*, atm) radiogenic and atmospheric derived argon
 %P = laser power percent

Raw data for muscovite incrementally heated (continued).